SPACE AND TIME IN THE HIPPOCAMUS

Doctoral Dissertation, 2009

BALÁZS UJFALUSSY

Department of Biophysics, KFKI Research Institute for Particle and Nuclear Physics of the Hungarian Academy of Sciences, Budapest, Hungary

Advisors:
Tamás Kiss, Ph.D.
Dr. Péter Érdi, Ph.D., D.Sc., Henry R. Luce Professor, Head of Department

Faculty of Sciences, Eötvös Loránd University, Budapest, Hungary

Ph.D. School: Biology
Head: Dr. Anna Erdei

Ph.D. Program: Neuroscience and Human Biology
Head: Dr. László Détári

"...In that Empire, the craft of Cartography attained such Perfection that the Map of a Single province covered the space of an entire City, and the Map of the Empire itself an entire Province. In the course of Time, these Extensive maps were found somehow wanting, and so the College of Cartographers evolved a Map of the Empire that was of the same Scale as the Empire and that coincided with it point for point. Less attentive to the Study of Cartography, succeeding Generations came to judge a map of such Magnitude cumbersome, and, not without Irreverence, they abandoned it to the Rigours of sun and Rain. In the western Deserts, tattered Fragments of the Map are still to be found, Sheltering an occasional Beast or beggar; in the whole Nation, no other relic is left of the Discipline of Geography. "

Travels of Praiseworthy Men (1698) by Suarez Miranda
In Borges, J. L. (1975): *A Universal History of Infamy*,
Penguin Books, London.

Acknowledgements

This work was carried out in the Computational Neuroscience Group, Department of Biophysics at the KFKI Research Institute for Particle and Nuclear Physics of the Hungarian Academy of Sciences during the years 2005-2009. The dissertation benefited a lot from the inspiring atmosphere of this ancient citadel of Hungarian scientific research. I also want to thank to my institute for its patience and support for the exciting field of computational neuroscience often strange for physicists.

I wish to express my deepest gratitude to my adviser, Dr. Péter Érdi, who introduced me to the fascinating area of computational neuroscience, for his continuous support and encouragement. My first own ideas in this field were conceived under his close supervision during my teaching and research assistantship at Kalamazoo College. His enthusiasm for new ideas in any fields of computational neuroscience initiated numerous fruitful discussions, collaborations and research papers.

I have been fortunate to obtain supervision from Tamás Kiss who provided me tremendous support to learn the tricks and techniques of computational neuroscience. I am grateful to him for never sparing his time when I asked him to discuss ideas or to critically read different versions of manuscripts.

My warmest thanks go to my co-worker, Dr. Mihály Hajós for his inspiring experiments that attracted me towards modelling the septo-hippocampal system.

I benefited a lot from reading the dissertations of ex-fellows of the group, specifically the works of Tamás Kiss, Máté Lengyel, and Gergő Orbán who kindly provided me their bookhack.tex file to improve the typography of this dissertation.

My special thanks belong to my close colleagues and co-workers Dávid Samu and Péter Erős for their kind collaboration during these years and also for their patience when I asked annoying technical questions during programming *Webots* or *C*. I owe my kindest thank to all other members of the lab for creating such a friendly atmosphere in which it was a real pleasure to work.

Preface

How does the brain process, represent and store information relevant for making fast and reliable decisions supporting adaptive behavior in different animals? These are arguably the core questions in the field of neuroscience especially in computational neuroscience (Bower and Beeman, 1998). The *hippocampus* is among the most intensively studied areas of the mammalian brain. Its relatively simple synaptic organization is well-conserved through the mammalian evolution, and its involvement in cognitive processes such as episodic memory or navigation makes the hippocampus an ideal candidate for studying neural information processing. The physical *location* of an animal is an abstract and hidden variable for them as they have to infer it based on their previous sequence of movements and the currently available set of sensory inputs. How the neural representation of the allocentric space changes in the hippocampus after environmental manipulations helps us understanding the information processing in the nervous system. Animals experience the continuous change of their environment on different *time* scales. Does the neural representation in the hippocampus reflect this continuous flow of information or the brain extracts discrete episodes in space, time and action? Although this question is still open, neural oscillations are naturally involved in binding and segmentation of the incoming information.

In the present dissertation we describe three lines of research focusing on different aspects of the questions posed in the previous paragraph. These three lines represent three different levels of hippocampal computations. First, on the microcircuit level, we give a new model for the generation of the septo-hippocampal theta oscillation and validate this model against experimental data. In the second line, on the macrocircuit level, we show that an integrated hippocampal spatial representation emerges from location dependent input, and we explore the interactions between the entorhinal and the hippocampal spatial representations under various experimental conditions. Finally, on the single-neuron level, we demonstrate that the dendritic morphology of different neurons shape their spatial receptive field within the hippocampus.

At the beginning of this dissertation we give an introduction to the structure, function and dynamics of the hippocampal formation (Arbib et al., 1997). This chapter serves as an ordered glossary for the rest of the dissertation not intended to give a critical

review of the issues covered. The advanced reader may simply skip this general introduction and start with the second part where a more specific introductions are given at the beginning of each chapter.

A note pertaining to style. As Koch wrote in the preface of his book (Koch, 1999) "science is a social endeavor: many, if not most, new ideas are born out of discussions with colleagues, reading books and papers, attending seminars and so on. We are often not even explicitly aware of these influences, but they are there non-the-less. It is to acknowledge this that I use the *pluralis modestati* form of the *we*" throughout this dissertation. This notation does not influence that the results (ideas, models, analysis of data, figures) described in the present dissertation reflect my own work unless the original author is explicitly referred.

Contents

List of Figures

Part I

Prelude

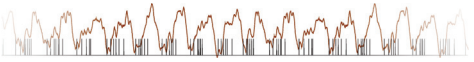

1

Introduction to the hippocampus

In this chapter we try to give a brief and concise introduction to the concepts used in the present dissertation. For those who take deeper interest in the hippocampus we recommend the recent comprehensive textbook, The Hippocampus Book (2007) (Andersen et al., 2007) which served as an authentic source of many information presented in this chapter. There are, of course, interspecies and age differences in hippocampal organization which will be ignored here for simplicity and, mostly data on the adult rat hippocampus will be presented.

The hippocampus: neural Rosetta Stone[1]

The hippocampus is one of the most widely studied regions of the brain not only because of its involvement in high level cognitive processes like memory formation (Scoville and Milner, 1957) and spatial navigation (O'Keefe and Nadel, 1978) but also because of its unique, relatively simple and feed-forward structure (Andersen et al., 1971). It is extensively studied at many different levels from biochemical signaling pathways through the physiology of single neurons to the behavior of large networks and this widespread research lead to fascinating discoveries like synaptic plasticity (Bliss and Lømo, 1973) or adult neurogenesis in the dentate gyrus (Kaplan and Hinds, 1977). Parallel to the accumulation of experimental data computational models have been constructed that shape our understanding the function of the hippocampal formation (Burgess, 2007).

[1] The term *neural Rosetta Stone* was borrowed from Andersen et al. (2007)

1.1 Structure

1.1.1 Gross anatomy

From an evolutionary point of view the hippocampus is an ancient part of the mammalian telencephalon. During ontogeny the hippocampus develops from the dorsomedial part of the pallium, called archipallium, and it is located in the medial temporal lobe in primates. When compared with the six-layered neocortex, the hippocampus has relatively simpler, ancient cytoarchitectonic structure, and is therefore called archicortex or allocortex. Both neocortical regions and the hippocampus are characterized by large, pyramid-shaped projection neurons and smaller interneurons, but principal neurons of the hippocampus are typically organized into a single layer. Moreover, the largely unidirectional passage of information through highly laminated intrahippocampal pathways and the distributed organization of intrinsic associational connections makes the neuroanatomy of the hippocampus unique.

The *hippocampal formation* consists of the *hippocampus proper* (or Ammon's horn, Cornu Ammonis, CA) the *dentate gyrus* (DG), the *subicular regions* and the *entorhinal cortex* (EC) (Fig. 1.1). Based on the size of the pyramidal cells, their input and output, the hippocampus proper is further subdivided into two major regions CA3 and CA1[2].

The main justification for including the four regions named above in the hippocampal formation is that they are linked, one to the next, by a largely unidirectional excitatory pathway. The majority of cortical inputs arriving to the hippocampus is originating from glutamatergic principal cells (*stellate cells* and *pyramidal cells*) of the superficial layers of the entorhinal cortex (EC). These fibers form the *perforant path* and terminate on the principal cells and interneurons (feed-forward inhibition) of the CA regions and the dentate gyrus. The EC itself is a higher order associative area collecting pre-processed information from each sensory modality.

[2]The region CA2 is a narrow zone between CA1 and CA3, and CA4 is the previously used name of the deep layer of the dentate gyrus.

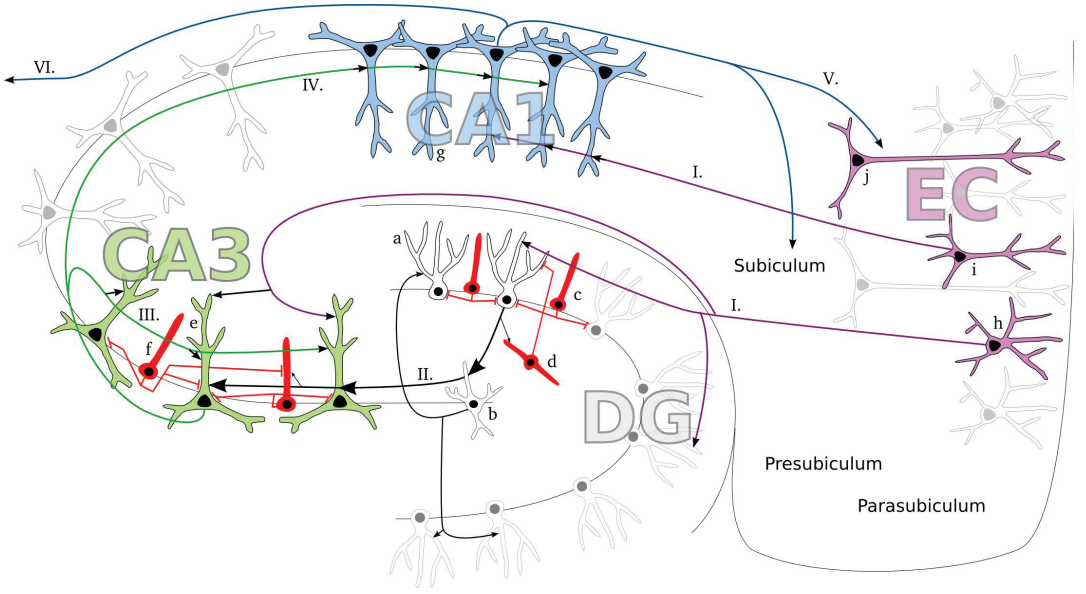

Figure 1.1: **Hippocampal circuits.** Simple drawing illustrates the key players of the hippocampal try-synaptic loop. EC: entorhinal cortex; DG: dentate gyrus, CA1 and CA3: subfields of the hippocampus proper. I: Perforant path, II: mossy fibers, III: recurrent connections within the CA3 region, IV: Schaffer collaterals, V: CA1 back-projection to the EC, VI: fimbria. a: dentate granule cells, b: dentate mossy cells, c-d: interneurons in the DG, e: pyramidal cell in CA3, f: interneuron in the CA3, g: CA1 pyramidal neuron, h: layer II stellate cell in the EC, i: layer III pyramidal neuron, j: deep layer pyramidal neuron

Neurons in layer II of the entorhinal cortex project to the dentate gyrus and the CA3 field of the hippocampus, while neurons in layer III project to the CA1 and the subiculum. The principal cells (called *granule cells*) of the dentate gyrus project to the CA3 field via the mossy fiber projections. Pyramidal neurons of the CA3 field project to the CA1 via the Schaffer collaterals while pyramidal neurons of the CA1 region project to the subiculum and both CA1 and subiculum project back to the deep layers (layer V and layer VI) of the entorhinal cortex. This internal excitatory circuitry of the hippocampus (Fig. 1.1) is often referred to as the hippocampal trisynaptic loop (Andersen et al., 1971):

$$
\begin{array}{lllllllll}
\text{EC} & \rightarrow & \text{DG} & & & & & & 1^{\text{st}}\text{ synapse} \\
 & & \text{DG} & \rightarrow & \text{CA3} & & & & 2^{\text{nd}}\text{ synapse} \\
 & & & & \text{CA3} & \rightarrow & \text{CA1} & & 3^{\text{rd}}\text{ synapse} \\
 & & & & & & (\text{ CA1} & \rightarrow \text{ EC} & 4^{\text{th}}\text{ synapse)}
\end{array}
$$

The hippocampus has extensive connections with subcortical structures, among them are the amygdala, the anterior thalamus and supramammillary area. Inputs from the locus coeruleus, the raphe and the septal nuclei (see section 2.1) reaches the hippocampus via the fimbria-fornix pathway. These pathways often, but not exclusively, use transmitters other than glutamate or GABA and have modulatory effect conveyed by metabotropic rather than fast acting ionotropic receptors.

1.1.2 Cytoarchitectonic organization

A transverse (coronal) section of the hippocampus reveals two C-shaped interlocking cell layers, the granular cell layer (*stratum [str.] granulosum*) of DG and the pyramidal cell layer (*str. pyramidale*) of CA regions.

Dentate gyrus. The dentate gyrus is comprised of three layers. Superficially is a relatively cell free layer, called molecular layer (*str. moleculare*) where dendritic branches of granule cells receive entorhinal and commissural afferents. The granule cell layer of the DG is made up of the densely packed somata of granule cells. These two outer layers form the smaller C-shaped structure that encloses a cellular region, the *polymorphic cell layer*, which constitutes the third layer of the dentate gyrus.

Cornu Ammonis. The larger C, representing Cornu Ammonis can be subdivided into five layers both in CA3 and CA1. The ventricular surface of the hippocampus is covered by a thin sheet of myelinated afferent and efferent fibers called the *alveus*. The narrow, relatively cell-free layer located below the alveus is called *str. oriens*. It contains the basal dendrites of pyramidal cells and several classes of interneurons. Next, the principal cell layer is called *str. pyramidale* and contains the densely packed cell bodies of pyramidal neurons as well as some classes of interneurons (basket, axo-axonic, bistratified cell). In the *str. radiatum* the radial oblique branches of pyramidal neurons receives recurrent connections in the CA3 and the Schaffer collateral input in the CA1 region. The most superficial layer of the hippocampus is called *str. lacunosum-moleculare*. It is in this layer that fibers from the EC terminate on the apical tuft of pyramidal neurons as well as on the dendritic tree of interneurons. As we emphasized above, the layered structure of the hippocampus is reflected in many aspects of its synaptic organization: different pathways form synapses in different layers, and the dendritic tree as well as the axonal arbor of interneurons are in register with one or another of these pathways.

Entorhinal cortex. The entorhinal cortex is a neocortical structure with the standard six-layered organization. *Layer II* is populated by stellate and pyramidal cells both projecting to the DG and CA3 as well as layer II of other regions of the EC. In *layer III*, the most numerous are the pyramidal cells which give rise to the perforant path projections to the CA1. *Layer V* is characterized by its large pyramidal neurons whose dendrites ascend towards the superficial portion of layer II and into layer I. Axons of these cells run into the deep white matter and additional collaterals innervate the superficial layers of the EC. It is not known which types of neurons in layer V-VI are the recipients of hippocampal back-projections. Based on its cytoarchitectonic organization and its connectivity with neocortical areas and the hippocampus the entorhinal cortex can be subdivided into two general areas: the lateral entorhinal area (LEA) and the medial entorhinal area (MEA). Lateral and medial entorhinal projections have a beautiful three dimensional organization with a number of functional implications. Layer II entorhinal cortex projections to the DG and CA3 terminate in a laminated fashion: the LEA projects more superficially in the molecular layer and the str. lacunosum-moleculare while the MEA projects deeper. In contrast, in CA1 and subiculum, layer III entorhinal projections are organized topographically: the LEA projects to the distal while MEA to the proximal CA1.

Interneurons. Whereas cell bodies of most principal cell types (i.e., glutamatergic stellate, granule and pyramidal cells) are organized into highly structured lamina (i.e., layer II in EC, *str. granulosum* in DG and *str. pyramidale* in CA3/CA1, respectively), the somata of local circuit GABAergic inhibitory interneurons are scattered throughout almost all layers of the hippocampus (Freund and Buzsáki, 1996). Moreover, despite representing only $\approx$10% of the total hippocampal neuron population, based on their dendritic and axonal morphology, their neurochemical content, their electrophysiological properties or firing patterns, inhibitory interneurons represent one of the most divers cell populations. However, even within a single region of the hippocampus interneurons have highly variable properties and classifications based on different criteria may not necessarily overlap (Parra et al., 1998; Maccaferri and Lacaille, 2003; Klausberger and Somogyi, 2008). The axons of these diverse cell populations make mainly short-range projections (but see (Jinno et al., 2007; Takacs et al., 2008)) and they are considered as regulators of principal cell activity. The axons of interneurons often target specific dendritic domains of principal cells as well as other interneurons therefore they play different roles in the timing of neuronal output, the regulation of synaptic transmission and plasticity, the modulation of dendritic excitability and the generation and pacing of large scale oscillatory activity.

1.2 Dynamics

1.2.1 Hippocampal Oscillations

Several patterns of electrical activity have been recorded from the hippocampus, and they have been correlated with different behavioral states. More than forty years ago, Vanderwolf placed a relatively large electrode into the hippocampus of a freely moving rat and recorded the EEG activity during wide range of behaviors (Vanderwolf, 1969). He identified three distinct states. First, the rhythmical theta state, occurring during various types of locomotor activity including exploratory, preparatory or other kinds of voluntary movements, during arousal as well as during REM sleep. Second, a large amplitude, irregular activity pattern (LIA) that is characteristic for consummatory behaviors such as grooming or eating. The third, a small amplitude, irregular activity occurs during behavioral transitions.

Theta activity. Hippocampal theta oscillation is a prominent, large amplitude (> 1 mV) field potential oscillation in the 4-12 Hz frequency band in the rat hippocampus first described by Green and Arduini (1954). The large amplitude of the extracellularly recorded oscillation reflects synchronous changes in the membrane potential of large number of principal neurons. Indeed, the subthreshold membrane potential and the firing activity of pyramidal cells, granule cells and most of hippocampal interneurons were shown to be modulated by theta oscillation (Skaggs et al., 1996; Kamondi et al., 1998; Klausberger et al., 2003). As different neurons are locked to different phases of the theta, the oscillatory signal itself emerges from the temporally ordered activity of many classes of neurons.

In the rat, theta is centered on the hippocampal formation but there are also reports of EEG and cellular activity phase locked to the hippocampal theta in many other areas including the cingulate cortex (Leung and Borst, 1987), prefrontal cortex (Hyman et al., 2005; Jones and Wilson, 2005; Siapas et al., 2005), posterior hypothalamus (Bland et al., 1995; Kocsis and Vertes, 1997), amygdala (Paré and Collins, 2000) as well as in the medial septum (Petsche et al., 1962; Stewart and Fox, 1989). Although theta activity is prominent in rats, dogs and cats it is controversial whether it can be recorded from either monkey or human hippocampus. However, difficulties in recording primate theta may arise from inappropriate behavioral paradigm and recording technique rather than from the absence of theta per se. Indeed, intracranial EEG recordings in epileptic patients during virtual spatial navigation tasks have demonstrated short episodes of activity with pronounced theta periodicity (Kahana et al., 1999; Caplan et al., 2003).

Theta, in turn, has been classified into two subtypes on the basis of behavioral correlate and pharmacological sensitivity (Kramis et al., 1975). *Type I* theta is faster (8-12 Hz), it occurs during voluntary movements and it is resistant to anticholinergic drugs such as atropine or scopolamine. This atropine-resistant component is sensitive to anaesthetics like urethane or ketamine, as well as to the lesion of the entorhinal cortex (Buzsáki, 2002). *Type II* theta is usually slower (4-8 Hz), occurs during psychological states such as arousal, attention or intention to move as well as during anaesthesia and is sensitive to cholonergic drugs (Kramis et al., 1975; Lawson and Bland, 1993). These two types of theta *does not* represent two mutually exclusive state of the hippocampal network, rather they are two relatively independent components of the emerging theta activity. Consequently, different, but cooperating parts

of the same neural circuitry are involved in the generation of these oscillations: the entorhino-hippocampal system in the generation of type I and the septo-hippocampal system in the generation of the type II theta (Buzsáki, 2002; Yoder and Pang, 2005).

Medial septal GABAergic neurons fire rhythmic bursts phase locked to the hippocampal theta (Petsche et al., 1962; Stewart and Fox, 1989; King et al., 1998) and they selectively innervate hippocampal interneurons (Freund and Antal, 1988). Based on these observations, it was suggested, that medial septal GABAergic neurons could drive hippocampal theta oscillation by rhythmically dis-inhibiting pyramidal neurons (Stewart and Fox, 1990; Tóth et al., 1997; Hangya et al., 2009). Cholinergic excitation from the medial septum seems to be involved in both types of theta oscillations (Yoder and Pang, 2005) by modulating both septal and hippocampal circuits and pushing them into a "theta mode" (Monmaur et al., 1997; Buzsáki, 2002).

Intrinsic hippocampal circuits have also been implicated in the generation of hippocampal theta activity (Chapman and Lacaille, 1999; Kocsis et al., 1999; Gillies et al., 2002; Orbán et al., 2006; Manseau et al., 2008) but it is not clear whether these regions are capable of generating theta activity on their own or their propensity to oscillate at theta frequency reflects a resonance mechanism (Leung and Yu, 1998; Hutcheon and Yarom, 2000).

Taken together, theta oscillation reflects a "global state" of the hippocampal formation where the highly organized activity of different neurons and microcircuits have specific role in hippocampal information processing.

Non-theta patterns. The faster gamma (40-100 Hz) oscillation is often temporally nested with the slower theta rhythm (Csicsvári et al., 2003) and have an important role in organizing cell-assemblies (Harris et al., 2003; Foster and Wilson, 2007) and in spike timing dependent plasticity (Bi and Poo, 1998).

During non-theta periods, large irregular activity (LIA) characterize the hippocampal EEG which is a relatively large amplitude but irregular activity pattern where the dominating frequencies are lower than theta. *Sharp waves* are extremely large amplitude ($>$1 mV), short (50-100 ms) events appearing irregularly in the hippocampal EEG during LIA. It was suggested that sharp waves are generated within the CA3 recurrent collateral system and then transmitted to the CA1 through the Shaffer collaterals (Csicsvári et al., 2000). Since an extremely large portion of pyramidal neurons discharge synchronously during sharp waves, they are considered as the most

synchronous physiological mode of the hippocampus (Buzsáki, 1986).

Around the time of the negative peak of the sharp wave, there is a high frequency oscillation between 120-300 Hz, whose peak amplitude occurs in the CA1 pyramidal layer (Buzsáki et al., 1992). During these *ripples* there is a synchronous burst in many pyramidal cells and several classes of interneurons (Klausberger and Somogyi, 2008) receiving feed-forward activation via Schaffer collaterals.

1.2.2 Single cell activity

During exploratory behavior different classes of hippocampal interneurons fire clock-like bursts locked to distinct phase of the ongoing theta oscillation at high rate ($>$10 Hz). Hippocampal pyramidal neurons, although they are also phase locked to the theta, have much lower baseline firing rate ($<$1 Hz), and, in rodents, their activity is usually restricted to a specific location (O'Keefe and Dostrovsky, 1971) or a particular configuration of sensory stimuli (Eichenbaum et al., 1999). Although the hippocampus is most likely involved in the rapid, one-trial encoding of arbitrary associations (Morris and Frey, 1997; Treves and Rolls, 1994), one of the most relevant stream of information, at least in rodents, is spatial location. This is supported by an enormous amount of data demonstrating forms of location dependent activity at different levels of hippocampal information processing.

Grid cells. The triangular grid-like firing (illustrated on Fig. 3.2A) of principal neurons in the medial entorhinal cortex was perhaps the most exciting discovery of the last decade in hippocampal research (Hafting et al., 2005). Grid cells, although most prominent in layer II, are found in all layers of the MEA (Sargolini et al., 2006). Grids of neighboring cells are offset relative to each other but share a common orientation (Barry et al., 2007). Colocalized cells have identical grid spacing but the spacing increases topografically from the dorsal to the ventral end of the medial entorhinal cortex. The grid fields are anchored to visual cues in the environment as they follow the rotation of landmarks (Hafting et al., 2005) or the deformation of the environment (Barry et al., 2007). However, grid cells maintained their firing after the removal of external landmarks (Hafting et al., 2005) suggesting that they are also driven by self-motion information. Unlike place cells (see below) grid cells were active in all environments (at least in all environments tested) and the relative offset of the nodes of different grid cells was invariant across environments (Fyhn et al., 2007). Their

coherent realignment suggest that grid cells form a topological map that serves as a universal coordinate system for navigation (McNaughton et al., 2006). The mechanism underlying the generation of the surprising regularity of grid cell's firing fields and their possible role in spatial navigation attracted many theoretical investigations (Guanella and Verschure, 2006; Fuhs and Touretzky, 2006; Hasselmo et al., 2007; Burgess et al., 2007; Rolls and Kesner, 2006; Solstad et al., 2006; Si and Treves, 2009; Huhn et al., 2009) (see Welinder et al. (2008) for a thorough discussion).

Interestingly, another cell type with location-dependent activity was described recently in the entorhinal cortex: neurons termed *border cells*, in the medial EC and adjacent parasubiculum were found to fire when the rat was close to a geometric border of the environment (Solstad et al., 2008; Lever et al., 2009). The existence of this pattern location dependent activity had already been predicted by computational models of Neil Burgess (Burgess and O'Keefe, 1996; Barry et al., 2006) where they suggested that hippocampal place cell activity is at least partially driven by the so called *boundary vector cells*.

Head direction cells. Another well characterized group of spatially selective cells recorded in the hippocampus is the class of *head direction cells* (HD cells, Wiener and Taube (2005)), found in the presubiculum (Taube et al., 1990) and in the entorhinal cortex (Sargolini et al., 2006). HD cells fire whenever the rat's head points in a specific direction relative to the environment irrespective of its location or whether it is moving or still. HD cells are anchored to distal sensory cues (Zugaro et al., 2001), but their firing remained stable in the absence of visual cues for short periods and the angular distance between any given pair remains constant (Taube et al., 1990). Based on the fact that HD cells, just as grid cells, fire consistently in all environments tested it has been suggested that these neurons provide directional and distance information, respectively, to the universal cognitive map (O'Keefe and Burgess, 2005; McNaughton et al., 2006; Huhn et al., 2009). Conjunctive representation of head direction and position in the MEA, where the firing of some grid cells is modulated by the animal's heading (Sargolini et al., 2006) supports this idea.

Place cells. The thirty-eight years old finding of O'Keefe and Dostrovsky (O'Keefe and Dostrovsky, 1971) that principal cells of the rodent hippocampus and the dentate gyrus (Jung and McNaughton, 1993) fire when the animal occupies a particular location within its environment, called its *place field*, attracted tremendous amount of research (for a comprehensive review see Redish (1999)). Probably because it was the

first demonstration that single neurons in the brain may signal an abstract variable, the location of the animal, rather than sensory events or motor commands.

It was clear since the first recordings that place cells are not controlled by single sensory stimuli (for example they tolerated radical changes in lighting) and their firing do not depend on the animal's motivation or incentive for visiting a location (O'Keefe and Dostrovsky, 1971; O'Keefe and Nadel, 1978). Rather they signal the animals location relative to an allocentric *reference frame* anchored to the configuration of available landmarks. Different groups of cells are active in different environments and, unlike in the case of grid cells and head direction cells, the relative position of place fields changes incoherently across environments. Manipulations like rotation of these landmarks (Muller and Kubie, 1987), parametric change in the shape of the recording box (O'Keefe and Burgess, 1996) or moving the start-box on a linear track (Gothard et al., 1996) all results in a shift in the reference frame accompanied by the coherent transformation of the place fields themselves. On the other hand, after larger changes in the environment the reference frame is replaced by a new one where place cells *remap*, i.e., the location of place fields and the maximal firing rate of place cells changes substantially compared to their activity under the original configuration (Lever et al., 2002; Leutgeb et al., 2005b). However, the fine details of this process are still not fully understood (see Tanila et al. (1997)), they differ according to the region being studied (Leutgeb et al., 2004) and probably depends on the details of the experimental procedure (Tsodyks, 2005) (compare Wills et al. (2005) and Leutgeb et al. (2005a)).

In open field environments place fields are omnidirectional (Muller et al., 1994) whereas on one dimensional environments like on a linear track (O'Keefe and Recce, 1993; Gothard et al., 1996) or a radial arm maze (Muller et al., 1994) they are highly directional. Whereas in the first situation each cell may be said to represent a location, in the second case they rather represent a serial position along a path. Whether omnidirectionality appears as soon as place fields develop or place fields start out with a directional bias and it is the result of further experience that they lose directionality is an open question (Káli and Dayan, 2000; Buzsáki, 2005). The complexity of the environment influence their directionality since placing various multimodal sensory cues along linear or circular tracks significantly increased the proportion of bidirectional place fields (Battaglia et al., 2004b).

In the absence of sensory input place cells can be controlled by self motion infor-

mation (Quirk et al., 1990; Sharp et al., 1995; Jeffery et al., 1997; Save et al., 2000) although the selectivity of spatial firing may be degraded in the dark (Markus et al., 1994). Once established, place cells can have the same firing pattern for months (Thompson and Best, 1990). The size of the place fields depends on the recording site: place fields are smaller (20 cm) in the dorsal hippocampus, while they become larger ($>$ 1 m) more ventrally (Jung et al., 1994; Maurer et al., 2005; Kjelstrup et al., 2008), parallel to the dorso-ventral increase in grid spacing (Hafting et al., 2005).

The firing of place cells provides information on the location of the animal in several ways: First, on a coarser scale, the firing of a given neuron signals that the animal entered its place field. Second, the firing rate of the place cell increases while the animal approaches the center of the place field and decreases after leaving it. In this way the neuron signals the distance of the animal from the center of the place field. Finally, the phase of firing relative to the ongoing theta oscillation changes monotonically with the distance traveled within the place field (O'Keefe and Recce, 1993; Skaggs et al., 1996), a phenomenon called *phase precession*. The dynamics of phase precession is characteristic for many classes of neurons in the hippocampal formation including dentate granule cells (Skaggs et al., 1996), pyramidal cells of the CA3 and CA1 regions (O'Keefe and Recce, 1993) and grid cells of the entorhinal cortex (Hafting et al., 2008). The detailed analysis of the astonishing dynamics of phase precession is beyond the scope of this introduction and can be found in the doctoral dissertation of Máté Lengyel (Lengyel, 2003).

While the location of the animal is the most consistent correlate of place cells' firing what else modulate their activity remained controversial and depends on the experimental design (O'Keefe, 1999; Eichenbaum et al., 1999). It was demonstrated that the firing of hippocampal units are modulated by the speed (McNaughton et al., 1983) and the direction of movement (McNaughton et al., 1983; Muller et al., 1994), by the path taken by the animal before arriving to the place field (Wood et al., 2000), by the location of the animal's goal (Ferbinteanu and Shapiro, 2003) etc. Some of the neurons fire only when the animal is engaged in a particular behavior e.g., eating, grooming or exploratory sniffling (O'Keefe, 1976). It was even suggested that the primary location dependent firing of place cells is caused by the experimental protocol where "the delivery of rewards and the onset, direction, speed, and punctuation of movements and other behaviors are all fully and intentionally randomized in time and space in an effort to *subtract out* their influence" (Eichenbaum et al., 1999). Record-

ing the hippocampal unit activity during a variety of specific non-spatial stimuli and behaviors in animals performing various tasks suggest, that individual hippocampal cells encode regularities present in the animal's every experience, including spatial and nonspatial cues and behavioral actions (Berger et al., 1983; Wiener et al., 1989; Wood et al., 1999). These studies indicate that nonspatial events are fundamental elements of hippocampal representation and support a more general function of the hippocampus in information processing associated with episodic memory.

Nevertheless, the rodent hippocampal formation has a remarkable ability to process and represent spatial information and mathematical models revealing the mechanism of these computations might help us to understand hippocampal function.

Despite a considerable effort, true place cells have not been observed in primates, although various types of sensory and response related activity is often gated by spatial variables (Rolls et al., 1989). For example, cells in the CA1 region of the monkey hippocampus, called *spatial view cells* respond more when the monkey is gazing toward one location in the room than toward other locations, even though most of the view details are obscured totally by curtains (Rolls et al., 1997). In humans, a substantial fraction of hippocampal neurons responded selectively to visual stimuli from different categories, including faces, natural scenes and houses, famous people and animals (Fried et al., 1997; Kreiman et al., 2000), to the sight of a particular word or face stimulus (Quiroga et al., 2005). Taken together, these data is consistent with the broad scope of spatial and nonspatial codings observed in rodents.

1.2.3 Synaptic plasticity

Beside the rich dynamics of neural activity characterizing the hippocampus, the connectivity between neurons is also subject to dynamic changes on various time scales. Short term depression and facilitation (Zucker and Regehr, 2002) characterize synaptic transmission at different pathways and have been implicated in many different hippocampal computations including regulation of excitatory/inhibitory balance of the mossy fiber pathway (Mori et al., 2004), the generation of the phase precession phenomenon (Leibold et al., 2008) and the formation of grid cells' firing fields (Kropff and Treves, 2008).

The pioneering work of Bliss and Lømo (1973) reporting that synaptic transmission

at the perforant path–granule cell synapses can be potentiated following a brief period of stimulation and this potentiation lasted for long time (hence its name: long term potentiation, LTP) was a paradigmatic step towards understanding the neural basis of memory (Bliss and Collingridge, 1993; Martin et al., 2000; Pastalkova et al., 2006). The induction of LTP required the nearly simultaneous activation of both pre- and postsynaptic site which were the necessary conditions for the synaptic basis of memory formation predicted on purely theoretical basis by Hebb (1949) .

Research during the four decades since its original description shed light on many details of the LTP phenomena, including the critical role of NMDA receptors in the induction of the LTP in many cases; the variety of signaling pathways that contribute to the induction, expression and maintenance of LTP; and its different variants observed in several neural structures including the neocortex, the cerebellum and the amygdala in several different preparations from *in vitro* to freely behaving animal. Other important advancements were the description of its counterparts, the long term depression (Lynch et al., 1977); the discovery of spike timing dependent plasticity (STDP) (Bi and Poo, 1998; Dan and Poo, 2006) that connects causality to neural networks or the description of homeostatic forms of synaptic plasticity (Turrigiano, 1999). The question, whether the postsynaptic signal required to its induction is global for the whole dendritic tree, as is the firing rate of the neuron, or it is the local to site of the stimulation has been raised already in the earliest experiments (McNaughton et al., 1978) and gained further attention recently (Magee and Johnston, 1997; Golding et al., 2002; Govindarajan et al., 2006; Harvey and Svoboda, 2007; Harvey et al., 2008).

1.3 Function

In 1957, Scoville and Millner reported that a patient, H.M., showed severe memory impairments after the surgical destruction of its hippocampus. Since their famous report one of the dominant theories about hippocampal function states that the primary function of hippocampus in humans is the formation of *episodic and declarative memory* (Eichenbaum, 2004). Indeed, patients with bilateral hippocampal lesions are unable to form new episodic memories and can not remember any events that occurred just before the surgery, but retain their memories for things that happened years earlier, such as in their childhood and they show intact procedural skills as well as general intelligence. The theory gained further support from additional lesion studies both in humans (Zola-Morgan et al., 1986; Vargha-Khadem et al., 1997) and in animals (Day et al., 2003) and from functional imaging experiments (Schacter and Wagner, 1999). The hippocampus has an essential role in the rapid encoding of information in relation to their spatio-temporal context (Morris and Frey, 1997) (but see Tse et al. (2007)), but it is still not clear whether after a certain period these memories are "consolidated", and stored elsewhere in the neocortex (Frankland and Bontempi, 2005) or they always remain hippocampus dependent (Nadel and Moscovitch, 1997). From a computational point of view, the single autoassociation network of the CA3 region is able to store arbitrary associations, the fragments of an episode, and the direct and indirect (through the DG) projections from the EC may be involved in the retrieval and the encoding of these memories, respectively (Treves and Rolls, 1992, 1994). This system enables the flexible, context dependent retrieval of the stored information based on noisy or partial cues. Another theories emphasize that the phase precession compresses sequences arriving at the behavioral time scale to the time scale of LTP (Skaggs et al., 1996), which enables the hippocampus to store sequences of events composing ongoing behavioral episodes (Jensen and Lisman, 1996; Eichenbaum et al., 1999; Lisman and Otmakhova, 2001; Jensen, 2005).

Another prominent theory on hippocampal function, largely based on place cell recordings in rodents, the *cognitive map* theory emphasizes its role in spatial cognition and navigation (O'Keefe and Nadel, 1978; Redish, 1999). According to this theory the processing and storage of spatial information is the primary and perhaps the exclusive role of the hippocampus, at least in the rat, it requires particular computations and the hippocampus has been evolved to fulfill this function (O'Keefe, 1999). Theories emphasizing spatial domains in hippocampal information processing gained further

support by the discovery of the phase precession phenomenon in many region of the hippocampal formation (O'Keefe and Recce, 1993; Skaggs et al., 1996; Hafting et al., 2008) and, more recently, by the description of the spatially periodic firing fields of entorhinal neurons (Hafting et al., 2005) (but see Lipton and Eichenbaum (2008)). Moreover, functional imaging experiments using virtual reality task demonstrated, that the hippocampus is involved in spatial navigation also in humans (Maguire et al., 1998; Burgess et al., 2002). The theory is criticized from several different directions: most of its support came from experiments on rodents, and it is hard to interpret the growing amount of data on nonhuman primates and human subjects under this spatial framework; and even the rodent experiments are sometimes inconsistent with a purely spatial function (Wood et al., 1999) and suggest a broader scope of hippocampal information processing. However, different interpretations of the same experimental data often coexist (compare O'Keefe (1999) and Eichenbaum et al. (1999)).

Part II

Fantasia and Fugue in C(A) minor

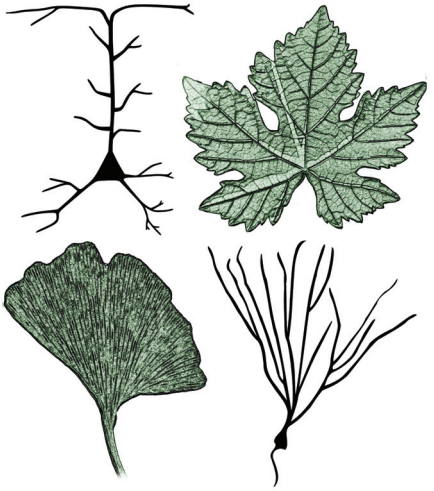

2

Time: The generation of the Septo-Hippocampal Theta Oscillation

2.1 The Role of the Medial Septal Nucleus in the Generation of Hippocampal Theta

The medial septum-diagonal band (MSDB) complex is believed to play a crucial role in the generation and maintenance of a typical hippocampal oscillatory activity the temporally nested theta (4-12 Hz) and gamma (40-60 Hz) rhythm (Petsche et al., 1962; Stewart and Fox, 1990; Vinogradova, 1995). The hippocampal theta oscillation, which is a large amplitude coherent oscillation, prominent during exploratory movements, REM sleep and anaesthesia (Vanderwolf, 1969; Vértes and Kocsis, 1997) is fundamental in several neural computations like memory formation (Hasselmo et al., 2002) and memory related tasks, such as navigation (O'Keefe and Nadel, 1978) in many different ways (see sections 1.2–1.3).

Originally, neurons in the MSDB were considered either cholinergic or GABAergic and these population differed both in their anatomical and electro-physiological properties (Brashear et al., 1986; Griffith, 1988; Kiss et al., 1990). GABAergic cells interconnected via axo-somatic synapses (Henderson et al., 2004) innervate different hippocampal interneurons (Freund and Antal, 1988) driving them by firing rhythmic bursts phase locked to the hippocampal theta rhythm (Green and Arduini, 1954; Bland et al., 1999; Brazhnik and Fox, 1997; Stewart and Fox, 1990). The *in vivo* activity pattern of cholinergic cells is more controversial: they fire either rhythmic bursts (Brazhnik and Fox, 1997, 1999) or single action potentials (Simon et al., 2006) and

they innervate both interneurons and pyramidal cells in the hippocampus (Frotscher and Leranth, 1985). Cholinergic activation, mediated by slow, muscarinic receptors (Cole and Nicoll, 1984), contributes to intrinsic, theta periodic oscillations both in the hippocampus (Konopacki et al., 1987; Fellous and Sejnowski, 2000) and medial septum (Goutagny et al., 2008) *in vitro*, and modulates the amplitude of theta (Lee et al., 1994; Monmaur et al., 1997; Yoder and Pang, 2005) *in vivo*. By analyzing the phase relationship between medial septal unit activity and hippocampal field theta oscillation a strong phase coupling was observed both in anaesthetized (Brazhnik and Fox, 1997) and in freely moving rats (King et al., 1998; Dragoi et al., 1999), but the preferred firing phase of different cell types remained controversial (King et al., 1998; Brazhnik and Fox, 1999). A recent study used combined immunocytochemical and electro-physiological methods to demonstrate that parvalbumin expressing (PV+), GABAergic cells show bimodal phase distribution during hippocampal theta activity (Borhegyi et al., 2004). *In vitro* studies on MSDB neurons showed that GABAergic cells express parvalbumin and exhibit fast-spiking activity (Morris et al., 1999; Sotty et al., 2003).

The first neuron type found to exhibit sustained rhythmic activity *in vitro* was a cluster-firing cell type described by Serafin et al. (1996). These neurons were considered as non-cholinergic, putative GABAergic neurons. Later, Sotty et al. (2003) using simultaneous electro-physiological and biochemical methods identified them as glutamatergic cells. The presence of a population of glutamatergic neurons in the MSDB has been recently confirmed by anatomical studies (Hajszan et al., 2004; Colom et al., 2005). These glutamatergic neurons form a network that is able to produce slow, synchronized bursting activity and innervate local GABAergic and cholinergic cells (Manseau et al., 2005). A recent *in vitro* study also showed that activation of glutamate receptors can synchronize MSDB neurons in theta frequency (Garner et al., 2005).

In the present chapter, we build a computational model in order to (*i*) determine the role of different cell types in the generation of synchronized bursting activity within the MSDB, (*ii*) demonstrate that burst-firing of medial septal GABAergic cells observed *in vivo* is an emergent network property and (*iii*) explain how the multimodal preferred firing phase distribution (Brazhnik and Fox, 1997; King et al., 1998; Borhegyi et al., 2004) of medial septal cells is generated. To achieve this we build a detailed computational model of the medial septal circuitry, with a conductance-based model

of GABAergic and glutamatergic neurons. Cholinergic neurons are assumed to play a slow, permissive role by modulating the excitability of the septo-hippocampal circuit and are not explicitly modeled here.

2.2 Methods

2.2.1 Neuron Models

Two types of neurons were simulated in the present study: a cluster-firing, glutamatergic cell and a fast-firing, GABAergic neuron. Details of the model equations can be found in the Appendix A.1.

Cluster-firing neuron. To model cluster-firing neurons in the MSDB we used the single compartment model described by Wang (2002) with unchanged parameters unless otherwise noted. This model contains spike generating currents (I_{Na}, I_{K}) and a slowly inactivating potassium current (I_{KS}). The membrane potential change is given by the following current balance equation:

$$C_{\mathrm{m}}\mathrm{d}V/\mathrm{d}t = -I_{\mathrm{Na}} - I_{\mathrm{K}} - I_{\mathrm{KS}} - I_{\mathrm{L}} - I_{\mathrm{syn}} + I_{\mathrm{ext}} \tag{2.1}$$

where $C_{\mathrm{m}} = 1\mu\mathrm{F/cm}^2$ is the membrane capacitance, I_{L} is the leakage and I_{syn} is the synaptic current. I_{ext}, the external current, is a constant depolarizing current representing background excitation mostly due to cholinergic innervation. The membrane noise term, originally introduced by Wang was omitted. For numerical integration of these equations the initial membrane potential of each cell was chosen randomly from a Gaussian distribution of mean $\mu(V_{\mathrm{init}}) = -64\,\mathrm{mV}$ and standard deviation $\sigma_{V_{\mathrm{init}}} = 30\,\mathrm{mV}$. The external current of this cell type was also taken from a Gaussian distribution ($\mu(I_{\mathrm{ext}}) = 0.02\,\mathrm{nA}$, $\sigma(I_{\mathrm{ext}}) = 0.002\,\mathrm{nA}$, mean and std, respectively). In control conditions an individual cell fires clusters of action potentials in the low theta frequency range (4-6 Hz) while the intracluster frequency is in the gamma range (40-50 Hz).

Fast-firing neuron. Medial septal fast-firing, non accommodating neurons were shown to express parvalbumin (Morris et al., 1999), a calcium binding protein, indicating that these neurons are GABAergic and project to the hippocampus (Freund, 1989).

To model these neurons we simplified the cluster-firing neuron model used in (Wang, 2002), described briefly in the previous section, by omitting the slow potassium channel, which is responsible for the cluster-firing behavior. The speed of the inactivation of I_{Na} and the activation of I_{K} were increased by changing the temperature factor ϕ from 5 to 10 so that the after-hyperpolarization following the action potential became smaller. The membrane potential change of the fast-firing cell is given by the following current balance equation:

$$C_{\text{m}}\text{d}V/\text{d}t = -I_{\text{Na}} - I_{\text{K}} - I_{\text{L}} - I_{\text{syn}} + I_{\text{ext}} \tag{2.2}$$

To introduce heterogeneity the initial membrane potential of each cell was chosen from a Gaussian distribution of mean $\mu(V_{\text{init}}) = -64\,\text{mV}$ and standard deviation $\sigma_{V_{\text{init}}} = 30\,\text{mV}$. The I_{ext} background current was an important parameter for synchronization of these neurons and were varied between $\mu(I_{\text{ext}}) = -0.008\,\text{nA}$ and $\mu(I_{\text{ext}}) = -0.026\,\text{nA}$. The response of the model to a tonic depolarizing current (Fig. 2.2B) is similar to physiological measurements from fast firing cells, except that the model lacks the depolarizing sag and spike frequency adaptation, which is present in most of the GABAergic cells in the MSDB (Sotty et al., 2003).

2.2.2 Synapse Models

Two types of synapses were simulated:

GABAergic synapse model. GABA-A IPSCs were described based on (Wang and Buzsáki, 1996) by the equation:

$$I_{\text{syn}} = \bar{g}_{\text{syn}} s (V - E_{\text{syn}}), \tag{2.3}$$

where $\bar{g}_{\text{syn}}$ is the maximal synaptic conductance, and the activation variable s was governed by the following first order kinetics:

$$\frac{\text{d}s}{\text{d}t} = \alpha F(V_{\text{pre}})\,(1 - s) - \beta s, \tag{2.4}$$

where the transmitter release probability ($F(V_{\text{pre}})$) was a function of the membrane potential of the presynaptic neuron:

$$F(V_{\text{pre}}) = \frac{1}{1 + \exp\left(-\frac{V_{\text{pre}} - \Theta_{\text{syn}}}{K}\right)} \tag{2.5}$$

Parameters characterizing synaptic contacts between different pre- and postsynaptic neurons were as follows: $\alpha = 14$ ms^{-1}, $\beta = 0.07$ ms^{-1}, $K = 2$ mV, $\Theta_{\text{syn}} = 0$ mV, $E_{\text{syn}} = -75$ mV. The synaptic conductance was set to $g_{\text{syn}} = 0.189$ nS.

Glutamatergic synapse model. Glutamatergic transmission was mediated by AMPA receptors described in Destexhe (2000). Briefly

$$I_{\text{AMPA}} = \bar{g}_{\text{AMPA}} s (V - E_{\text{AMPA}}) \tag{2.6}$$

$$\frac{\mathrm{d}s}{\mathrm{d}t} = \alpha T(V_{\text{pre}})(1 - s) - \beta s \tag{2.7}$$

Here, $\alpha = 1.1$ mM^{-1}ms^{-1}, $\beta = 0.19$ ms^{-1}, $E_{\text{AMPA}} = 0$ mV, $g_{\text{AMPA}} = 0.1$ nS on glutamatergic and $g_{\text{AMPA}} = 0.15$ nS on GABAergic cells. The transmitter release probability ($T(V_{\text{pre}})$) was a function of the presynaptic membrane potential,

$$T(V_{\text{pre}}) = \frac{1}{1 + \exp\left(-\frac{V_{\text{pre}} - \Theta_{\text{syn}}}{K}\right)}, \tag{2.8}$$

where $\Theta_{\text{syn}} = 2$ mV, and $K = 5$ mV.

2.2.3 Modeling the Effect of Zolpidem

Zolpidem is known to bind to the benzodiazepine binding site of the GABA-A receptors. Modeling the effects of this drug was based on the following observations. First, benzodiazepines, such as zolpidem are known to increase the affinity of the GABA-A receptor to its endogenous agonist GABA (Mohler et al., 2002), increasing the frequency of opening of the associated chloride ion channel in the presence of the GABA. This causes an increase in the decay time constant and also the amplitude of the IPSCs when the receptor occupancy is incomplete (Eghbali et al., 1997). In the case of hippocampal interneurons (and pyramidal cells) 10 μM zolpidem increased the conductance of IPSCs to 140% (135%) and the decay time constant to 184% (173%) of the control value (Hájos et al., 2000), which is more than a two fold increase in the net synaptic current. Second, zolpidem is a preferential α_1 GABA-A receptor positive allosteric modulator. Third, α_1 GABA-A receptors are expressed by septal GABAergic cells (Gao et al., 1995), hippocampal pyramidal cells and in several hippocampal interneurons including hippocampal horizontal cells (Gao and Fritschy, 1994) projecting to the MSDB. Thus, in our phenomenological model application of zolpidem was hypothesized to either increase the maximal synaptic conductance or decreasing

the rate of channel closing (parameter β in equation 2.4) of every GABA-A synapses. These different manipulations led to qualitatively similar results[1]

2.2.4 Softwares and Mathematical Analysis

Simulations were performed using the GENESIS (version 2.2) software package (Bower and Beeman, 1998) under the Linux operating system. Mathematical analysis of the results were performed using the GNU octave (version 2.1.69).

To quantify the synchronization of the neuronal firing in the network, we introduced a *coherence index* based on the correlation between the activity of cell pairs from the same network. The activity of each cell was defined by dividing the simulation time T into small bins of τ width and the value of a given bin was 1 if the cell fired during that interval or 0 if not. Thus, the coherence index of a network is calculated as the mean correlation between the activity of all cell pairs from the network. We calculated gamma coherence with $\tau = 5\,\text{ms}$ and theta coherence with $\tau = 50\,\text{ms}$.

To define the *firing phase* of a cell a periodic reference signal was required. Since the hippocampal regions are not included in the simulations we can not relate the firing phase of the individual cells to a hippocampal signal like in experimental studies. Instead, we quantified the relative preferred firing phases of neurons via an arbitrarily chosen reference signal and compared these relative values with experimental findings. The reference signal used in our calculations was the mean firing rate versus time function of one of the glutamatergic population (see Fig 2.1B). 0° was chosen to be the trough, 180° the peak of this sinusoid-like signal. Mean firing rate of the neuron populations was calculated as the mean of its cells' approximate firing rate. The approximate firing rates were calculated by convolving the series of firings by a Gaussian of 1 ms standard deviation according to Dayan and Abbot (2001). The phase (Φ) of each spike was calculated relative to this signal, i.e. the minimum and the maximum between which the spike occurred were identified and the phase of the spike was calculated by

$$\Phi = \begin{cases} 180^\circ \dfrac{t}{t_{\max} - t_{\min}} & \text{if} \quad t_{\max} > t_{\min}, \\ 180^\circ \dfrac{t}{t_{\max} - t_{\min}} + 180^\circ & \text{if} \quad t_{\max} < t_{\min}. \end{cases} \tag{2.9}$$

[1] For a more detailed analysis of the interactions of GABA, benzodiazepines and the GABA-A receptor see Baker et al. (2002); Érdi et al. (2006).

where t is the time when the spike was emitted, $t_{\min}$ and $t_{\max}$ are the time of the minimum and the maximum, respectively, of the mean firing rate of the glutamatergic population. This phase was regarded as a vector of unit length and of angle Φ. The sum of these vectors calculated for all spikes of a cell divided by the number of spikes fired was considered as the *preferred firing phase* of a given neuron. Mean phases of the populations were calculated by taking the circular average of the phase vectors of cells belonging to a given population.

2.3 Results

Our hypothesis was that the structure of local synaptic connections between glutamatergic and GABAergic cells in the MSDB is responsible for their synchronization and for the generation of the preferred firing phase.

In our original paper (Ujfalussy and Kiss, 2006) we gave two different models for theta and gamma synchronization in the medial septum. However, in the present dissertation we describe in detail only the *feed-forward model*, as since the publication of the models, this one is supported by a larger number of experimental data. We compare the assumptions and predictions of different models of septo-hippocampal theta generation in the discussion, section 2.4.

2.3.1 Glutamatergic Neurons Act as Pacemakers for Septal Theta rhythm

Glutamatergic cells are described by the cluster-firing cell model and are interconnected into a network by fast (AMPA-type) glutamatergic synapses (see Methods). We systematically varied the structure of the network and demonstrated that cluster-firing neurons display robust in-phase synchronization if connected via glutamatergic synapses even in the presence of significant heterogeneity in the population. Due to excitatory interactions the emerging population rhythm is slightly faster than the theta periodic clusters of disconnected neurons. Simulations show that spikes and clusters of spikes of coupled glutamatergic neurons are synchronized to each other (Fig. 2.1A) and theta or gamma coherence is high and does not depend on the structure of connectivity within the network (data not shown). Glutamatergic cells show in-phase synchronization since these neurons fire their spikes and clusters simultaneously in

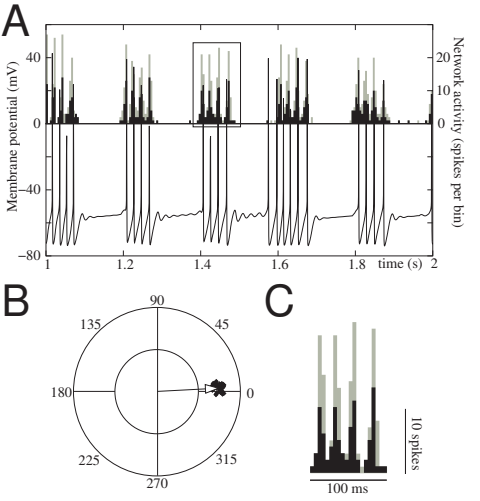

Figure 2.1: **Robust synchronization in the glutamatergic network.** A, Population activity of the network with random connectivity (gray and black bars indicate the activity of two arbitrary subpopulations; grey bars are drawn on top of black bars) and the membrane potential of a representative neuron. Action potentials and clusters are synchronized in the whole population. B, The polar plot shows that the preferred firing phase of the cells are similar. C, Discrete peaks of population activity enlarged from *A* show that the spikes of the cells are synchronized within the clusters.

the whole network (Fig. 2.1A,C) and the mean phase of all cells' firing are similar (Fig. 2.1B). This robust in phase synchronization allows the glutamatergic network to be a local theta periodic pacemaker for a network of fast-firing GABAergic neurons in the medial septum.

2.3.2 Glutamatergic Neurons Transmit the Theta Rhythm to Local GABAergic Network

In the *feed-forward model* we modeled two subpopulations (SPs) of fast-firing GABAergic neurons (Fig. 2.2A-B). All fast-firing neurons are interconnected via fast GABAergic (GABA-A) synapses, but only neurons in one of the two SPs are innervated by lo-

cal glutamatergic cells with connection probability $p_{\mathrm{UA}} = 0.5$. This subpopulation is therefore called Excitatory Driven SubPopulation (*ESP*, Fig. 2.2A,). The other SP, that lacks glutamatergic innervation but receives GABAergic input from the ESP is called Inhibitory Driven SubPopulation (*ISP*, Fig. 2.2A). Neurons in this latter subpopulation (ISP) need stronger background constant excitatory current (I_{ext},, representing cholinergic activation) to maintain similar firing rate as the cells in the other subpopulation (ESP) driven by rhythmic glutamatergic EPSPs. The connectivity between glutamatergic and GABAergic cells in the feed-forward model was motivated by the works of Brazhnik and Fox (1997). They found, that a part of medial septal neurons fire bursts of action potentials on the peak of rhythmic EPSPs, while other neurons are active when released from theta-periodic inhibition. Moreover, intact cholinergic transmission was found to be critical for burst-firing of the inhibitory driven cells as their theta related firing was blocked by the local application of scopolamine (Brazhnik and Fox, 1997).

When fast-firing GABAergic neurons are innervated by the glutamatergic network GABAergic cells from the two SPs fire alternating clusters of action potentials (Fig. 2.2C, D). On one hand, the action potential generation of cells in the ESP is the result of the interplay between their intrinsic dynamics and their excitatory innervation. Since the intracluster-frequency of glutamatergic EPSPs interfere with their intrinsic oscillatory dynamics, the activity of these neurons is highly irregular (Fig. 2.2C). On the other hand, the ISP lacks phasic synaptic input during its active state (it is inhibited while the ESP is active and starts firing when released from inhibition) so the firing pattern of these neurons is more regular and governed solely by its intrinsic membrane dynamics (Fig. 2.2D). Both gamma and theta coherence of the GABAergic SPs are high in the feed-forward model (data not shown).

The three different neuronal population (one glutamatergic and two GABAergic) have different preferred firing phase relative to the reference oscillatory signal. As hippocampal dynamics was not modeled here, we used the population activity of glutamatergic neurons as a reference signal. Therefore the preferred firing phase of the glutamatergic population was, by definition, zero. The GABAergic subpopulation driven by excitatory synapses (ESP) neurons followed the glutamatergic cells with a small (25 ms, 45$^{\mathrm{o}}$) delay (Fig. 2.3A). The ISP start firing when released from the inhibition, therefore they are approximately anti-phasic with the ESP (Fig. 2.3A). However, the delay between the preferred firing phase of the two GABAergic subpopulation is

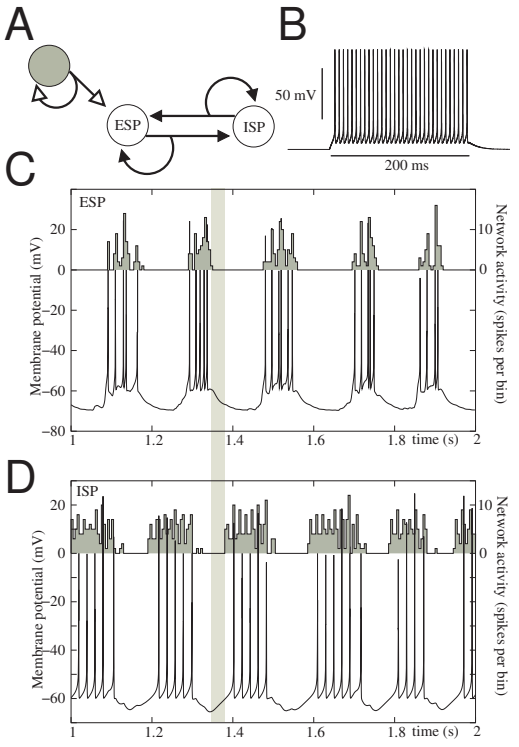

Figure 2.2: **Interactions between septal glutamatergic and GABAergic neurons – the feed-forward model.** A, Randomly interconnected network of glutamatergic neurons innervate one of the subpopulations, the ESP, of fast-firing GABAergic cells. The GABAergic neurons from a random network (shaded circle: cluster-firing, glutamatergic neuron, open circle: fast-firing, GABAergic neuron, open arrow: glutamatergic connection, filled arrow: GABAergic connection). B, Response of a fast-firing neuron to an external current pulse (dI=0.025 nA). C-D, Activity of the two GABAergic subpopulations and the membrane potential of a representative neuron from the subpopulations (C, ESP and D, ISP). The neurons in the two subpopulations fire intermittent clusters. The shaded box shows the delayed onset of firing in the ISP after released from inhibition. Parameters: $I_{\text{ext,ESP}} = -0.0225\,\text{nA}$, $I_{\text{ext,ISP}} = -0.012\,\text{nA}$

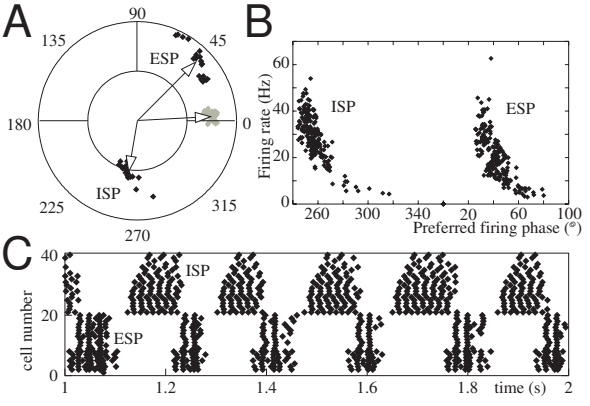

Figure 2.3: **Phase relationships in the feed-forward model.** A, Polar plot shows the phase relationship between glutamatergic (gray dots) and GABAergic (black dots) cells. Cells from the ESP have a slight phase delay ($\sim 45°$) relative to the glutamatergic cells. Cells from ISP have a phase delay more than $\sim 180°$ relative to cells from ESP due to their delayed activation (see Fig. 2.2C, D). B, Correlation between the firing rate and the preferred firing phase was significantly negative (for the ESP: -0.53; for ISP: -0.75). C, Neurons on the raster plot are ordered according to their preferred firing phase. Cells with smaller number (earlier phase) usually have higher firing rate within the SP.

larger than 180° (Borhegyi et al., 2004) since cells in the ISP need some time to reach the firing threshold (see shaded box on Fig. 2.2C-D).

While local glutamatergic neurons innervated only a part of the septal GABAergic network, the synaptic connectivity among septal GABAergic neurons was random. Increasing the strength of GABAergic synaptic connections in the network did not change the theta rhythmic activity of the cells. However it decreased the firing rate of GABAergic neurons through feed-back inhibition (Fig. 2.4A-B). This prediction of the *feed-forward model* is in sharp contrast with the predictions of other models of septo-hippocampal theta generation (Wang, 2002; Ujfalussy, 2005). In these models, namely in the *ping-pong model* (Ujfalussy and Kiss, 2006; Ujfalussy, 2005) and in X.-J. Wang's model Wang (2002), GABAergic synaptic coupling regulates the frequency of the emerging slow oscillation but not the firing rate of individual cells (Fig. 2.4C-D). In the following section our collaborators used juxtacellular record-

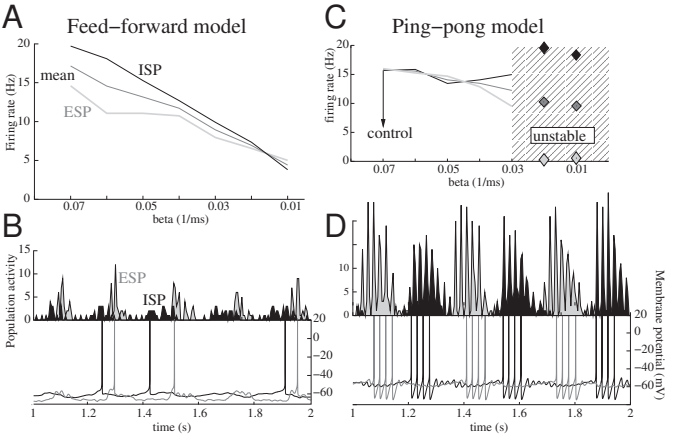

Figure 2.4: **The effect of GABAergic synaptic modulation on the network activity in different models.** A-B, Feed-forward model. A, The firing rate of GABAergic cells in both subpopulations decreases with the strength of the GABA-A synapse (beta is defined by equation 2.4). B, The activity of the two subpopulations and the membrane potential of two representative neurons with increased GABAergic conductance. Compare with the population activity and the membrane potential of the cells on Fig. 2.2C-D. C-D: Ping-pong model, which is described in detail in Ujfalussy and Kiss (2006). C, The firing rate of GABAergic cells decreases only moderately with stronger GABAergic synapses and the network becomes unstable above a critical value. D, The activity of the two subpopulation and the membrane potential of two representative neurons with increased GABAergic conductance.

ing from anaesthetized rats before and after the application of a GABA modulator zolpidem to test the response of the septal network to the modulation of the synaptic connections.

2.3.3 Experimental Test of the Model

Our collaborator, Mihály Hajós (Pfizer Global Research and Development, Pfizer Inc., Groton, CT, USA) recorded extracellularly from single neurons in the medial septum and the local field potential in the pyramidal layer of the hippocampal CA1 region

from anaesthetized rats ($n = 6$)[2]. Single units in the medial septum fired rhythmic bursts and their firing rate was high (25 ± 10 Hz). The septal unit activity was phase coupled to the ongoing hippocampal theta oscillation (Fig. 2.5A). Systemic administration of zolpidem (0.1-1 mg/kg, IV, n = 6), a preferential positive allosteric modulator of GABA-A receptors containing α_1 subunit, instantaneously attenuated or abolished theta oscillation of the septo-hippocampal system. In the hippocampus zolpidem significantly reduced EEG power at the theta frequency range (Fig. 2.5B). Parallel to changes in hippocampal activity zolpidem significantly inhibited the firing activity of MSDB neurons by reducing the firing rate to approximately 10% of baseline activity ($p < 0.01$, Fig. 2.5C). In addition, the periodicity of MSDB neurons was significantly reduced by zolpidem (32% of baseline, $p < 0.01$), as revealed by their autocorrelation (Fig. 2.5D). Subsequent administration of flumazenil (Ro 15-1788, 1 mg/kg, IV) a non-selective antagonist at the benzodiazepine binding site of GABA-A receptors, reversed, at least partially, zolpidem-induced inhibition of theta activity of both MSDB neurons and hippocampal EEG (data not shown). The pronounced decrease in the firing activity of medial septal neurons found in this experiment is more consistent with the *feed-forward* model (compare Fig. 2.4B with Fig. 2.5B) than with alternative models of medial septal theta generation (compare Fig. 2.4D or Figure 7. of Wang (2002) with Fig. 2.5B).

2.4 Discussion

In this section we will discuss the predictions of the *feed-forward model* and compare them with experimental data as well as with the predictions of other models of the septo-hippocampal circuitry. Table 2.1 showing the similarities and the differences between the these models serves as an ordered summary for the following paragraphs.

[2]The detailed description of the methods of the experiments as well as the discussion of the results can be found in the cited paper Ujfalussy et al. (2007). Since I was involved in computational modelling and data analysis, I do not include the technical details of the experiments in this theoretical dissertation.

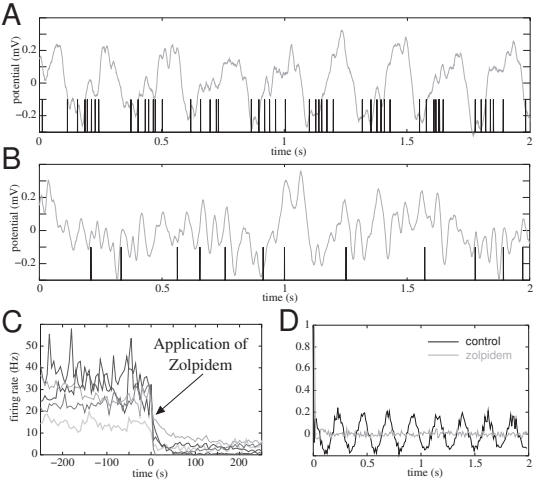

Figure 2.5: **The effect of zolpidem on septo-hippocampal activity.** A, Hippocampal local field potential and simultaneous septal single unit activity in control condition. B, Representative example of hippocampal LFP and septal unit activity after the application of zolpidem. C, The change in the firing rate of five different septal unit after the application of zolpidem. D, Autocorrelation of unit activity reveals that septal neurons loose their rhythmicity after the application of zolpidem. This Figure is based on the experiments conducted by Mihály Hajós.

PHENOMENON	WANG MODEL	PING-PONG MODEL	FEED-FORWARD MODEL
Theta synchronization in medial septal slice is	not possible	possible	possible
GABAergic neurons are *in vitro*	cluster-firing cells	cluster-firing cells	fast-firing cells
Theta periodicity in GABAergic cells is caused by	a slow potassium current	a slow potassium current	synaptic input
Pahase distribution of GABAergic cells	unimodal	bimodal	bimodal
Cells are synchronized through	GABAergic	GABAergic	glutamatergic and GABAergic synapses
Correlation between firing rate and preferred firing phase	?	no correlation	cells with lower firing rate fire later
Locale application of glutamate antagonist	has no effect	has no effect	disrupt hippocampal and septal theta oscillation
Application of GABA modulator	change the frequency of the oscillation	change the frequency of the oscillation	change the firing rate of the cells

Table 2.1: The similarities and the differences between different computational models of septal theta generation (Wang, 2002; Ujfalussy and Kiss, 2006).

2.4.1 Electrophysiology of the Medial Septum

Experimental evidence support that periodic firing of MSDB neurons *in vivo* remain after chronic isolation from the brainstem or from the hippocampus (Vinogradova et al., 1980; Vinogradova, 1995). Moreover, theta burst of different medial septal neurons remain coherent even in the absence of hippocampal theta (Stewart and Fox, 1989). These results suggest that neurons in the MSDB can act as autonomous pacemaker. Indeed, coherent extracellular oscillation at theta frequency in the MSDB slice preparation was observed in the presence of kainate, a glutamate receptor agonist (Garner et al., 2005). However, in this study putative GABAergic and cholinergic neurons fired single action potentials in each theta cycle rather than clusters. In another study Manseau et al. (2005) observed synchronized glutamatergic bursts under epileptogen conditions *in vitro* in various cell types in the MSDB. Although the frequency was much slower and the duration of these bursts was much longer than under *in vivo* conditions, it is remarkable that in both studies the synchronized activity in the MSDB is linked to the activation of glutamatergic receptors as in our feed-forward model. These experimental results served as rationale on which we based the hypothesis that intraseptal mechanisms alone might serve as generators of the theta pacemaker activity and proposed models that are in accordance with the above observations. Indeed, a recent study using *in vitro* rat septohippocampal preparation demonstrated, that upon optimal excitation, the MSDB alone is able to generate hippocampal oscillations in the theta frequency band (Goutagny et al., 2008).

Contrary to *in vitro* preparations where GABAergic cells exhibit fast-firing activity (Griffith and Matthews, 1986; Morris et al., 1999; Knapp et al., 2000) these cells were found to display theta periodic burst-firing activity only *in vivo* (King et al., 1998; Brazhnik and Fox, 1999; Borhegyi et al., 2004; Simon et al., 2006). Moreover, further studies (Griffith, 1988; Griffith et al., 1991; Henderson et al., 2001; Sotty et al., 2003) underpin the notion that under *in vitro* conditions medial septal cells do not exhibit sustained cluster- or burst-firing activity in the theta frequency range. Following this line of thoughts, we might conclude that there exist some conditions favoring burst-firing *in vivo*, which have not been reproduced *in vitro* yet. In the presented computer simulations we conclude that even if GABAergic cells are not cluster-firing cells they can exhibit clustering properties due to their periodic input, which could explain the apparent duality of GABAergic cell firing properties *in vivo* and *in vitro*.

Arrangement of spikes in theta periodic clusters can rely both on intrinsic or extrinsic mechanisms. A specific ion channel might serve as the basis of a mechanism of intrinsic theta modulation of activity as in our modeled cluster-firing cell. Like the regulation of the H-current is mediated by metabotropic receptors via the intracellular concentration of the cyclic AMP (Wainger et al., 2001), the regulation of an ion channel responsible for cluster-firing behavior may require specific extracellular environment (e.g. neuromodulators from the brainstem) that is not present *in vitro*. Interaction between neurons through synapses can also results in a rhythmic firing pattern as in our feed-forward model. In this case modulation by the fast synaptic dynamics causes a substantial change in the firing pattern of the neurons (see further discussion in Sec. 2.4.3, 2.4.4).

Correlation between the firing rate and the preferred firing phase characterize neurons within the same SP in our feed-forward model, whereas no such correlation was found in other models. This correlation has not been studied yet experimentally.

2.4.2 Network Structure and Preferred Firing Phase

Brazhnik and Fox (1997) found that theta periodic membrane oscillation of brief-spike cells is mediated by glutamatergic EPSPs, while rhythmic firing of long-spike cells are driven by GABAergic IPSPs. Based on spike-waveform statistics they suggested that one of these two subpopulations is GABAergic, the other is cholinergic. However, recent recordings from immuncytochemically labelled neurons revealed that cholinergic neurons fire single spikes at very low rate during theta (Simon et al., 2006) instead of bursts of action potentials. This suggest, that both brief spike cells and long spike cells in the study of Brazhnik and Fox (1997) were GABAergic, and probably correspond to our excitatory driven and inhibitory driven subpopulations, respectively, in our feed-forward model. Moreover, Brazhnik and Fox (1997) found that the two subpopulations fired in the opposite phase of the dentate theta. Indeed, in a recent experiment by Borhegyi et al. (2004) GABAergic neurons, identified based on their parvalbumin immunoreactivity, formed two distinct populations according to their preferred firing phases relative to the hippocampal theta oscillation.

Why experimental recordings failed to observe the three different neuron population locked to different phases of hippocampal theta? First, the phase of the hippocampal theta depends on the exact location of the recording electrode: there is a 180^{o}

phase shift between *stratum pyramidale* and *stratum lacunosum-moleculare* (Buzsáki, 2002). This limits the comparison of recordings from different animals. Second, hippocampal theta oscillation is not an ideal sinusoid signal, but it is a complex oscillatory signal with many different frequencies. Both the amplitude and the dominant frequency in the theta band changes continuously. The phase of a spike therefore depends on the method used to decompose the recorded signal. More exactly, a certain amount of error always remain in the phase estimation which limits the precision of the preferred firing phase of a single neuron even within the same recording session. Third, according to our feed-forward model, different septal neuron populations fire at different, but overlapping time windows during hippocampal theta cycles. Moreover, in the model the preferred firing phase of a neuron depends not only on which population it belongs to, but also on its synaptic input and the level of background excitation. Specifically, GABAergic neurons with higher firing rate tend to fire earlier in the theta cycle in the model (Fig. 2.3B-C). These differences within populations may mask differences between populations.

2.4.3 Pharmacological Modulation of the Septal Theta Rhythm

Pharmacological modification of synapses among medial septal neurons may be a convenient tool to reveal the network connectivity. Synaptic connections play a fundamental role in signal propagation and information processing in neural networks and the modification of these connections likely results in the alternation of its activity characterized by changes in the firing rate of a given neuron or synchrony between pairs of neurons. Physiological evidences suggest that rhythmic burst-firing of different neurons in the medial septum rely on phasic activation through cholinergic, GABAergic and glutamatergic synaptic connections (Stumpf et al., 1962; Stewart and Fox, 1989; Brazhnik and Fox, 1997).

Brazhnik and Fox (1999) showed that intraseptal blockade of GABAergic transmission eliminated rhythmicity of long spike cells, whereas rhythmicity of brief-spike neurons remained unchanged. As we have already discussed above, brief spike cells correspond to the ESP in our model, while long spike cells form an ISP, and therefore these findings are in a good agreement with our model. They (Brazhnik and Fox, 1999) also found that local injection of scopolamine (a cholinergic antagonist) abolishes the burst-firing activity of long-spike cells but not that of brief spike cells

in anaesthetized rats. In our model neurons in the ISP required an extra amount of constant excitation to fire at high rate when released from inhibition. We suggested that this background excitation is mediated via slow muscarinic acetylcholine receptors. The cholinergic blockade therefore also disrupts theta bursting in the ISP in the feed-forward model.

Zolpidem is a specific modulator of GABA-A channels containing α_1 subunit. Most subcortical nuclei, including monoaminerg or cholinerg ones (Rodriguez-Pallares et al., 2001) express GABA-A receptors containing the $\alpha_{2/3}$ subunit just as medial septal cholinergic cells (Gao et al., 1995). In the medial septum only GABAergic but not cholinergic neurons (Gao et al., 1995) express GABA-A receptors containing α_1 subunits (Gao and Fritschy, 1994; Nusser et al., 1996). Our computational model demonstrated that the decrease in the firing rate of septal neurons can be explained by the effect of zolpidem on the intra-septal GABAergic network. With a decreased activity the medial septum was unable to pace hippocampal theta in anaesthetized animals, and an aperiodic signal from the hippocampus could contribute to the decrease in the periodicity of medial septal neurons (Ujfalussy et al., 2007). Indeed, the elimination of the hippocampal theta rhythm was sufficient to decrease the periodicity of septal neurons in several cases (Brazhnik and Fox, 1997, 1999; Borhegyi et al., 2004; Ujfalussy et al., 2007).

For example, L-838417, an $\alpha_{2/3}$ selective modulator of GABA-A receptors, potentially acting through septal cholinergic system (Gao et al., 1995) eliminate hippocampal theta oscillation (Ujfalussy et al., 2007) since hippocampal theta, under anaesthesia, depends critically on the integrity of cholinergic transmission (Vanderwolf, 1988). After the application of the drug the periodicity of septal units were also decreased, but their firing rate remained unaltered (Ujfalussy et al., 2007). Hippocampal interneurons projecting to the medial septum receive excitation from local pyramidal cells (Blasco-Ibanez and Freund, 1995; Jinno et al., 2007; Takacs et al., 2008). These interneurons provide an effective feed-back to septal GABAergic neurons (Tóth et al., 1993) and regulate the state of the septal rhythm generating circuit (Manseau et al., 2008; Hangya, 2009). It has been suggested that decreased periodicity of medial septal neurons during hippocampal non-theta states is caused by the non theta-periodic firing of these hippocampo-septal neurons (Ujfalussy et al., 2007).

2.4.4 Glutamatergic Neurons

The robust in phase synchronization of glutamatergic cells in our model raise the possibility that this circuit can serve as theta periodic pacemaker for septal and also for hippocampal neurons. Blocking AMPA receptors in the medial septum does not abolish hippocampal theta in the behaving rat (Leung and Shen, 2004) but under urethane anaesthesia local infusion of AMPA receptor antagonists to the MSDB disrupt hippocampal theta oscillation triggered by intraseptal cholinergic activation (Puma and Bizot, 1999). These studies suggest that glutamatergic neurons are critically involved in the generation of the atropine sensitive theta in the hippocampus.

Manseau et al. (2005) observed large glutamatergic bursts in various cell types including putative glutamatergic neurons. These neurons fired clusters of action potentials in response to constant depolarization but in the presence of 4-AP (a potassium channel blocker) and bicuculline (a GABA-A antagonist) they fired prolonged bursts on the top of a large excitatory wave. The frequency of the bursts were much slower than the frequency of the theta oscillation. Their study demonstrates that glutamatergic neurons are able to pace synchronized rhythmic activity in the MSDB. On the other hand, these experiments did not explain how large excitatory bursts could emerge in a network of cluster-firing neurons.

The effect of local application of glutamate receptor antagonists to the firing pattern of MSDB neurons have not been studied. Our feed-forward model predicts that the local application of an AMPA receptor antagonist would result in desynchronization of glutamatergic cells and would disrupt cluster-firing activity of GABAergic neurons. However, if hippocampal theta remains after the drug injection a feed-back from the hippocampus may also be able to maintain synchronized burst-firing activity in a part of the network.

* * *

In the present chapter we built a computational model that describes several aspects of the generation of the theta oscillation within the septo-hippocampal system. The theta oscillation is the dominant EEG pattern in wide range of behaviors and seems strongly coupled to information processing within the hippocampus. In the next two chapters we study how neural circuits of the hippocampus support its role in information processing.

3

Space I: Robust path integration in the entorhinal grid cell system with hippocampal feed-back

3.1 Introduction

During the course of their evolution animals have developed several types of sensory organs. Information collected by these can be used by the animal to execute several tasks required for its survival. One such task is navigation for which animals at different levels of development use different types of sensory inputs. In rodents these types include auditory, tactile, visual (allothetic) and self-motion (idiothetic) information (Maaswinkel and Whishaw, 1999). Integration of these modalities into a unified representation of the environment might serve as the basis for navigation in animals at a high level of phylogenetic development. Electrical recordings from single cells in the rat hippocampus showing highly spatially correlated cell activity (O'Keefe and Dostrovsky, 1971), indicated that this structure might be the site of integrated spatial representation in the rat brain (O'Keefe and Nadel, 1978). Indeed, the integration of different modalities in the hippocampus is supported by both the anatomy of this structure (Amaral and Witter, 1989; Amaral and Lavenex, 2007) and the influence of the different types of modalities on the place representation by the hippocampal cells (Wiener et al., 1995; Jeffery, 2007). For example, on one hand, changing the visual appearance of the testing environment by modifying its shape (Muller and Kubie, 1987; Leutgeb et al., 2007) or rotating the landmarks supposedly used for self-localization (Jeffery and O'Keefe, 1999) would alter the firing pattern of place cells in a way systematically corresponding to changes in the environment. On the other hand, self-motion information has an effect on place cell firing both in the angular (Jeffery and

O'Keefe, 1999) and in the linear (Gothard et al., 1996) domain. Most intriguingly, rats are able to switch back-and-forth between vision and path integration depending on their reliability in case they are in conflict (Jeffery, 1998).

Path integration is performed using self-motion information (Etienne and Jeffery, 2004), which originates from the visual-flow, the vestibular system, proprioceptive motor copies, etc. Theoretical considerations (McNaughton et al., 2006) suggest that path integration in rats, using this multimodal information, is performed in the attractor network of the recently discovered entorhinal grid cell system (Hafting et al., 2005), which functions as a preprocessing stage in the generation of the hippocampal place code. These cells found in all layers of the medial entorhinal cortex (EC) were shown to fire on a regular hexagonal lattice, tessellating the space (Hafting et al., 2005; Sargolini et al., 2006).

Path integration alone, however, can not be used by animals or robots for proper navigation as errors in the measurement of speed and direction increasingly accumulate, and after the animal proceeds a certain distance this error would invalidate self localization. Fortunately, combining allothetic and idiothetic information offers a way to ameliorate path integration and get rid of the harmful noise. There is evidence showing that in humans, when the visual and the self-motion information are in conflict either the visual system resets the self-motion system based on a remembered location of landmarks or the two information are integrated (Nardini et al., 2008). Specifically, adults when facing conflicting cues use a weighted average of cues in determining their location, while young children alternated between the use of either information source without combining them. In rats, however, when vision and self-motion are in conflict place cells generally prefer to follow the visual stimulus (Knierim et al., 1995; Jeffery, 1998; Maaswinkel and Whishaw, 1999). Moreover, depending on the precision needed to achieve a goal, animals might swap the different navigation strategies. For example, during homing, hamsters first follow a relatively straight line indicating the use of path integration (Séguinot et al., 1993), however, when they get close to their nest, they switch to follow a circular trajectory in a search for familiar (visual) cues (for a review see Etienne et al. (1996); Etienne and Jeffery (2004)).

The exact mechanism of how grid cells and place cells interact with each other to form a robust representation of the environment is still to be elucidated. Building on experimental observations several components of the underlying neural structures have been studied by theoretical tools. The first models explaining the generation

of hippocampal place cell activity from visual inputs used the distance from and the bearing to identified landmarks as input to the hippocampus (Zipser, 1985; Sharp, 1991; Burgess et al., 1994; Touretzky and Redish, 1996; Barry and Burgess, 2007). Hippocampal place cells were activated when the currently perceived scene matched the stored landmark configuration. However, these models require exact object recognition, and representation of distances and angles between objects in the EC. If such a representation is present, place cell activity, i.e. a partitioning of the environment into place fields, emerges from the combination of a Hebbian-like learning between the EC and hippocampal cells and competition among hippocampal place cells (Sharp, 1991). Later it was shown (Ujfalussy et al., 2008) that similar Hebbian mechanism is able to produce place cell like activity even if the representation of the sensory input is less elaborated.

An other theory proposed by Burgess and O'Keefe (1996) suggests that hippocampal place cell activity is based on the firing of so called boundary vector cells (Barry et al., 2006). A neural network model based on this theory was successfully implemented in a mobile robot (Burgess et al., 2000), which used real-word inputs: sensory input cells, feeding their output into entorhinal cortical cells, were selective to the distance of a wall in a particular direction. Interestingly, very recently this model was supported by experimental evidence, whereby cells, termed border cells, in the medial EC and adjacent parasubiculum were found to fire when the rat was close to a geometric border of the environment (Solstad et al., 2008; Lever et al., 2009). These cells might serve to produce a reference frame for location determination and could be used to error correction, when the animal reaches the border, or even more, a corner of the environment. However, the question how the error accumulating in the path integrator while the animal moves from border to border still requires further elaboration.

Here, we ask the question how errors accumulating in path integration is corrected in the entorhino-hippocampal system in a biologically plausible way. Specifically, in the present study we propose a mechanism, which combine path integration via entorhinal grid cells and vision to create a unified representation of the environment by hippocampal place cells. We assume that the projection from CA1 and subiculum to the deep layers of the entorhinal cortex can influence the attractor dynamics in the entorhinal cortex, and that these connections are established through Hebbian learning when the environment is novel. This approach is consistent with the idea proposed by O'Keefe and Burgess (2005), who suggested that a feed-back innervation from hip-

pocampal place cells to entorhinal grid cells facilitates the association of grid cells to sensory inputs and associations between different sets of connected grid cells. Furthermore, we show that these feed-back connections empower the system to correct self-localization errors originating from noisy path integration.

3.2 Methods

For numerical simulations of the entorhino-hippocampal model, we set up a virtual environment and a simple robot model in the Webots (Michel, 2004) mobile robotics simulation software. All physical events happening to the robot (displacing it, turning it, blocking its movement when hitting obstacles), as well as maintaining the communication between the external word and the neural network model via robotic sensors were handled by Webots. To explore its environment, the robot moved forward in a straight line for three time steps, then turned randomly left or right 0.3 radians. A time step in the simulations was 0.125 seconds and the robot's speed was 0.22 meters per second.

The neural model – the whisker cell, local visual cell, grid cell and the place cell models – was run within the robotic simulation using inputs from the robot's sensors. Outputs – firing rates of cells – were saved and processed off-line in the R software environment (R Development Core Team, 2005). Control of the robot was not connected to the neural model in any way, the robot moved randomly and sampled the environment.

3.2.1 Overview of the Neural Network Model

The neural network model consisted of neurons in the barrel cortex, entorhinal cortical grid cells, local visual cells and hippocampal place cells (Fig. 3.1A). Inputs from the external world originated from the robot's sensors and were represented as firing rates in the entorhinal and barrel cortical part of the model. As we intended to study how allothetic information can be used to ameliorate path integration, we used noisy proprioceptive input in the simulations. Error accumulated in the path integrator and invalidated the neural representation of position.

Cortical neurons (the input layer) innervated hippocampal cells via modifiable synapses.

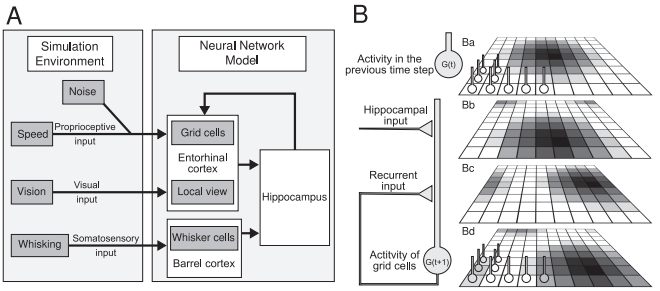

Figure 3.1: **Overview of the computer model.** A, The neural network model – consisting of the model of the entorhinal cortical grid cells, local visual cells, whisker cells and the hippocampal place cells – was run in a simulated robot in the Webots environment. Inputs of the model, represented as firing rates of grid, local visual and whisker cells respectively, came from the sensors of the robot sampling a virtual environment. White noise was added to the proprioceptive input (wheel rotation). Neurons in the input layer innervated hippocampal place cells, which in turn fed-back onto the entorhinal grid cells. B, The inputs and the activity of the entorhinal grid cells system. Simulated grid cells of a given population receive recurrent inputs from other grid cells of the population and afferent input from the hippocampus, both of which influence the change of grid cell activity in time (left). Grid cells are organized in a matrix, represented in the right panel, where darker color of a square indicates higher grid cell activity. The topology of the recurrent connections initiates the formation of an activity bump (Ba) after a few simulation time steps. When the animal moves the noisy proprioceptive input modulates the recurrent connectivity between grid cells and the input of the neurons in the corresponding directions is increased (Bc, see Sec. 3.2.4 and Guanella and Verschure (2006) for more details). The recurrent synaptic (Bc) input is integrated with the feed-back input from the hippocampus (Bb) and finally the activity bump shifts according to the estimated direction of motion (Bd).

Hippocampal cells in turn exhibited spatially correlated firing similar to experimentally observed place cells. In the present model hippocampal cells integrated the three types of modalities represented in the cortical models. We used this integrated place representation to stabilize the spatial firing pattern of grid cells via a feed-back excitation from the hippocampus to grid cells.

In the following sections of the Methods we describe the parts of the model in more detail.

3.2.2 Inputs of the Model

The neural network model receives three types of inputs from the environment. First, 20 distance sensors represented by 20 rate models were used to simulate the whisking of rats. Whenever the robot moved close enough to a wall, activity of these neurons increased from 0 continuously to 1. These sensors were also used to perform low-level obstacle avoidance reflex.

Second, one row of the panoramic camera image was taken as the visual input. The robot was constrained to move in the central portion of the environment, thus the striped wall it sensed by its cameras always remained in a distance serving distal visual cues. To enable the robot to establish its orientation a cue card was simulated. Whenever the robot moved it calculated its orientation relative to the direction of the cue card. The panoramic camera image was then rotated using the robot's self established head direction such that a pixel in a given direction (e.g. the view to the north) was always mapped to approximately the same local visual cell, irrespective of the orientation of the robot. Thus, the reference frame in our case was given by the location of the robot and the direction of the cue card relative to the robot at the beginning of the simulation. Altogether, we simulated 120 visual cells. Firing rate of a visual cell corresponded to the gray scale value of the respective camera pixel normalized in the $[0\,..\,1]$ interval.

Third, the rotation of the differential wheels was registered and a speed vector was calculated serving an input to the entorhinal grid cell system consisting of 270 neurons. The speed vector was considered to be noisy as it is in real animals and robots, giving rise to an inaccurate update of the position's representation by the grid cells, which integrated this noisy speed vector as described in the Sect. 3.2.4.

The noisy speed was simulated according to the following equation:

$$s' = s * (1 + \xi), \tag{3.1}$$

where s is the constant noiseless speed measured from the rotation of the robot's wheels, s' is the noisy speed used to update the grid cell system, and ξ is a random variable following the normal distribution with standard deviation σ.

3.2.3 The Simulated Hippocampal Network and the Learning Rule

The purpose of the hippocampus model in the present simulations was to integrate its inputs and generate a unified representation of the environment by place cells. To achieve this goal we followed the theory proposed by Rolls (1995), which explains how the hippocampal formation operates to serve as an episodic memory device. However, when input patterns are functions of the position, hippocampal cells show place correlated firing activity similar to the behavior of experimentally observed place cells. To achieve this behavior we implemented a Hebbian-like learning algorithm between neurons in the input layer and hippocampal place cells and competition among place cells (Sharp, 1991).

In the present model we simulated 1000 hippocampal cells described by a rate vector $\mathbf{H}$ (Fig. 3.1). These cells were innervated by neurons of the input layer (described by the rate vector $\mathbf{I}$) consisting of grid cells ($\mathbf{G}$), local view cells and whisker cells, but not by other hippocampal cells. The simulation was divided into two phases (Rolls, 1995), learning and active feed-back, respectively.

During the learning phase (Sect. 3.3.2) first, the afferent innervation from the input layer was used to calculate the activation ($\mathbf{h}$) of hippocampal neurons

$$h_j = \sum_i C_{ij} I_i, \tag{3.2}$$

where C_{ij} describes the strength of each synapse between the input layer and the hippocampus. Second, from the activation vector firing rates were calculated using a nonlinear activation function $f(\cdot)$

$$\mathbf{H} = f(\mathbf{h}, \chi), \tag{3.3}$$

where χ is the desired sparseness of the coding and $\mathbf{h}$ is the hippocampal activation vector. The function $f(\cdot)$ was implemented by an iteration, which selected the most active neurons and scaled their activation into the $[0 \,..\, 1]$ interval such that the desired sparseness χ was reached:

$$\frac{<\mathbf{H}>^2}{<\mathbf{H}^2>} \stackrel{!}{=} \chi \tag{3.4}$$

During learning the connection matrix (C_{ij}) was modified by a Hebbian-type learning rule

$$\Delta C_{ij} = \alpha H_j \left(I_i - C_{ij}\right), \tag{3.5}$$

Parameter	Value	Description
N	1000	Number of cells
α	0.05	Learning rate
χ	0.01	Sparseness of coding
μ	0.6	Mean synaptic strength
ρ	0.1	Deviation of synaptic strengths from mean

Table 3.1: **Default parameter values used in simulations of the hippocampal model**

where α is the learning rate.

During the active feed-back phase (Sect. 3.3.3) cell activities were calculated by the same set of equations 3.2 – 3.4, but C_{ij} was fixed.

In the simulations all-to-all connections were applied in C_{ij}. Initial matrix elements were picked from a normal distribution:

$$P(C_{ij} = w) = \frac{1}{\sqrt{2\pi}\rho} \mathrm{e}^{-\frac{(w-\mu)}{2\rho^2}}, \quad \text{if } 0 < w < 1 \tag{3.6}$$

Table 3.1 lists parameters used in the hippocampal model.

3.2.4 The Grid Cell Model

In a previous version of this model (Ujfalussy et al., 2008) grid cells were described by their firing rate, which was implemented as a periodic function of the animal's spatial location, following Blair et al. (2007). This simple approach is computationally efficient and allows the simulation of several grid cells at the same time. However, for our present purposes a dynamical description of grid cells is required as we intend to describe the deterioration of the hexagonal spatial firing pattern due to the noisy inputs and its restoration by modifiable connections between place cells and grid cells. Thus we incorporated the dynamical model of Guanella and Verschure (2006) into our model framework.

This artificial neural network model implements a continuous attractor system on a two dimensional neural space (Fig. 3.1B). Activity of a neuron is represented by a scalar variable denoting the firing rate of the neuron. The connection among neurons

Parameter	Layer I	Layer II	Layer III
Gain	1	1.5	2
Bias	0	0	0
Spacing [m]	0.80	0.55	0.40

Table 3.2: **Parameters used in the simulations.** Parameters used in our simulations of the grid cell model by Guanella and Verschure (2006). Other parameters were kept as in the original paper. Spacing in the model is a function of the gain parameter.

is all-to-all and to return the hexagonal spatial firing property of grid cells, the connections are implemented on a twisted torus topology of the neural tissue (see Fig. 1 and 2 of Guanella and Verschure (2006)). Starting from a random initial condition, first an activity bump is formed somewhere in the neural space depending on the initial state, which is the stable solution of this continuous attractor system. Integration of the animal's speed – i.e. the displacement of the activity bump – is implemented through the modulation of the connections by shifting them in the direction of the animal's motion. In our simulations we followed the same principle but used the noisy version of the speed vector (Eq. 3.1).

According to recordings from freely moving rats we used 3 layers of grid cells in the simulations, neurons within each layer sharing a common spacing and all layers had the same orientation (Barry et al., 2007). Each layer consisted of 9·10 neurons, each neuron had a different spatial phase. For generating these neurons we used the parameters listed in Table 3.2, other parameters were kept as in the original paper by Guanella and Verschure (2006).

Additionally to the original model (Guanella and Verschure, 2006) calculation of the grid cell activity was modified by the feed-back connections (Fig. 3.1). Specifically, equation 2 of Guanella and Verschure (2006) was changed into the following form

$$\mathbf{G}_i(t) = n\left(n(A_i(t)) + n\left(\sum_{j=1}^{N} W_{ij}^{(\mathbf{H},\mathbf{G})} H_j\right)\right), \tag{3.7}$$

where A is the original, $\mathbf{G}$ is the modified activity of the grid cells, $\mathbf{H}$ is the rate vector, N is the number of the simulated hippocampal cells, and $n(\cdot)$ is the linear normalization function

$$n(V_i) = \frac{V_i - min(\mathbf{V})}{max(\mathbf{V}) - min(\mathbf{V})}\,. \tag{3.8}$$

3.2.5 Development of the Hippocampo–Cortical Feed-back

In order to study the error correcting capability of the integrated hippocampal place representation we had to adjust the $\mathbf{W}^{(\mathbf{H},\mathbf{G})}$ weight matrix of the feed-back connection projecting from the simulated hippocampal cells to the grid cell population. Each element of the $\mathbf{W}^{(\mathbf{H},\mathbf{G})}$ matrix was initialized to 0. To evolve this matrix we used the following presynaptic gating learning rule:

$$\Delta W_{ij}^{(\mathbf{H},\mathbf{G})} = \gamma * H_j * \left(G_i - W_{ij}^{(\mathbf{H},\mathbf{G})} \right) \tag{3.9}$$

3.2.6 Evaluation of the Feed-back

To quantify the error correcting capability of the integrated hippocampal place representation in the grid cell system, we calculated the Pearson correlation at each time point t between the grid activity vector in the noiseless situation ($\mathbf{G}(t)$) and the corrected grid activity when noise was present in the system together with the hippocampo-entorhinal feed-back correction ($\mathbf{G}'(t)$) and averaged for the whole course of the active feed-back phase (2000 time steps):

$$C_X = \langle \mathsf{cor}\left(\mathbf{G}(t), \mathbf{G}'(t)\right) \rangle_{t=[2001\,..\,4000]} \tag{3.10}$$

for all three ($X \in \{\text{I, II, III}\}$) grid cell layers (Table 3.2).

Another approach to quantify the efficiency of the feed-back was the estimation of the robot's position based on the firing of grid cells. First, we calculated the two dimensional firing rate map of each grid cell during the learning period. Second, we obtained a probabilistic robot location map by multiplying point-wise the rate maps of all simultaneously active grid cells during the recall period. Finally, the maximum of this map gave us a rough estimation of the current position of the robot. This measure was used in Figures 3.3 and 3.4.

3.3 Results

Part of this work, including the implementation of the grid cells system and the hippocampal feed-back as well as basic exploration of the error-correction ability of the

network (Fig. 3.2 of this dissertation) was done by our master student, Dávid Samu (Samu, 2008). Péter Erős was involved as a graduate student in modeling place field formation in the hippocampus. Other parts of this chapter (Fig. 3.3-Fig. 3.6) are the work of Balázs Ujfalussy under the supervision of Tamás Kiss and Péter Érdi.

3.3.1 Simulation of the Model

Initially, all firing rates and the C_{ij} synaptic matrix elements were set randomly and were modified during the course of the simulation. The $\mathbf{W}^{(\mathbf{H},\mathbf{G})}$ matrix was initialized to 0. To solve the problem of the separation of concurrent learning and exploitation of acquired knowledge, we separated the simulation into two phases as described below.

3.3.2 Learning Phase

During the first (learning) phase of the simulation the cortico-hippocampal connections were modified by Eq. 3.5, and the feed-back connections as described in Section 3.2.5. This part of the simulation lasted for 2000 simulation time steps. During the learning phase, however, the feed-back connections did not influence the activity of the entorhinal grid cells. During this phase the network initialized itself in two ways: First the initially random activity in the grid cell system was stabilized and formed an activity bump due to the attractor dynamics of this subsystem. The bump was formed and path integration started within a few simulation time steps. As noise was turned off initially, grid cells exhibited a robust hexagonal spatial activity pattern (Fig. 3.2A-B).

Second, due to the competition between hippocampal neurons and the self-organizing synaptic modification, input patterns were transformed into a sparse and orthogonal representation in the hippocampus. As described earlier, (Rolls et al., 2006; Ujfalussy et al., 2008) spatially correlated inputs generate place cell activity in the model hippocampus during the learning phase of the simulation. Generation of the place code was fast, place fields remain stable after a few visit of a certain location.

An important difference between the previous version of this model (Ujfalussy et al., 2008) and its present version is that previously, similarly to other modeling works (Solstad et al., 2006; Rolls et al., 2006), we used multiple orientations and spacings in the grid cell part of the model. In the present version, however, only one orientation is

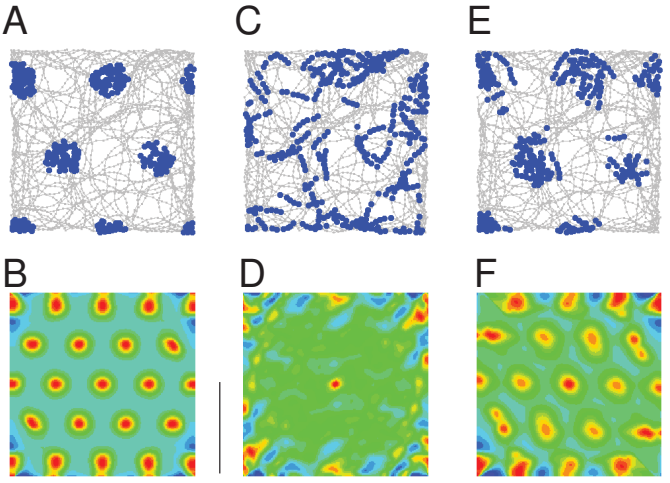

Figure 3.2: **Spatial activity pattern in the grid cell system.** A-B, Without noise and without hippocampal feed-back. The zig-zagging line on A represent the path of the robot with small black dots at sampling points where sensory information was processed, big dots show where a certain grid cell had non-zero activity. On B the spatial auto-correlation function calculated from the rate map. C-D, Spatial activity pattern in the grid cell system with noise and without hippocampal feed-back. Note that introducing noise in the proprioceptive information distorted the regular firing activity of grid cells. E-F, Spatial activity pattern in the grid cell system with noise and hippocampal feed-back. Grid cell parameters were: gain 1.5 and bias 0. The scale bar denotes 0.5 meter for ACE and 1 meter for BDF. This figure is based on the works of Dávid Samu.

used and only three spacings (Barry et al., 2007), still, integrating the grid input with the visual input results in well expressed place fields in the hippocampus.

3.3.3 Active Feed-back Phase

During the second (active feed-back) phase (2000 time steps) synaptic weights did not change and all synaptic pathways influenced their target regions. Also, noise was added to the signal of the rotation sensors of the robot's wheels, which deteriorated the regular activity of the grid system (Fig. 3.2C-D) and invalidated the path integration. As a result, two third of the cortical input vector contained noisy information, which

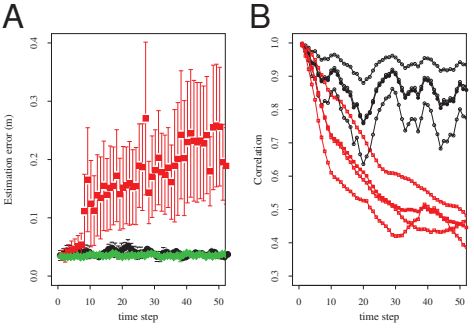

Figure 3.3: **Continuous error correction by feed-back.** A, Estimation of the robot's position based on the grid system (see Sec. 3.2.6). Symbols show mean, error bars SEM of the position without error correcting feed-back (red, squares), with feed-back (black, diamonds) and without noise (green, dots). B, Error accumulation in the grid cell system quantified by the correlation between different realizations of the grid-system (see Eq. 3.10). Open red squares represent the correlation of the noise-free grid-system with the noisy system without hippocampal feed-back for the three simulated grid layers. Open black circles denote correlations of the noise-free system with the noisy system, when its activity is corrected by the hippocampal feed-back, given for the three layers of the grid-system. Filled symbols represent the mean for the three layers. This figure is based on the average of ten runs. See text for details.

had an impact on the hippocampal place representation, reflected by distorted place fields. Simulation results show, however, that activating the hippocampal feed-back resulted in restoring both the grid and the place code (Fig. 3.2E-F).

Next we studied the continuous nature of the error correction by hippocampal feed back. While the robot traversed place fields that were not associated to grid fields by the feed-back during learning, the path integrator run free of the hippocampal influence, thus accumulated the sensory noise. However, the robot explored the whole arena during the initial learning phase, and thus place fields cover uniformly the available space. Therefore hippocampal place fields continually influence grid cell firing and the sensory noise has simply not enough time to accumulate (Fig. 3.3). On the whole, we found that after the sufficient amount of learning was accomplished (about 700 time steps in our case) error correction in the grid cell system took place and an appropriate place representation was generated.

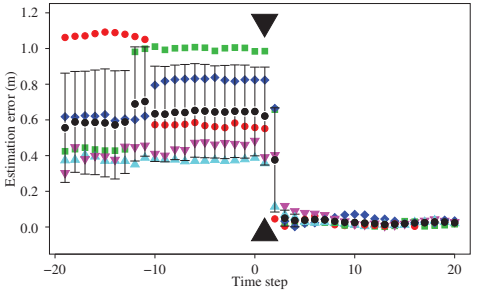

Figure 3.4: **Recovery after disorientation.** The error of the position estimation based on the grid-cell activity is high after disorientation but decreases suddenly after turning on the visual input (at $t = 1$). The five symbols show the error of the position estimation (see Sec. 3.2.6) for five runs, the symbols with the error bars show their average and standard deviation.

3.3.4 Predictions of the Model

We studied the properties of the simulated grid cell – place cell system in situations when the environment around the robot changes. In the first set of experiments we tested how the grid- and place cell systems are able to identify the location of the robot in an already learned, familiar, environment after disorientation (Fig. 3.4). For this experiment, the robot first learned positions in the environment for 2000 time steps. Then, the grid activity was randomized and the robot wandered from a random starting point for 200 time steps with the visual input turned off. Third, the visual input was turned back on, and the robot kept wandering for another 200 time steps.

As shown on Fig. 3.4 after the visual input is turned back (black arrows), the estimation of the robot's position based on the grid cell system (see Sec. 3.2.6 for the methodology) or the place cell system (data not shown) rapidly improves, showing that the grid cell system and the place cell system runs in accordance with the previously learned pattern, i.e. the robot is able to recover from a disorientation and recognizes an already visited environment.

In a second set of experiments the robot was put into a novel environment. Specifically, the robot was first put into an environment and learned the locations as described in Sect. 3.3.2. After learning in the first environment the striped pattern on the walls was changed to simulate a new environment and the robot was allowed to learn again

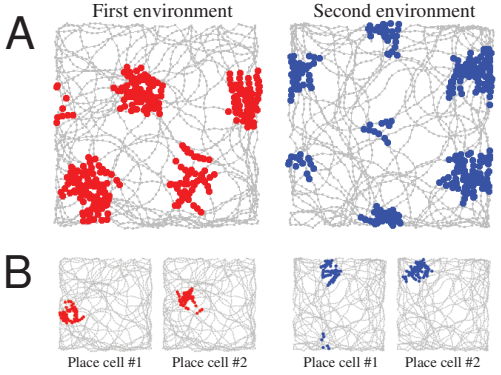

Figure 3.5: **Remapping in a new environment.** Left column: first environment, right column: second environment. Panel A shows a selected grid cell, and B two place cells in the first and in the second environment, respectively. For details see the text.

for 2000 time steps. After learning spatial receptive fields of grid and place cells were evaluated (Fig. 3.5). We found that grid cells remap coherently, as expected. Any two grid cells will preserve their relative phase, each grid cell will have the same spacing and their orientation change the same degree, in accordance with experimental observations (Fyhn et al., 2007).

Place cells perform global remapping. Some place cells were only active in one of the environments (approximately 40% of the cells in the first only, about 30% in the second only), some in both (about 10%) and some remained silent in both. Place fields of those cells that were active in both environment were independent. We also found that place fields in the second environment were slightly larger than in the first (data not shown). These observations can be explained by taking into account the competitive learning mechanism used in the hippocampal system. Cells that learned to represent a certain location will have synaptic strength associated to them such that only the input pattern describing the location of their place field will activate them, thus in the new environment they will not be able to learn. Naive cells, which were not involved in the representation of the first environment, on the other hand, will be able to learn new places. Also, as in the second environment less cells are able to learn, their resulting place field will be bigger.

Finally, to explicitly test how visual and proprioceptive inputs are combined, in a third set of experiments we simulated the morphing of the environment. The oversimplified visual system used in the model did not allow us to simply stretch the arena together with the striped pattern on its wall because in this case the robot did not recognize the distorted visual input.

However, to simulate the conflict between the visual and the proprioceptive system, we developed an other method. During the learning phase the gain parameter (see Table 3.2) of the grid cell system was modified, while the environment was kept unchanged. During the active feed-back phase, the gain parameter was set back to its original value, thus simulating a mismatch between the proprioceptive and the visual inputs. Specifically, the gain parameter of the grid cells was changed from 1 to 1.5 in the vertical direction and kept 1 in the horizontal direction for learning. As a result, during learning the hippocampal feed-back was associated with a distorted grid pattern that moved 1.5 times faster in the vertical direction than in the horizontal direction. During recall the gain parameter in the vertical direction was set back to 1, simulating that the side of the arena corresponding to the vertical direction was shortened 1.5 times while the visual cues remained unchanged. Without hippocampal feed-back, the grid activity exhibited the regular hexagonal pattern according to its proprioceptive input (Fig. 3.6 A). However, when the hippocampal feed-back was turned on, the grid pattern was compressed 1.5 times in the vertical direction (Fig. 3.6 B). During recall, the hippocampal feed-back forced the grid activity to change faster in the vertical direction, due to the associations learned previously, resulting in the compressed grid pattern.

Thus we conclude, that the visual input is able to continuously influence the entorhinal path integrator system via an integrated hippocampal place representation.

3.4 Discussion

We have analyzed a computer model of the rodent cortico-hippocampal system from the perspective of place learning and recognition. The main result of our study is that a representation of locations integrating visual and proprioceptive information can be used to decrease the harmful effect of sensory noise accumulating in the path integrator subsystem. Specifically, we have shown that although the noisy self locomotion

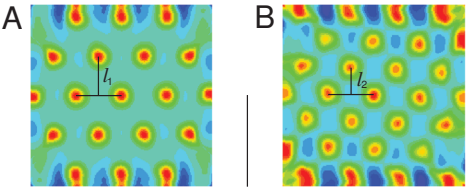

Figure 3.6: **Visual input is able to distort the grid system.** Effect of scaling the proprioceptive input relative to the visual input on the grid cell activity. The spatial autocorrelation function of one representative grid cell is shown without (A) and with (B) hippocampal feed-back. During learning a vertically compressed grid cell activity were associated with the hippocampal place representation. As shown on panel A, after rescaling the proprioceptive input during recall, the regular hexagonal spatial firing pattern of grid cells were reestablished *in the absence of* hippocampal feed-back. However, panel B shows that the visual input induce vertical rescaling in the grid cell system via the hippocampal feed-back. The magnitude of the vertical rescaling ($\frac{l_1}{l_2} = 1.5$) was exactly the same as modulation of the corresponding gain parameter.

information would distort the firing pattern of entorhinal cortical grid cells a feed-back excitation from hippocampal place cells can restore the correct pattern and at the same time improve the properties of place fields themselves as well, in a circularly causal manner.

Based on experimental evidence (Wilson and McNaughton, 1993) in a theoretical framework McNaughton et al. (1996) proposed that the visual information might be used both to establish the initial location of rodents – initialize its path integrator system – and to correct for accumulating error. Following this idea, there have been attempts to explain how a stable representation in the path integrator system might emerge. For example, Arleo and Gerstner (2000) have presented a model in which they define abstract extra-hippocampal path integrator neurons (in fact, rather similar to grid cells found five years later), which integrated wheel rotation. They also faced the problem of accumulating error and used visual cues to eliminate its harmful effect. Namely, after a certain amount of time their robot stopped exploration and searched for familiar visual cues. When a cue was found to be reliable enough the path integrator was reset to the current location determined by the visual stimulus.

Our model fits in this general theory as it uses the visual information to correct path integration (we hypothesize that olfactory, auditory or whisking inputs could also be used for this corrections as these modalities are similar to vision in that noise does

not cause error to accumulate in their representations). However, in our model not only the visual, but the integrated (visual & proprioceptive) information was used to correct the path integration error (c.f. O'Keefe and Burgess (2005)). Moreover, we did not introduce discrete time points or set up thresholds when a re-calibration becomes necessary, instead building on the anatomy of the hippocampus (Amaral and Witter, 1989) and implementing the modifiable hippocampo-cortical feed-back, continuously corrected the path integrator. This continuous influence of allothetic information on the path integration system is supported by the fact that entorhinal grid cells' firing fields rescaled in response to environmental deformation (Barry et al., 2007).

Theories on the hippocampo-cortical feed-back mostly hypothesize on its functional role in respect of the episodic memory aspect of the cortico-hippocampal system (Treves and Rolls, 1994; Lőrincz and Buzsáki, 2000; Witter et al., 2000). According to these theories the hippocampus is able to rapidly form a new representation upon passing through a new episode e.g., visiting an unknown location. After the memories are formed the feed-back activation could provide information useful to the neocortex in the building of new representations by recalling previous memories, which process would constitute a form of memory consolidation (Rolls and Kesner, 2006). Also, a closed loop connecting layer II-III of the entorhinal cortex to the hippocampus and from the latter to the deep layers of the entorhinal cortex (Witter et al., 2000) might serve to continuously compare new inputs and temporarily stored information in order to facilitate the decision whether a new or an already stored experience is encountered.

An other aspect of the feed-back connection might be that when only a fragment of the episode is presented, it is able to recall the whole episodic memory through the back-projection pathways from the hippocampus to the cerebral neocortex, resulting in reinstatement of neuronal activity in association areas of the cerebral neocortex similar to that present during the original episode (Treves and Rolls, 1994). Similarly, in our model the location of the animal can be continually recalled based on visual cues. Conversely, in the absence of vision (e.g., in darkness) the animal could retrieve visual landmarks associated with its location based on its position information coming from path integration.

The model proposed by Gaussier et al. (2007) suggests a different role for the hippocampo-entorhinal feed-back, including an explanation of spatially correlated processes as well. In this model there is again a continuous interplay between the hippocampus and the entorhinal cortex, where the latter stores and recognizes input configurations,

while the former identifies transitions from the present towards new states. This approach is somewhat similar to ours in that the entorhinal grid cell system is partly driven by the hippocampus, but differs in that Gaussier et al. (2007) do not assume attractor dynamics as the basis for the generation of grid cells but suppose that the operation of an extra-hippocampal system endowed with "long-distance" path integration capabilities creates the grid activity in the entorhinal cortex given some properties of the connections between the two structures.

In our model, the representation of the anatomy of the entorhinal cortex and the hippocampal feed-back is not detailed. It is known, however, that the hippocampus sends afferents to the deep layers of the entorhinal cortex and receives efferents from the superficial layers (Witter et al., 2000). It is also known, that classical grid cells can primarily be found in layer II of the EC, while deeper layers (III, V, and VI) contain grid cells, head-direction cells and conjunctive grid and head-direction cells (Sargolini et al., 2006). Interestingly, there is an extensive system of connections among entorhinal cortical layers too (van Haeften et al., 2003; Kloosterman et al., 2003), which implicates that the grid representation and the path integration in the entorhino-hippocampal system is an emergent property, which requires all participating regions and layers.

In the presented model we used the approximation that noise in the proprioceptive input was only simulated when the synaptic connections were already established. This is due to the fact that we primarily intended to show that an integrated place representation can be used to correct one of its constituent part. The learning process was necessary to set the appropriate weight matrix for the feed-back connection. However, we propose that the shown mechanism can be utilized by animals as well, considering their exploratory strategy. Animals (from arthropods to rodents) were shown to start the exploration of a new environment by short trips, initially frequently returning to their nest or an other initial location (Collett and Zeil, 1998; Etienne et al., 1998) and move further away only after they are familiar with their immediate surrounding. This exploration strategy is in favor of our proposed model as during the short trips only small error accumulates in the path integrator. If the learning process lasts only for a short time – and our simulation results showed that a learning converges rapidly –, and after learning the feed-back is used to correct the path integrator, than with a gradual exploration and learning the animal is able to enlarge its map while keeping the hippocampus and entorhinal cortex always in register.

Theoretically, the allothetic information could reach the path integrator system directly, or indirectly through an integrated representation from the hippocampus. Manipulations resulting from a coordinated alteration of both the hippocampal and the entorhinal representations like rotation of the environmental landmarks (Hafting et al., 2005), deformation of the enclosure (Barry et al., 2007) or induction of simultaneous global remapping in the hippocampus and grid cell realignment in the EC (Fyhn et al., 2007) can be interpreted within both the direct and the indirect framework. Our model predict, however, that after the inactivation of the hippocampus, firing of grid cells would remain location dependent but would become more dispersed and would not follow environmental manipulations. Indeed, recordings on a linear track showed that although hippocampal inactivation did not disrupt the spatially confined firing of the grid cells, the fields became wider and less stable (Hafting et al., 2008) supposedly because of the accumulating error in the path integrator system.

In our simulations the hexagonal firing pattern of the grid cells was generated by an attractor network of entorhinal neurons that requires specific connectivity pattern (Guanella and Verschure, 2006; McNaughton et al., 2006; Fuhs and Touretzky, 2006). Our basic idea, that allothetic information reaches the grid cells indirectly though the hippocampus can also be applied to an other class of grid cell models (Hasselmo et al., 2007; Burgess et al., 2007), where grid cell firing arises from interference of theta frequency membrane potential oscillations in single neurons. In this case, hippocampal place cells should continually reset the phase of the dendritic oscillations of entorhinal grid cells. Spike timing dependent plasticity rules during exploration could be used to set up the proper connectivity (Lengyel et al., 2005b). Hippocampal and entorhinal phase precession (Hafting et al., 2008) and subthreshold oscillation of entorhinal grid cells (Giocomo et al., 2007) support this scenario.

* * *

In the present chapter we used a highly simplified model of hippocampal place representation in order to demonstrate that the combined allothetic and idiothetic information can be used to correct for the accumulating noise in the entorhinal path integration system. However, different hippocampal subfields are characterized by various types of location dependent activity parallel to their specific role in information processing. In the next chapter we will describe the neural computations behind the generation of multiple, independent place fields of granule cells in the dentate gyrus.

4

Space II: Parallel Computational Subunits in Dentate Granule Cells Generate Multiple Place Fields

4.1 Introduction

Neurons possess highly branched, complex dendritic trees, but the relationship between the structure of the dendritic arbor and underlying neural function is poorly understood (Hausser and Mel, 2003). Recent studies suggest that dendritic branches form independent computational subunits: Individual branches function as single integrative compartments (Polsky et al., 2004; Losonczy and Magee, 2006), generate isolated dendritic spikes (Wei et al., 2001; Milojkovic et al., 2005) linking together neighbouring groups of synapses by local plasticity rules (Golding et al., 2002; Gordon et al., 2006; Harvey and Svoboda, 2007). Coupling between dendritic branches and the soma is regulated in a branch-specific manner through local mechanisms (Losonczy et al., 2008), and the homeostatic scaling of the neurotransmitter release probability is also regulated by the local dendritic activation (Branco et al., 2008).

The computational power of active dendrites had already been demonstrated by several computational studies (Segev and Rall, 1988; Mel, 1993; Mel et al., 1998; Koch, 1999; Archie and Mel, 2000; Poirazi and Mel, 2001), but how local events influence the output of the neuron remained an open question. Using the cable equation (Rall, 1989) or compartmental modelling tools one can calculate the current or voltage attenuation between arbitrary points in a dendritic tree (Koch, 1999), which is in good agreement with *in vitro* recordings. However, cortical networks *in vivo* are believed to operate in a balanced state (Shu et al., 2003; Haider et al., 2006), where the inhibitory drive is continuously adjusted such that the mean activity of the population

is nearly constant (Buzsáki, 1984; Assisi et al., 2007). In this case, the firing of an individual neuron is determined, beyond its own input, by the activity distribution of the population. A simple cascade model (Herz et al., 2006) incorporating numerous dendritic compartments allowed us the statistical estimation of the activity distribution of neurons within the population. We used this model to study how localized dendritic computations influence the output of the neuron.

In the present chapter we derive mathematical framework that can be applied to various neurons with different dendritic arborization. Next we use this framework to infer signal processing in hippocampal granule cells. Compared to pyramidal neurons granule cells have relatively simpler dendritic arborization: They lack the apical trunk and the basal dendrites, but are characterized by several, equivalent dendritic branches, extended into the molecular layer (Claiborne et al., 1990) (Fig. 4.1A). Recordings from freely moving rats revealed that like pyramidal neurons, granule cells exhibit clear spatially selective discharge (Jung and McNaughton, 1993; Skaggs et al., 1996). However, granule cells had smaller place fields than pyramidal cells, and had multiple distinct subfields (Jung and McNaughton, 1993; Leutgeb et al., 2007). It has also been recently shown that these subfields are independent, i.e., their distribution was irregular and the transformation of the environment resulted in incoherent rate change in the subfields (Leutgeb et al., 2007). The dendritic morphology of granule cells suggest that parallel dendritic computations could contribute to the generation of multiple, distinct subfields of these neurons.

In this chapter we analyze how synaptic input arriving to dendritic subunits influence the neuronal output. First, we introduce the model used in this study and we define statistical criteria to measure if a dendritic branch alone is able to trigger somatic spiking. We show, that generally neurons perform input strength encoding i.e., input to the whole dendritic tree but not activation of a single branch is encoded in the somatic firing. In other words, most of the branches contributes a little to the activity of the neuron. Next we demonstrate that if the local response is enhanced by active mechanisms (dendritic spiking and synaptic plasticity) then neurons switch to feature detection mode during which the firing of the neuron is usually triggered by the activation of a single dendritic branch. Furthermore we show that moderately branched dendritic tree of granule cells is optimal for this computation as large number of branches favor local plasticity by isolating dendritic compartments, while reliable detection of individual dendritic spikes in the soma requires low branch number. Dendritic branches

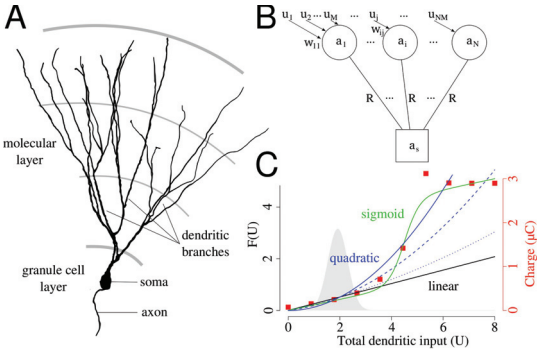

Figure 4.1: **The structure of the model.** A, Anatomical reconstruction of the dendritic tree of a mature granule cell from mice. The dendritic tree is dominated by the long parallel dendritic branches in the outer two third of the molecular layer. Note the lack of basal dendrites and the apical trunk compared to a pyramidal neuron. Based on the figure of Dr. Josef Bischofberger. B, Model for the somato-dendritic interactions in dentate granule cells. Distal dendritic compartments are represented by circles, and the soma by a square. Further details are in the text. C, The different dendritic integration functions used in this study. Black: linear, blue: quadratic, green: sigmoid function. Red, square symbols indicate the nonlinearity of dendritic integration in a conductance based model of hippocampal granule cell (Ujfalussy et al., 2009). Dashed and dotted lines show different degrees of nonlinearity. The distribution of the total dendritic input with uniform synapses is shown in the background.

of dentate granule cells could therefore learn different inputs; and the cell, activated through different dendritic branches, could selectively respond to distinct features (locations), participating in different memories. Finally using spatially organized input we illustrate that our model explains the multiple independent place fields of granule cells and these dendritic computations increase the pattern separation capacity of the dentate gyrus.

4.2 Model

We set up a cascade model (Herz et al., 2006) to study the somato-dendritic interactions in neurons, that is simple enough for mathematical analysis but can be adequately fitted to experimental data. The long, parallel branches of dentate granule cells are represented by distinct compartments connected to the somatic compartment

of the model (Fig. 4.1B). The activation of the somatic (a_s) and dendritic (a_i) compartments are described by the following equations:

$$C_m \frac{\mathrm{d}a_i}{\mathrm{d}t} = -\frac{a_i}{R_m} + f(\sum_{j=1}^{M} w_{ij} u_j) + \frac{a_s - a_i}{R_a}, \tag{4.1}$$

$$C_m \frac{\mathrm{d}a_s}{\mathrm{d}t} = -\frac{a_s}{R_m} + \sum_{i=1}^{N} \frac{a_i - a_s}{R_a}, \tag{4.2}$$

where C_m is the membrane capacitance, R_m^d and R_m^s are the total dendritic and somatic membrane resistances, respectively, and R_a is the axial resistance between the dendritic and the somatic compartments. Each of the N dendritic branches are contacted by M presynaptic axons, u_j is the firing rate of axon j, and w_{ij} is the synaptic strength between the dendritic branch i and presynaptic axon j (see Methods for parameters specific to hippocampal granule cells). $f(U)$ is the dendritic integration function that specifies the form of the local integration of synaptic inputs, and $U_i = \sum_j w_{ij} u_j$ is the total synaptic input to a given branch. Because the firing rate of the presynaptic entorhinal neurons depend mostly on the location of the animal (Sargolini et al., 2006) we assume, that input varies slowly compared to the membrane's time constant in dentate granule cells ($\tau_m \approx 37$ ms, (Schmidt-Hieber et al., 2007)). Therefore, we rewrite Equations 4.1-4.2 to their steady-state form:

$$a_i = R_m f(U_i) + (a_s - a_i)\frac{R_m^d}{R_a} = F(U_i) + \frac{a_s - a_i}{R^d} \tag{4.3}$$

$$a_s = \frac{R_m^s}{R_a} \sum_i (a_i - a_s) = \frac{1}{R^s} \sum_i (a_i - a_s) = \frac{\sum_{i=1}^{N} a_i}{R^s + N} \ , \tag{4.4}$$

where $F(U) = R_m^d f(U)$ and $R^x = R_a / R_m^x$ is the proportion of the axial and the membrane resistivity. In granule cells the area and the electrical resistance of the somatic membrane is similar to the membrane area and resistance of a single dendritic branch (Schmidt-Hieber et al., 2007) (see Methods). Therefore, in the following calculations we use $R = R^s = R^d$ to denote the electrical isolation between somatic and dendritic compartments. Three different functions were used in this study to approximate the local integration of synaptic inputs within the dendritic branches of hippocampal granule cells (Fig. 4.1C, Ujfalussy et al. (2009)): a linear ($F_L(U) = 0.26U$) and a quadratic ($F_Q(U) = 0.13U^2$) function were used in the analytical calculations; but the results were also tested with a sigmoid ($F_S(U) = \dfrac{3.4}{1 + \exp\left(\frac{4.5-U}{0.3}\right)} + U/4.7$) function. We also performed some of the analytical calculations by decreasing the degree of nonlinearity, where we used $F_C = 0.07U^2 + 0.12U$ or $F_C = 0.02U^2 + 0.22U$.

Note, that the action potential generation is not incorporated in the model, and all active properties of the dendrites are modeled by the integration function $F(U)$.

Distribution of the Somatic Activation. Supposing that firing rates of presynaptic neurons (u_j) are independent and identically distributed we assume that the total input of the dendritic branches $U_i = \sum_j w_{ij}u_j$ is drawn randomly from a Gaussian distribution with mean μ and variance σ^2:

$$p[U_i] = \mathbb{G}(U_i|\mu, \sigma^2) \tag{4.5}$$

where $p[U]$ indicates a probability distribution over U (Fig. 4.1C; see Eq. 4.17 in Methods for parameters specific to hippocampal granule cells). More specifically, $\mathbb{G}(U_i|\mu, \sigma^2)$ indicates the distribution of the magnitude of possible total inputs to a single dendrite over many different instances. Based on the distribution of the total dendritic input, we can compute the distribution of the somatic activation a_s, and determine the firing threshold (β) according to the proportion of simultaneously active cells (the sparseness of the representation, sp_{DG}) in the DG (Jung and McNaughton, 1993). First, we rearrange Eq. 4.3 using the input distribution to express the distribution of a_i:

$$a_i = \frac{RF(^{\mathbb{G}}U_i) + a_s}{R+1}, \tag{4.6}$$

where $^{\mathbb{G}}U$ indicates that the inputs of the dendritic branches are randomly sampled from a Gaussian distribution. We substitute Eq. 4.6 into Eq. 4.4, and we get

$$a_s = \frac{\sum_{i=1}^{N} F(^{\mathbb{G}}U_i)}{R+N+1}. \tag{4.7}$$

We can assume again, that the inputs (U_i) of the dendritic branches are independent and identically distributed variables. (Note, that while the activations a_is are not independent because of the back-propagation of currents from the soma, the inputs are.) If N is high enough, we can approximate the sum in Eq. 4.7 with a Gaussian distribution, and rewrite the equation:

$$p\left[a_s\right] = \mathbb{G}\left(a_s|\frac{N\mu_F}{R+N+1}, \frac{N\sigma_F^2}{(R+N+1)^2}\right) \tag{4.8}$$

where $p[a_s]$ indicates a probability distribution over a_s, while μ_F and σ_F^2 are the expected value and the variance of the dendritic integration function $F(U)$ given the

input distribution ${}^{\mathbb{G}}U$:

$$\mu_F = \int_{-\infty}^{\infty} p[U]F(U)\mathrm{d}U = \int_{-\infty}^{\infty} \mathbb{G}(U|\mu,\sigma^2)F(U)\mathrm{d}U, \tag{4.9}$$

$$\sigma_F^2 = \int_{-\infty}^{\infty} \mathbb{G}(U|\mu,\sigma^2)(F(U)-\mu_F)^2\mathrm{d}U. \tag{4.10}$$

We calculated the integrals 4.9-4.10 with two different forms of dendritic integration of synaptic inputs: a linear and a quadratic function (Fig. 4.1C). The details of these calculations are in the Appendix A.2.

We do not model inhibitory neurons in the dentate gyrus, however, we assume, that they play a substantial role in continuously adjusting the firing threshold of principal neurons and regulating the activity of the network (Buzsáki, 1984; Assisi et al., 2007). As a result of this regulation always the most depolarized neurons are able to fire, and the proportion of simultaneously active neurons is characteristic for different hippocampal areas (Barnes et al., 1990; Jung and McNaughton, 1993). Given that all neurons share a common input statistics and have similar internal dynamics, equation 4.8 also describes the distribution of a_s across the granule cell population at a given time. If only the most depolarized 1-5% of the population are able to fire (Barnes et al., 1990), this also means that only those neurons exceed their firing threshold whose activation is within the uppermost 1-5% of the distribution described by Eq. 4.8. Therefore, the proportion of simultaneously active neurons within the dentate gyrus sp_{DG} (Barnes et al., 1990; Jung and McNaughton, 1993) also determine the firing threshold β for granule cells.

Criteria for Independence in the Output. We approach the dendritic independence by focusing on the statistical distributions of the input to dendritic branches, as these branches form the basic computational subunits in our model. We ask whether the input of a single branch could be sufficiently large to significantly depolarize not only the given branch but also the soma of the neuron. We defined two conditions to study whether the spiking of the neuron is caused by the activation of a single dendritic branch or by the simultaneous depolarization of multiple branches.

First, the conditional probability $H(U_k) = p[a_s > \beta|U_k]$ is the probability of firing given that any branch k has total input $U_k = \sum_j w_{kj}u_j$, while inputs to all other branches are random and independent samples from the distribution of $\mathbb{G}(U|\mu,\sigma^2)$ (Figure 4.2A). At those U_k values where this probability is close to 1 the cell tends to fire when any of the dendritic branches gets that input. Second, the conditional

distribution $K(U^*) = p[U^*|a_s > \beta]$ is the distribution of the synaptic input of the most active branch U^* at the time the depolarization of the soma exceeds the firing threshold (β) (Figure 4.2A). $K(U^*)$ can be regarded as the marginal of the joint distribution of $p[a_s, U^*]$ above the firing threshold (Figure 4.2B). The probability mass of this function shows the typical maximal input (U^*) values when the neuron fires.

These two conditions together determine whether a single branch can be sufficiently depolarized to trigger somatic spike or not. If the probability of firing is high ($H(U) \approx 1$) at typical input values ($K(U^*)$) then the firing of the cell is caused by a *single branch*. With the definition of Gasparini and Magee (2006) we call this form of information processing as *independent feature detection*. On the other hand, if the firing probability is low ($H(U) << 1$) even if one of the branches receive extremely large input (U^* is high) then the cell mostly fires when the *overall* dendritic activation is high, and even the most depolarized branch usually fails to make the neuron fire. We use the expression *input strength encoding* (Gasparini and Magee, 2006) to denote this second type of computation. The calculation of the two functions $H(U)$ and $K(U^*)$ is described in the Methods section.

4.3 Results

4.3.1 Constant Synaptic Weights: Input Strength Encoding

First we chose unstructured synaptic input, i.e., the firing of entorhinal neurons were independent and the strength of all synapses were equal. In this case we approximated the total synaptic input U to a branch with a Gaussian distribution (Eq. 4.5, Fig. 4.1C). Given the input distribution we asked whether the excitation of single branches can be sufficiently large to cause significant depolarization in the soma.

The typical largest input values, indicated by the probability mass of $K(U^*)$ (Fig. 4.2C-D) are unable to sufficiently depolarize the soma and determine the neuronal output (indicated by the low $H(U)$ values) in the case of both the linear (Fig. 4.2C) and the quadratic (Fig. 4.2D) integration functions. Wherever $K(U^*)$ has high values, $H(U)$ is low in both cases, which indicate, that these branches are not able to independently influence the output of the neuron. Only coactivation of several branches could make the neuron fire in this case, and the output of the neuron encodes the

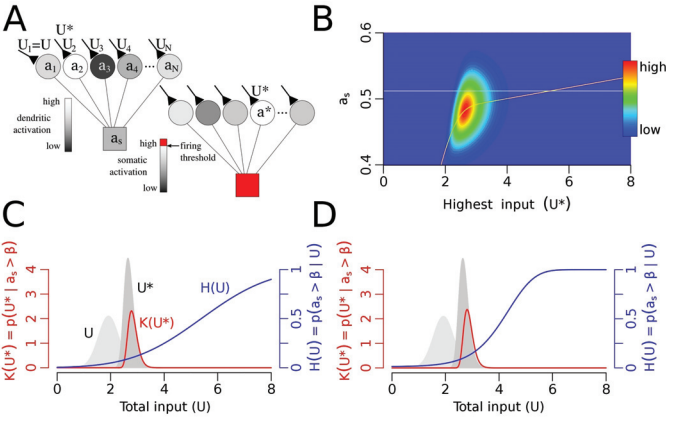

Figure 4.2: **Input strength encoding with uniform synapses.** A, The figure shows two neurons (or the same neuron with two different input sets). We calculated the probability of firing ($H(U)$) given that one of the branches has exactly U synaptic input (e.g., $U_1 = U$) while inputs of other branches ($U_2, U_3, \ldots, U_N$) are drawn independently from the input distribution. Second, we calculated the distribution of the maximal input ($K(U^*)$) given the depolarization of the soma exceeds the firing threshold. B, Color coded joint probability distribution of the somatic activation and the maximal dendritic input, $p[a_s, U^*]$ with the linear integration function. Red is maximum, dark blue is zero. The color-code emphasizes low probability events and it is not linear. The horizontal line is the firing threshold; the yellow line shows the conditional expectation of a_s given U^*. If dendrites were independent high and low U^* values could be separated by a somatic threshold of action potential generation. C-D, Dendritic independence with linear (C) and quadratic (D) integration functions. Left axis, red: $K(U^*)$, the distribution of the maximal dendritic inputs during firing. Right axis, blue: the $H(U)$ function, which is the probability of firing given that one of the dendrites has U total input. The probability of triggering output by a single branch is low ($H(U) < 0.25$) even with reasonably large input (as revealed by the low $H(U)$ values at the probability mass of $K(U^*)$). This indicates that a single dendritic subunit is unable to reliably activate the neuron with these integration functions. Background light gray is the distribution of U while dark grey shows the distribution of U^*. Parameters: $R = 0.01$, $N = 30$.

strength of the summated dendritic input. As $H(U)$ converges to 1 for high input values extremely high inputs to a single dendrite could reliably trigger somatic firing. In the next sections, however, we study how synaptic plasticity selectively modifies individual synapses and contributes to the sparse occurrence of extraordinarily high input values.

4.3.2 Hebbian Synapses: Feature Detection

During Hebbian learning synapses contributing to postsynaptic activation are potentiated while other synapses may experience compensatory depression (Lynch et al., 1977; Turrigiano, 1999). We simulated the learning process by showing a finite number of uncorrelated samples from the input distribution (see Methods) to the model neuron initiated with uniform synaptic weights. The synaptic weights of those dendritic branches where the activation exceeded a threshold, β_d were modified according to the following Hebbian plasticity rule (Gerstner and Kistler, 2002) that incorporates heterosynaptic depression (Lynch et al., 1977):

$$\Delta w_{ij} = \gamma \mathbb{H}(a_i - \beta_d)(u_j - w_{ij}) \tag{4.11}$$

where a_i is the local dendritic activation, u_j is the presynaptic firing rate and w_{ij} is the synaptic strength. $\mathbb{H}()$ is the Heaviside function and $\gamma < 1$ is a constant learning parameter. Note, that the learning rule is local to the dendritic branches: the synaptic change depends on the local activation but not on the somatic firing.

Next, we calculated the total input to the branches $U_i = \sum_j w_{ij} u_j$ after modification of synapses (Figure 4.3A), and recalculated the two functions $H(U)$ and $K(U^*)$ defined previously with the new input distribution (Eq. 4.18). As shown on Figure 4.3A the total synaptic input in response to a learned pattern increases significantly after learning (compare blue and grey curves on Fig. 4.3A), while untrained patterns generate smaller synaptic inputs (compare grey and black curves on Fig. 4.3A). The main consequence of synaptic plasticity is that the trained patterns generate much larger local response than untrained patterns, which raise the possibility of their detection in the soma. Note, that an unspecific increase of synaptic weights would result in an upward shift of both the input distribution (Eq. 4.5) and the firing threshold, but would not affect the somatic detection of individual dendritic events.

The neuron is able to selectively respond to the dendritically learned patterns if a sin-

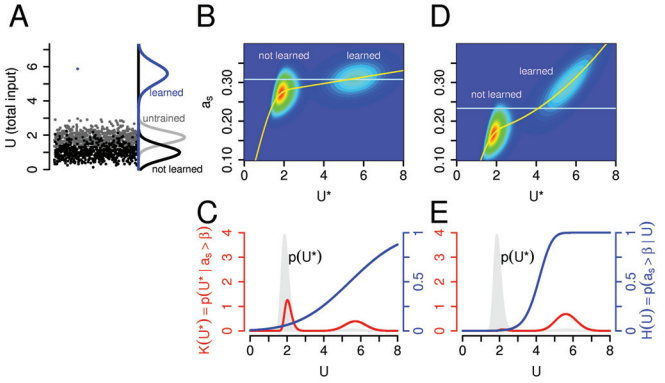

Figure 4.3: **Independent feature detection with Habbian synapses.** A, Synaptic plasticity separates the inputs. Before learning the total synaptic input to a dendritic subunit come from a Gaussian distribution (600 samples are shown with grey circles) with the calculated density function shown on the right (Eq. 4.5). During the learning process each branch learns its largest input and the response increases to the learned input (blue circle), while it decreases to all other inputs (black circles). The black and blue Gaussian curves show the density functions for the non-learned and learned inputs, respectively (Eq. 4.19). BD, Color-coded joint distribution of the somatic activation and the maximal dendritic input ($p[a_s, U^*]$) in the linear (B) and quadratic (D) case. The horizontal lines indicate the firing threshold. CE, The distribution of the maximal dendritic input when the cell fires ($K(U^*)$ in red) and the probability of firing with a given input ($H(U)$ in blue). The distribution of U^* is shown in the background. In the linear case, 50% of firing occurs when one of the branches receives its preferred input, while with quadratic integration function more than 95%. Parameters: $R = 0.01$, $N = 30$.

gle branch, when facing with its preferred input, is able to induce significantly more depolarization at the site of the action potential initiation compared with the case when all branches get random, not learned input. Figure 4.3B-E shows the dendritic input and the activation of the soma after learning. If the maximal input U^* is small (left bumps on Fig. 4.3B,D) and none of the branches got its preferred input then the somatic activation is usually small. If U^* is high (Fig. 4.3B,D; right bumps), which means that one of the branches receives its preferred input pattern, then the somatic activation is increased. The increase of the somatic activation with learned input is only moderate in the linear case (Fig. 4.3B,C) resulting in an incomplete separation of learned and not learned inputs by the somatic firing threshold. However, if synaptic inputs are supra-linearly (quadratically) integrated within the dendritic branches, effi-

cient separation is possible: the probability that the presentation of a learned pattern elicits supra-threshold somatic response, called *dendritic spike detection probability* was over 95% (Fig. 4.3D,E). In this case the output of the neuron encodes whether or not one of the stored features was present in the neuron's input and not simply the strength of the total input arriving to the whole dendritic tree. In other words, if dendritic nonlinearity enhance the response of a given branch to its preferred input, then this branch alone is able to trigger somatic spiking. In the following sections we use the term *dendritic spiking* to refer to these supra-linear dendritic events. Although there is no data available on the synaptic induction of local dendritic spiking in hippocampal granule cells, voltage dependent Ca^{2+} currents are present in the membrane of granule cells (Blaxter et al., 1989; Fisher et al., 1990) and whole-cell recordings from these neurons suggest that T-type Ca^{2+} channels can generate dendritic action potentials at least in young neurons (Schmidt-Hieber et al., 2004) or under hyperexcitable conditions (Blaxter et al., 1989; Fricke and Prince, 1984).

4.3.3 Independent Learning in Isolated Branches

Next, we explored how the independent feature detection ability of the model depends on the resistance between the somatic and dendritic compartments with nonlinear dendritic integration. In the passive cable model of dendritic trees the space constant of the membrane $\lambda_m \approx (R_m/R_i)^{1/2}$ plays a substantial role in determining the voltage attenuation among two sites. Consequently, an increase in the intracellular resistivity R_i or a similar decrease in the membrane resistance R_m will contribute to the separation of dendritic subunits by decreasing the membrane's space constant λ_m. In the present study we used the inverse of the space constant $R \approx R_i/R_m$ to characterize the degree of electrical resistivity between the somatic and dendritic compartments. Indeed, an increased resistivity (R) between the compartments (smaller space constant) induced larger degree of electrical isolation as the somatic response to the same amount of dendritically applied current decreased (compare Figure 4.4A left and right panels). However, this isolation did not modify the dendritic spike detection probability in the soma: Large dendritic spikes localized to a single compartment could be reliably separated from subthreshold events with a somatic firing threshold at a wide range of resistances R (Fig. 4.4A-B). This was also true for the selective alternation of the somatic or the dendritic membrane resistance (Fig. 4.4B).

On the other hand, the resistance parameter had a substantial impact on the isolation of different dendritic compartments which might be necessary for the independence of synaptic plasticity. To measure the isolation of the dendritic subunits we calculated the influence of other compartments on the activation of a given branch (external influence) quantified by the standard deviation of $p[a_i|U_i]$. Figure 4.4C shows the activation of a dendritic branch in the function of its input at different R values. If the resistance is small ($R = R_a/R_m = 0.01$, Fig 4.4C, left), then the local activation depends only slightly on the local input and the external influence is high (Fig 4.4D). In this case the local input spread out to the entire dendritic tree and activates similarly all branches. On the other hand, if the resistance is high ($R = 1$, Fig 4.4C, right) then the external influence is small, and the depolarization of a dendritic branch depends mostly on the local input. Interestingly, decreasing the resistance of the perisomatic membrane (R_m^s) alone was more efficient in separating the dendritic subunits than decreasing the resistance of the dendritic membrane or both (Fig 4.4D). The extensive GABAergic (Douglas et al., 1983; Halasy and Somogyi, 1993) and glutamatergic (Buckmaster et al., 1996) innervation of the proximal dendritic and perisomatic region of granule cells may therefore contribute significantly to the isolation of the dendritic compartments.

The impact of a single branch on the somatic activation, and also the coupling between dendritic branches may depend highly on the relative size of the subunit compared to the whole dendritic tree. Therefore we varied the number of dendritic subunits, N, and calculated the probability of detecting dendritic spikes in the soma and the external influence on the dendritic subunits (Figure 4.5). The probability of detecting a dendritic spike in the soma decreased gradually after a few ($N \approx 30$) number of branches from 1 to 0.3 ($N \approx 1000$, Figure 4.5A-B). If the number of branches was low, then the effect of a single branch on the soma was relatively high, and the somatic detection of single dendritic events was reliable. Conversely, one out of hundreds of branches had relatively low impact on the neuron's output even if the local depolarization was significant.

The electrical coupling between the dendritic subunits characterized by the external influence on the local activation also decreased with the number of branches, (Figure 4.5C-D). In the model the branches are connected through the somatic compartment, and because the variance of the somatic activation decreases if N increases (Eq. 4.8), the external influence will also decrease. Therefore, in a complex den-

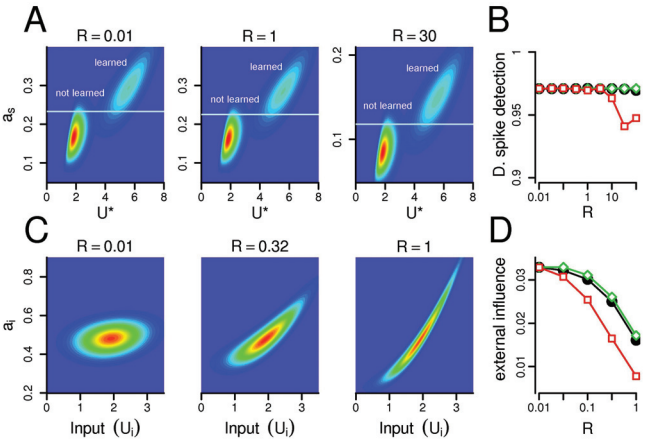

Figure 4.4: **Changing the resistance influence the isolation of compartments, but not the detection of dendritic spikes.** A, The joint distribution of the somatic activation a_s and the maximal dendritic input U^* with different resistances. B, The probability of detecting a dendritic spike remains constant even if the resistance changes 2-3 orders of magnitude. Black circles: both somatic and dendritic resistances are altered; green diamonds: only resistance of the dendritic membrane (R^d_m) is changed while $R^s_m = 0.01$; red squares: somatic membrane resistance (R^s_m) is changed, $R^d_m = 0.01$. Although the distribution of the somatic activation scales with the resistance (see panel A and Eq. 4.7), the detection probability of a single dendritic event remains relatively constant. C, The joint distribution of the activation of a dendritic branch a_i and its own input U_i . When the resistance is low (left), the local activation depends only slightly on the input. Conversely, if the resistance is higher (right) the local input has substantial impact on the activation of the branch. D, The external influence decreases as the resistance increases. Symbols are the same as on panel B. Note, that decreasing the resistance of the perisomatic membrane (red squares) is the most efficient in separating the dendritic compartments (recall, that $R_s = R_a/R^s_m$). $N = 30$

dritic tree containing higher number of subunits the branches are electronically more isolated which is required for local plasticity. To keep the probability of dendritic spike detection high and the dendritic coupling low at the same time, the number of branches should therefore be as high as possible, but not higher than $N \approx 60$.

As we showed on Figure 4.4, the dendritic coupling depends on the resistance R, as high resistance separates better the subunits. Therefore we conclude, that a medium number of branches with relatively high resistance is ideal for parallel dendritic com-

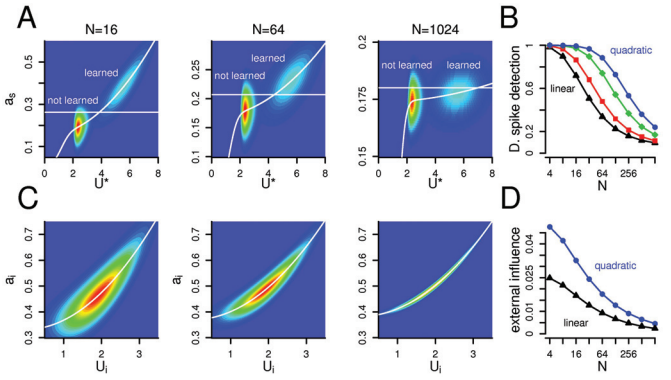

Figure 4.5: **Moderate number of branches allows the isolation of subunits and the detection of dendritic spikes.** A, The joint distribution of the somatic activation a_s and the maximal dendritic input U^* . As the number of branches grow (from left to right), the somatic depolarization caused by a dendritic spike in a single compartment decreases gradually. Consequently, if N is high, than the somatic threshold (horizontal line) can not separate small and large dendritic events. B, The probability of detecting a dendritic spike decreases as the number of dendritic subunits increases. Different colors indicate different degrees of nonlinearity (blue circles: quadratic; black triangles: linear integration function). C, The joint distribution of the activation of a dendritic branch a_i and its own input U_i. Increasing the number of compartments decrease the variance of the distribution and the impact of other branches. D, The external influence decreases with the number of branches both with linear (triangles) and quadratic (circles) integration function. $R = 0.3$

putations. The optimal number of dendritic subunits, however, depends on the size of the dendritic event determined by the local integration of the synaptic inputs (Fig. 4.5B). Appropriate detection of dendritic responses to learned patterns with linear integration is possible only in very small dendritic trees, whereas supra-linear integration allows the detection of individual dendritic events also in a larger dendritic arbor. Nonlinear integration by dendritic spiking therefore permits the neuron to selectively respond to a larger number of distinct input pattern.

4.3.4 Verification of the Model with Location Dependent Input

During the calculation above we assumed, that the activity of the presynaptic neurons are independent and that the samples from the distribution are uncorrelated. It

is known, however, that the firing of entorhinal neurons are not independent: At least half of layer II cells in the medial entorhinal cortex (EC) are grid cells, whose firing depend mostly on the position of the animal (Sargolini et al., 2006). Moreover, in reality animals do not face with discrete uncorrelated samples, but they experience the continuous change of their environment which is mirrored by the activity of the entorhinal neurons. In order to test our model under more realistic conditions, we simulated the activity of the rodent's EC during exploratory behavior as input to our modeled granule cell. The EC consisted of two neuron population: A population of grid cells (1000 neurons, 5 spacing, 5 orientations) representing a path integrator system (McNaughton et al., 2006) and a population of visual cells (1200 units), representing highly processed sensory information available in the EC (Burwell, 2000). In these simulations we used the $Webots^{®}$ mobile robot simulator (Michel, 2004).

The firing statistics of the entorhinal neurons was the same as used in the analytical calculation except that the activity of the neurons was location dependent. Moreover, as we simulated the trajectory of the rat during continuous foraging for randomly tossed food pellets (Leutgeb et al., 2007) the subsequent input patterns were highly correlated. We simulated a single granule cell with $N = 20$ dendritic branches each of them receiving a total number of $M = 100$ synaptic contacts from entorhinal neurons. The resistance was $R = 1$, we used the quadratic integration function and the neuron was tested in 5 different environments. During the 5 min. learning period (while 2000 spatial locations was sampled with an average running speed of 0.22 m/s) 0 - 8 branches learned usually at different spatial locations in each of the 5 environments. In most of the time synaptic plasticity in different branches occurred at different places, therefore the subunits were able to learn independently. Moreover, learning occurred only in naive branches, i.e., each branch learned only in one environment at a specific location and synapses of trained branches did not engage in learning at a different location. After the training period the synaptic weights of those branches that were subthreshold for synaptic plasticity ($\beta_d = 1.11$) in all environments were scaled down manually.

Next we studied the spatial activity pattern of the somatic and dendritic compartments while the robot was moving on a different track in the same environments. The dendritic branches responded with high activation ("dendritic spikes") to subsequent visit of places close to their preferred locations leading to the formation of dendritic place fields (Figure 4.6). Moreover, since the activation of the soma was substantially in-

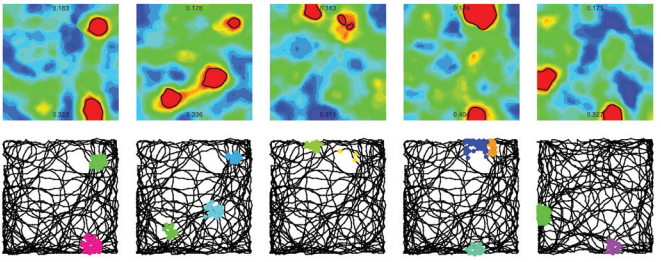

Figure 4.6: **Location dependent input and parallel dendritic computations generate multiple place fields.** The behavior of the same granule cell in five different environments (columns). Upper row: color-coded maps ("ratemaps") show the somatic activation on the 1x1 meter large maze. Red: high activation (spiking), blue: silent. The highest and the lowest value of the somatic activation is indicated on each ratemap. The places where the activation exceed the threshold ("place fields") are surrounded by black lines. We used the same, linear color-code in all panels. Lower row: the track of the robot and the location of the dendritic spikes. Dendritic place fields of different branches of the same neuron are marked by different colors. Somatic firing usually coincide with the activation of single dendritic branches.

creased in each of these dendritic place fields, the neuron had a multi-peaked activity map in several environments (Figure 4.6).

Finally we explored the effect of the size of the dendritic tree on the spatial firing pattern of the neuron (Figure 4.7). If there were only a few functional dendritic subunit than the neuron obviously had a small number of dendritic place fields (Fig. 4.7A), but the individual branches had strong influence on the somatic activity. Therefore the correlation between the somatic activation a_s and the maximal dendritic input U^* was high (Fig. 4.7B,C), as predicted by the analytical calculations. On the other hand, in neurons with large number of dendritic subunits there were more dendritic place fields (Fig. 4.7A), but a single branch had only a little impact on the activity of the neuron (Fig. 4.7D). Accordingly, the correlation between the maximal dendritic input and somatic activation was reduced (Fig. 4.7B). In these cases the cell fired when the overall excitation was high or when more than one branch were simultaneously excited. Therefore, the moderately branching dendritic tree of granule cells seems optimal for parallel dendritic computations since extensive branching inhibits the detection of individual dendritic events.

We conclude, that clustered plasticity together with dendritic spiking may be an ad-

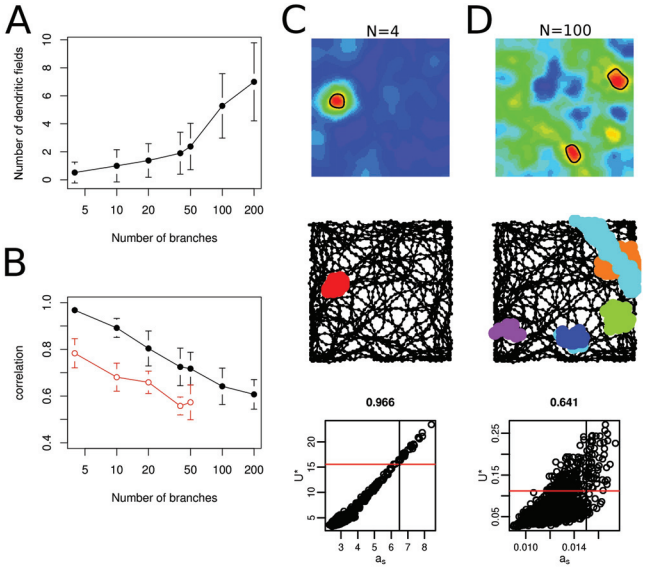

Figure 4.7: **Spatial firing patterns with different number of dendritic subunits.** A, The number of dendritic place fields increases with the number of subunits although the probability that one of the branches is supra-threshold for synaptic plasticity with naive synapses were kept constant. B, The correlation between the somatic activity (a_s) and the maximal input (U^*) decreases if the number of dendritic subunits increases. Open circles: correlation in environments where dendritic spikes were absent. Error bars on A and B show the standard deviation of 50 trials in 5 different environment. CD, Spatial firing patterns with $N = 4$ (C) and $N = 100$ (D) dendritic subunits. Upper and middle row is the same as on Fig. 4.6. Lower row: scatter plot showing the joint distribution of the somatic activation a_s and the maximal dendritic input U^*. Threshold for synaptic plasticity in the branches (horizontal line) and somatic firing (vertical line) are indicated. The correlation between the two variables is shown above the panels. If the neuron has a small number of dendritic subunits than the number of dendritic fields is small (A, C) but the activity propagates efficiently to the soma. Conversely, a neuron with a large number of dendritic subunits might have numerous dendritic fields, but the individual dendritic spikes have a little impact on the somatic activation.

equate cellular mechanism to explain the generation of multiple place fields in the DG.

4.4 Discussion

In this chapter we set up a statistical criteria to determine the effect of single dendritic events on the output of the neuron. Using this criteria we demonstrated that by supra-linear dendritic integration, given that branches have learned different input patterns, individual dendritic branches are able to trigger somatic firing. Next we have shown that high resistivity and large number of branches supports the segregation of dendritic subunits required for local plasticity. On the other hand, a single branch has a substantial effect on the output of the neuron only if the number of branches is sufficiently low. Finally using spatially organized input we have demonstrated that parallel computational subunits explain multiple, independent place fields of hippocampal granule cells.

4.4.1 Dendritic Spiking

Dendritically generated spikes mediated by voltage-gated Na^+ (Losonczy and Magee, 2006) and/or Ca^{2+} channels (Schiller et al., 1997) as well as glutamate-activated N-methyl-D-aspartate (NMDA) channels (Schiller et al., 2000) have been described in a variety of neurons (for a review see Hausser et al. (2000) or Johnston and Narayanan (2008)) including hippocampal granule cells (Fisher et al., 1990; Fricke and Prince, 1984; Blaxter et al., 1989; Schmidt-Hieber et al., 2004). We used a quadratic integration function in order to analytically model supra-linear dendritic integration (Archie and Mel, 2000) which differs from the sigmoid form of nonlinearity realized by dendritic spiking (Losonczy and Magee, 2006; Wei et al., 2001; Schiller et al., 2000). We believe, however, that at this level of abstraction the exact form of nonlinearity does not affect our results: As that is the difference between the dendritic responses to learned and not learned patterns that influence the somatic detection of dendritic events, a sigmoid integration function give qualitatively similar results (Ujfalussy et al., 2009). Moreover, we studied only passive interactions between individual dendritic events as the effect of voltage (Jung et al., 1997; Colbert et al., 1997) and calcium dependent currents (Cai et al., 2004; Tsay et al., 2007) regulating the

propagation of dendritic spikes were not included in the model. Future studies using a compartmental model equipped with dendritic spiking could support our results and clarify further details.

Our analysis has revealed that a moderately branched dendritic tree is optimal for the independent branches model, and we have shown that this mechanism could contribute to the spatial firing properties of granule cells in the DG. The dendritic tree of cerebellar Purkinje cells as well as the apical dendrites of hippocampal and neocortical pyramidal cells is typically larger, and more ramifying (Spruston, 2008). Their morphology is suitable for local plasticity within single branches (Golding et al., 2002; Harvey and Svoboda, 2007), and although it seems that individual branches may function as single integrative compartments (Losonczy and Magee, 2006; Wei et al., 2001; Ariav et al., 2003; Poirazi et al., 2003a), dendritic spikes localized to these compartments fail to propagate to the soma and directly influence the neuron's output (Vetter et al., 2001). Larger dendritic events, active spread of dendritic spikes towards the soma or interactions among dendritic subunits could contribute to the generation of somatic action potentials in this case. The dendritic tree of pyramidal neurons is, however, far more complex than that of granule cells: it has several morphological and functional subregions with different afferent inputs and membrane excitability (Spruston, 2008). Full understanding how their spatial firing characteristics arise from their cellular properties would require at least a different model structure and is beyond the scope of this study.

Whether individual dendritic events influence the output of the neuron depends - beyond the structure of the dendritic tree - on the size and the frequency of the large dendritic events and the output sparsity. The size of the events depends on the exact form of the dendritic integration function and the plasticity rule while the input statistics determine the frequency of such events. We have shown that given the sparseness of the output, sufficiently large, localized dendritic events arriving with appropriate frequency are able to separately determine the output of the neuron. Whether a local event is sufficiently large depends on the geometry of the dendritic tree: A smaller event may be sufficient if there are only a few subunits, or if the events actively propagate to a large part of the entire dendritic tree (e.g, the apical tuft in pyramidal neurons, (Williams, 2004)). Conversely, in neurons such as cerebellar Purkinje cells with large, ramifying dendritic tree, where individual events are localized to small branches, very large dendritic spikes would be required to influence the output. Indeed, detailed com-

partmental modelling of dendritic morphology revealed that the forward propagation of the action potential initiated in the apical trunk of pyramidal neurons was very effective, while in Purkinje cells dendritic action potentials were rapidly attenuated (Vetter et al., 2001).

4.4.2 Isolation of Branches

Clustered plasticity allows the neuron to simultaneously learn several different patterns but requires the electrical and/or biochemical isolation of the dendritic compartments (Larkum and Nevian, 2008; Govindarajan et al., 2006). However, the intracellular resistance (R_a) in dentate granule cells is relatively low and granule cells are usually regarded as electrically compact neurons (Schmidt-Hieber et al., 2007). Indeed, signal propagation from somata into dendrites *in vitro* is more efficient in granule cells compared with CA1 pyramidal cells and distal synaptic inputs from entorhinal fibers can efficiently depolarize the somatic membrane of granule cells (Schmidt-Hieber et al., 2007). However, *in vitro* studies do not take into account that neurons are embedded in a network of spontaneously active cells. As thousands of synapses bombard the dendritic tree *in vivo*, the dendritic membrane becomes "leakier" and, consequently, the membrane's space constant decreases significantly (Bernander et al., 1991). Moreover perisomatic inhibition (Sik et al., 1997) and feed-back excitation (via hilar mossy cells (Buckmaster et al., 1996)) further decrease the resistance of the proximal membrane contributing to the separation of the somatic and dendritic compartments (Williams, 2004; Chen et al., 1997). More specifically, we predict, that the membrane resistance of granule cells is considerably smaller at the perisomatic region than in the distal dendrites. Indeed, computational studies predict a 7-30 fold increase in the somatic leak conductance due to the synaptic background activity (Destexhe and Paré, 1999). On the other hand, large space constant at long terminal branches facilitate interactions among synapses distributed on the same branch. Therefore the long dendritic branches of dentate granule cells may act as single integrative computational subunits, separated from each other by the perisomatic region of the cell. Furthermore, in the present study we used steady-state approximations and we neglected temporal characteristics of the input and the integration. For rapidly varying inputs the coupling between dendritic sites and the soma is much smaller than for slowly varying currents since the distributed capacitance throughout the tree will absorb the charge before it reaches the soma (Koch, 1999). Therefore dendritic compartments

in a passive tree are more isolated for transient events, such as dendritic spikes, than for steady-state current. Finally, biochemical compartmentalization is likely to play a substantial role in the cooperative induction of LTP in both hippocampal (Harvey et al., 2008) and neocortical neurons (Gordon et al., 2006).

If, on the other hand, dendritic branches are not isolated during the learning process and synapses across the whole dendritic tree are modified simultaneously then different dendritic branches will be sensitive for different component (modalities) of the same episode. A new episode with partial overlap with the previously learned one may trigger dendritic spiking in the corresponding dendritic branch. As the somatic detection probability of dendritic spikes does not depend on the degree of electrical isolation (Figure 4.4), individual branches trigger somatic spiking, and, in this way the dentate gyrus contributes to the associative recall of the previously encoded episode in the hippocampus.

4.4.3 Synaptic Plasticity

Since the first description of LTP at perforant path - granule cell synapses (Bliss and Lømo, 1973) synaptic plasticity has become widely accepted as the physiological basis of memory (Martin et al., 2000). As Hebbian plasticity is intrinsically unstable, simply because it is a positive feed-back, multiple stability-promoting mechanisms have been proposed, including heterosynaptic depression (Stent, 1973; Lynch et al., 1977). Indeed, in the present model synaptic plasticity results in an average decrease of synaptic strengths (Fig. 4.3A), which have several functional consequences: First, as the dendritic response to untrained patterns and likewise the baseline activation of the cell decreases during training, the somatic detection of individual, large dendritic events becomes easier. Consequently, feature detection is less efficient in semi-trained neurons where synaptic weights at only a part of the dendritic tree has already been modified due to the learning precess. Therefore, in this model, appropriate training of each dendritic branch is required for proper functioning. Second, increased excitability stimulates learning in naive branches, while decreased responsiveness of previously trained branches prevents overlearning. Indeed, newly generated granule cells are more excitable than the neighboring old neurons (Schmidt-Hieber et al., 2004), and they are preferentially incorporated into functional networks in the dentate gyrus during acquisition of new memories (Kee et al., 2007).

One of the most interesting prediction of the present model is how the number of presynaptic spikes required for the postsynaptic induction of dendritic spiking changes during the course of learning. We can calculate this by dividing the total input U needed for dendritic spiking with the mean synaptic weight parameter (μ_w) before and after learning. Our model predicts, that while in young neurons the simultaneous occurrence of $\approx 70 - 80$ presynaptic spikes (randomly distributed across the presynaptic neurons) would trigger a postsynaptic dendritic spike, after learning (i.e., in matured neurons) two times more, $\approx 130 - 160$ would be required.

A recent study showed that the homeostatic regulation of the neurotransmitter release probability at neighbouring synapses depends on the local dendritic activity (Branco et al., 2008): Increased dendritic depolarization elicits a local homeostatic decrease in the release probability and vice versa. This mechanism may also prevent overlearning in trained branches, where dendritic spikes has sufficiently high rate, by reducing the excitability of that branch. On the other hand the same mechanism may stimulate learning new patterns in naive or disused branches where dendritic spikes are not present.

One of the key elements of our model was the local nature of the synaptic plasticity, i.e., the change of the synaptic weights was controlled by the local dendritic but not the somatic activity (Golding et al., 2002; Gordon et al., 2006; Harvey and Svoboda, 2007). Specifically, in hippocampal granule cells the induction of LTP was shown to be independent of the discharge of the neurons during the high-frequency stimulation (McNaughton et al., 1978). Our model predicts that, if the postsynaptic signal for synaptic plasticity is localized to individual dendritic branches than, due to the associative nature of the LTP, the synapses from entorhinal cells with overlapping firing become potentiated. If LTP is accompanied by structural remodeling, than the entorhinal neurons with overlapping place fields project to the same dendritic branches of granule cells as also proposed by (Hayman and Jeffery, 2008).

The variation in the strength of perforant path-granule cell synapses was found to be critical in the generation of multiple place fields in a recent modelling study (de Almeida et al., 2009). This heterogeneity caused a greater average synaptic excitation in a fraction of granule cells. The extra excitation therefore selects the subpopulation of neurons active within a given environment similar to the proposed role of contextual inputs in the model of Si and Treves (2009). One possible source of synaptic heterogeneity is synaptic plasticity (Song et al., 2000) which was also crucial in the present

model to amplify the local responses to learned patterns.

4.4.4 Hippocampal Circuitry

Hippocampal granule cells receive afferent fibers from the medial and the lateral portion of the entorhinal cortex, and these two pathways differ both in their pattern of termination (Forster et al., 2006; Amaral and Lavenex, 2007) and information content (Hargreaves et al., 2005). Fibers originating in the lateral EC display weak spatial selectivity and terminate on the most distal branches of granule cells, while medial entorhinal neurons innervate the middle third of their dendritic tree and show strong spatial selectivity (Hargreaves et al., 2005; Hafting et al., 2005). It has been recently suggested by modelling studies (Hayman and Jeffery, 2008; Si and Treves, 2009) that inputs originating from the lateral EC conveys contextual information to granule cells. In these models the contextual input select a subpopulation of neurons (or dendritic branches in Hayman and Jeffery (2008)) that can be activated within the given context (environment) while medial entorhinal fibers determine the exact location of the place fields. The selection of a subpopulation by contextual inputs can also contribute to the multiple firing fields of granule cells by reducing the number of available neurons within the given environment (Si and Treves, 2009; de Almeida et al., 2009). However, the spatial distribution of the individual place fields become regular (grid-like) if the multiple firing peaks are the consequence of an incomplete competition between neurons (Solstad et al., 2006), especially if the input grid cells are organized into a finite number of ensembles (Barry et al., 2007).

In this chapter we have shown that synapses, irrespective of their origin, arriving at different branches of hippocampal granule cells can be modified at different spatial locations. We have also shown, that in granule cells each dendritic branch is able to activate the neuron, therefore each subfield on the cell's multi-peaked activity map corresponds to a dendritic place field. The segregation of contextual and positional information could explain the sensitivity of the subfields to contextual manipulations (Leutgeb et al., 2007; Hayman and Jeffery, 2008) and is consistent with the role of DG in context discrimination (McHugh et al., 2007).

Along with the laminar organization of excitatory input, different interneurons innervate different dendritic domains of granule cells (Halasy and Somogyi, 1993; Freund and Buzsáki, 1996). It appears, that distinct types of interneurons have evolved to se-

lectively and locally modulate the computations performed by the postsynaptic membrane (Sik et al., 1997; Somogyi and Klausberger, 2005). According to our model, basket and axo-axonic cells may continually adjust the inhibitory drive such that the mean activity of the population remains nearly constant; HICAP cells, targeting the proximal dendritic domain of granule cells together with the excitatory mossy cells (Buckmaster et al., 1996) may increase electrical isolation of distal dendritic regions by raising the conductance of the proximal membrane; whereas MOPP and HIPP cells associated with the entorhinal afferents may contribute to the de-inactivation of calcium channels required to dendritic spiking by providing rhythmic hyperpolarization to distal dendritic branches.

4.4.5 Functional Consequences

What is the additional computational power gained from the present model? We argue, that smaller and uncorrelated place fields may help pattern separation in the dentate gyrus. Theoretical considerations suggest that the DG contributes to the hippocampal storage of new episodes by producing sparse representations via competitive learning (Treves and Rolls, 1994; Acsády and Káli, 2007; Treves et al., 2008). It was demonstrated by modelling studies that competitive learning on spatially organized input results in the formation of place fields (Rolls and Kesner, 2006; Solstad et al., 2006; Si and Treves, 2009) that is a sparse and nearly orthogonal representation of the input space. In this study we proposed that parallel dendritic computations explain the formation of multiple, independent place fields of hippocampal granule cells even within a relatively small environment (Jung and McNaughton, 1993; Leutgeb et al., 2007).

Pattern separation by the DG can be more efficient if granule cells have multiple, irregularly placed fields and the individual fields are smaller. The neural representation of neighbouring locations is more similar if neurons have one, larger field than if they have several but smaller fields (Ujfalussy et al., 2009). In our model the place fields of dendritic branches are analogous with the single place field of an electrically compact neuron. The multi-peaked somatic firing of granule cells mirrors the several *dendritic fields* of the same neuron. We argue, that if the size of the somatic firing fields is limited by competition between simultaneously active neurons (Takahashi and Sakurai, 2007), then the place fields of granule cells could be smaller than the corresponding

dendritic fields. If the individual place fields of granule cells become smaller, than the neural representation of adjacent places becomes less correlated which further increase the pattern separation ability of the DG. Therefore independent dendritic subunits increase the computational power of the DG while keeping the number of cells and their sparsity constant. Moreover, clustering of different inputs into different dendritic domains could explain the remapping of hippocampal place cells under several experimental conditions (Leutgeb et al., 2007; Hayman and Jeffery, 2008).

The impact of both dendritic nonlinearity and clustered plasticity on the computational power of neurons was rarely addressed by modeling studies. Poirazi and Mel (2001) predicted, that nonlinear dendritic integration with local (structural) plasticity rule increase the representational capacity of neural tissue. They showed on binary input, that the number of attainable input-output functions (representational capacity) is maximal if the neuron has many, relatively short branches, and the performance of the model in a linear classification task correlates remarkably well with the logarithm of representational capacity. However, in order to approach the combinatorial bound of the representational capacity in a neural tissue and to amplify slight differences in the input extremely large subunit nonlinearity was required (they used $F(U) = U^{10}$). In the present study we showed that a moderate increase in the memory-capacity can be achieved with local, Hebbian learning rule and slightly supra-linear dendritic integration. We emphasized that under certain conditions a single branch is able to evoke somatic output. However, if the amplitude of the individual events is smaller, a larger spatial extent involving the depolarization of additional branches will be required to trigger output spiking. This mechanism could induce a combinatorial increase in the representational capacity as shown by Poirazi and Mel (2001).

According to our model hippocampal granule cells can be regarded as a two layer neural network of abstract integrate and fire elements: In the first layer corresponding to the terminal branches the units integrate separately their inputs and they innervate a common output unit (second layer, the somatic compartment) that implements a logical OR computation. The idea that a dendritic tree may perform logical computations was originally proposed by Koch et al. (1983) to explain directional selectivity of retinal ganglion cells. Shepherd and Brayton (1987) further elaborated this approach but instead of branches they used dendritic spines as basic computational subunits. Our approach is more similar to how Poirazi et al. (2003b) describe hippocampal pyramidal cells, however, in that model the output unit performs (nonlinear) summation prior

to final thresholding. Another similar model was proposed by Gasparini and Magee (2006), in a paper where they showed that the apical trunk of hippocampal pyramidal neurons integrate spatially clustered and synchronously arriving synaptic inputs nonlinearly, whereas distributed or asynchronous inputs are linearly integrated. They suggest that processing in the nonlinear mode could functionally separate the dendritic arbor into a large number of independent nonlinear computational units, each sending its own output to the soma. In the present study, we showed that a single computational units is powerful enough to determine the output of the neuron only if there are not too much similar units ($N < 100$) and if the local integration is sufficiently nonlinear.

A similar picture emerged form a recent series of *in vitro* experiments performed on the basal dendrites of neocortical pyramidal neurons: These branches behave as independent computational subunits as nearby inputs on the same branch summed sigmoidally due to the presence of local NMDA spikes (Polsky et al., 2004; Schiller et al., 2000; Nevian et al., 2007) and synaptic plasticity required the pairing of local NMDA spikes with biochemical signals (Gordon et al., 2006). Moreover, an NMDA-spike localized to a single basal dendrite could efficiently induce somatic UP-state like depolarization accompanied by bursts of action potentials (Milojkovic et al., 2005). These results suggest that our model describes remarkably well the neuronal computations performed by the basal dendritic tree of pyramidal neurons. More recently, NMDA spikes with similar properties have been described in the fine distal tuft dendrites of these neocortical pyramidal neurons (Larkum et al., 2009). The authors suggest that there are two major site for integration of basal and apical dendritic inputs: the apical calcium and axosomatic sodium integration points (Larkum et al., 2009).

4.4.6 Experimental Predictions

Although we tried to fit our model to the available experimental data we had to make some assumptions regarding the integration of neighbouring inputs in dentate granule cells. Moreover, based on the model described in this chapter we make some explicit predictions. Both the assumptions and the predictions of our model should be tested experimentally.

1. Large synaptic inputs induce a nonlinear increase in the activation of the terminal branches of dentate granule cells. The form of the dendritic integra-

tion function in granule cells, like in pyramidal neurons (Losonczy and Magee, 2006; Schiller et al., 1997, 2000), could be determined by patch-clamp recordings from hippocampal slices.

2. Dendritic spiking in individual branches of young versus old granule cells can be triggered by at least 70 - 80 versus 130 - 160 simultaneous presynaptic spikes, respectively. The unitary EPSCs and the failure rates (Bartos et al., 2001) at the perforant path synapses should be determined and compared with the current required for the initiation of dendritic spiking in young and old granule cells.

3. Individual dendritic branches of dentate granule cells function as a single integrative compartment. *In vitro* experiments using two-photon imaging and glutamate uncaging (Polsky et al., 2004; Losonczy and Magee, 2006; Milojkovic et al., 2005) could be used to test this prediction.

4. The dendritic branches of dentate granule cells are isolated from each other - at least during training - by the low input resistance of the perisomatic region. Simultaneous recording from the soma and different branches (Milojkovic et al., 2005) together with perisomatic conductance injection (Williams, 2004) or detailed compartmental model paying attention to interneuronal firing rates and anatomical connectivity could determine the degree of isolation between the individual branches.

5. As the result of the local Hebbian learning rule, we predict that the presynaptic entorhinal cells with overlapping firing project to the same dendritic branches of the granule cells.

6. Different place fields of dentate granule cells are caused by excitation through different dendritic branches. This prediction could be tested *in vivo* using high resolution electrode arrays and single-cell current source density analysis (Takahashi and Sakurai, 2007; Somogyvari et al., 2005) or fiberoptic system combined with fluorescent dyes (Murayama et al., 2007, 2009).

4.5 Methods

4.5.1 Estimation of the Membrane Parameters for Hippocampal Granule Cells

We used the data from Schmidt-Hieber et al. (2007) to estimate the passive membrane parameters of the granule cells the DG (Table 4.1). First we computed the membrane area of a single branch (A_{dend}) falling into the perforant path termination zone (the outer two third of the dendritic tree):

$$A_{dend} = \frac{2}{3}\frac{\alpha l_d d_b \pi}{N} = 310\ \mu m^2, \tag{4.12}$$

where l_d is the total length of the dendritic tree, $d_b = 1.1\ \mu$m is the average diameter of a single branch, N is the number of branches and $\alpha = 1.9$ is a correction factor for the membrane area of dendritic spines. Similarly, the area of the somatic compartment (A_{soma}), assuming a sphere with diameter d_s:

$$A_{soma} = d_s^2 \pi = 315\ \mu m^2. \tag{4.13}$$

The area of the cross section of a single branch is $A_b = d_b^2\pi/4$, and the length of the proximal third of the branches, that do not receive input from the entorhinal cortex is $l_{ds} = 50\ \mu$m. Finally, we estimate the parameters in Eqs. 4.1-4.2:

$$R_m^s = \mathbb{R}_m / A_{soma} = 12.1\,\mathrm{G\Omega} \tag{4.14}$$

$$R_m^d = \mathbb{R}_m / A_{dend} = 12.3\,\mathrm{G\Omega} \tag{4.15}$$

$$R_a = R_i l_{ds} / A_b = 102\,\mathrm{M\Omega} \tag{4.16}$$

where $\mathbb{R}_m$ and R_i are the membrane resistance and the intracellular resistivity, respectively. As the somatic and the dendritic membrane area (and hence the resistance) were similar, we used that $R_m = R_m^s = R_m^d$. The parameter R used in our calculations was $R = R_a / R_m 0.01$ for a passive granule cell in the DG. Note that due to the synaptic conductances activated *in vivo* the membrane resistance of neurons is certainly lower than the *in vitro* estimates (Destexhe and Paré, 1999).

4.5.2 Estimation of the Synaptic Input

A single dentate granule cell receive synaptic input from $n_{\mathrm{EC-DG}} \approx 2500 - 4000$ entorhinal layer II cells distributed on $N \approx 25 - 40$ branches, whereas a single branch

Table 4.1: **Membrane parameters of hippocampal granule cells.**

Parameter	Description	Value
N	Number of branches	32 ± 3
M	Num. of presynaptic terminals/branches	100
$\mathbb{R}_m$	Membrane resistance (kΩcm^2)	38 ± 2.3
R_i	Intracellular resistivity (Ωcm)	194 ± 24
l_d	Total length of dendritic tree (μm)	2264 ± 133
d_b	diameter of branches: proximal, distal (μm)	$1.51 \pm 0.11, 0.73 \pm 0.04$
d_s	diameter of the soma (μm)	10
a	Surface area (1000μm^2)	13.3 ± 0.9
α	The increase of the surface area by dendritic spines (%)	190

Electrophysiological data from Schmidt-Hieber et al. (2007) used to estimate the parameters of the model.

receives $M \approx 100$ synapses in the rat's hippocampus (Schmidt-Hieber et al., 2007). According to Amaral and Lavenex (2007), there are $n_{\mathrm{DG}} \approx 1.2 \cdot 10^6$ granule cells in the rat's DG, and $n_{\mathrm{EC}} \approx 0.11 \cdot 10^6$ projection cells in the layer II of the entorhinal cortex. It is known, that a given location in the hippocampus may receive inputs from more than 25% of the dorsomedial- to-ventrolateral axis of the medial entorhinal cortex (Dolorfo and Amaral, 1998; Witter et al., 1989). Therefore, while a single dendritic branch get its $M \approx 100$ synaptic inputs randomly from nearly 25000 entorhinal cortical neuron, we assume that each synapse on a dendritic branch comes from different entorhinal neurons.

By electrical recordings from different hippocampal regions one can estimate the proportion of simultaneously active cells within a reasonable time window. We call this number the sparseness of the representation in the given area. Specifically, 1–5% of the granule cells are active simultaneously in the DG (Barnes et al., 1990; Jung and McNaughton, 1993), therefore we used $sp_{\mathrm{DG}} = 0.05$. The sparseness of the entorhinal input is somewhat larger, $sp_{\mathrm{EC}} = 0.2$ (Frank et al., 2001; Fyhn et al., 2004; Sargolini et al., 2006).

Experimental data provide a good estimate for the mean firing rate of these neurons, however, they give the variance of the mean across neurons, but not the variance in the firing rate of individual cells. To estimate the variance in the firing rate of an individual cell, we generated random spike trains based on the ISI histogram on Fig. 5

of Frank et al. (2001). The expected value and the variance of the number of spikes in a $100\,\mathrm{ms}$ time bin (corresponding to one period of the hippocampal theta rhythm) was $\mu_{EC'} = 0.32$ and $\sigma^2_{EC'} = 0.4$ and there was at most 4 spikes during $100\,\mathrm{ms}$ in the case of an entorhinal excitatory cell. We scaled these values relative to the maximal firing rate, so we had $\mu_{EC} = \mu_{EC'}/4 = 0.08$ and $\sigma^2_{EC} = \sigma^2_{EC'}/16 = 0.025$ characterizing the distribution of the presynaptic firing u_j. Possible differences in firing statistics across different (medial-lateral or dorsal-ventral) regions in the EC and across individual neurons are neglected here.

Next, we start with originally equal synaptic weights, $\forall w_{ij} = w = 3 \cdot \mu_{EC}$. In this case, if we assume that the firing of entorhinal neurons are independent and identically distributed, we can approximate the total input to a branch with a Gaussian distribution:

$$U = \sum_{j=1}^{M} w u_j = w \sum_{j=1}^{M} u_j = 3\mu_{EC} \sum_{j=1}^{M} u_j,$$
$$p[U] = \mathbb{G}(U|3M\mu^2_{EC}, 3^2\mu^2_{EC}M\sigma^2_{EC}) = \mathbb{G}(U|\mu, \sigma^2), \tag{4.17}$$

where $\mu = 3M\mu^2_{EC} = 1.92$ and $\sigma = 3\mu_{EC}\sigma_{EC}\sqrt{M} = 0.38$. The distribution of the total input U is shown on Fig. 4.1C.

Synaptic Input after Learning. Learning alters the distribution of the total input $U_i = \sum_j w_{ij}u_j$ of dendritic branches (Eq. 4.17) by modifying synaptic weights. From Eq. 4.11 used to describe synaptic plasticity, we can see that synaptic weights converge to a fixed point $w_{ij} = u_j$ whenever the activity of the postsynaptic branch i is above threshold β_d. In the stationary state, the weight vector $\overline{w}_j$ reflects a presynaptic firing pattern $\overline{u}$. In other words, the learned presynaptic firing pattern is stored in the corresponding synaptic weights.

In order to stimulate initial plasticity in naive branches and prevent learning in those branches that have already learned a pattern, we initialized the synaptic weights to $w_{ij} = w = 3\mu_{EC}$, which is higher than their expected value at the fixed point (μ_{EC}). This initialization ensured that the response (U) to unlearned inputs decrease during the process of learning, and prevented interference in branches that already have learned a specific pattern. Indeed, synaptic plasticity is enhanced in newly generated granule cells of the hippocampus compared with mature neurons already integrated into functional circuits (Schmidt-Hieber et al., 2004; Song et al., 2005; Kee et al., 2007).

After learning we can approximate the distribution of the total synaptic input U to a branch by the sum of two Gaussians representing the total input in the case of learned ($\mathbb{G}_l$) and not learned patterns ($\mathbb{G}_n$), respectively:

$$p[U] = p_l \mathbb{G}_l(U|\mu_l, \sigma_l^2) + p_n \mathbb{G}_n(U|\mu_n, \sigma_n^2), \tag{4.18}$$

where p_l (p_n) is the probability that one of the branches receive a learned (not learned) input, and μ_l and σ_l^2 (μ_n and σ_n^2) are the mean and the variance of the response to learned (not learned) inputs. If we have a finite number (N_S) of different inputs, and each branch learns one of them, then

$$p_n = \frac{N_S - 1}{N_S} \qquad p_l = \frac{1}{N_S}. \tag{4.19}$$

Distribution of the total input to the dendritic branches before and after learning is shown on Figure 4.3A. Parameters $\mu_n = 1$, $\sigma_n = 0.39$, $\mu_l = 5.6$ and $\sigma_l = 0.58$ were estimated numerically based on the reconstructed firing characteristics of entorhinal neurons. We assumed that each branches learned one of the samples and the probability that one of the branches receive its learned input (N/N_S) was the sparseness in the DG ($sp_{\mathrm{DG}} \approx 0.05$). Note, that the distribution of $\mathbb{G}_l(U)$ is the theoretical distribution of the responses to learned inputs, from which each branch draw only a few (perhaps one) sample because learning is very sparse.

We recalculated the two functions $H(U)$ and $K(U^*)$ with the new input distributions by replacing μ and σ with μ_n and σ_n in Equations 4.9-4.10 and 4.27-4.28, and by changing the distribution of U in Eq. 4.29 from Eq. 4.17 to Eq. 4.18. In these calculations, we neglected the possibility that two (or more) branches may both get their learned input at the same time. Finally, we determined the firing threshold by solving the following integral to β (see Eq. 4.24-4.25):

$$p[a_s > \beta] = \int_\beta^\infty \int p[a_s, U^*] \mathrm{d}U^* \mathrm{d}a_s = sp_{\mathrm{DG}}. \tag{4.20}$$

4.5.3 Criteria for Independent Firing

In the case of continuous variables we can write that $H(U_i) = H(U)$. The function $H(U)$ has the form:

$$\mathrm{H}(U) = p[a_s > \beta|U] = \int_\beta^\infty p[a_s|U] \mathrm{d}a_s. \tag{4.21}$$

The conditional probability $p[a_s|U]$ has a form similar to Eq. 4.8, except that we have only $N-1$ random variables from the Gaussian distribution of U (Eq. 4.17) with parameters μ_F and σ_F^2, therefore we can write that:

$$p[a_s|U] = \mathbb{G}\left(a_s|\frac{(N-1)\mu_F + F(U)}{R+N+1}, \frac{(N-1)\sigma_F^2}{(R+N+1)^2}\right). \tag{4.22}$$

We can compute the second function $K(U^*)$ as follows:

$$\mathrm{K}(U^*) = p[U^*|a_s > \beta] = \frac{p[U^*, a_s > \beta]}{p[a_s > \beta]} \tag{4.23}$$

$$p[a_s > \beta, U^*] = p[a_s > \beta|U^*]p[U^*] \tag{4.24}$$

$$p[a_s > \beta|U^*] = \int_\beta^\infty p[a_s|U^*]\mathrm{d}a_s, \tag{4.25}$$

where $p[a_s|U^*]$ is the conditional distribution of the somatic activation a_s and the maximal dendritic input U^*. The distribution $p[a_s|U^*]$ is similar to the distribution of $p[a_s]$ in Eq. 4.8 with two important differences: First, we have only $N-1$ random variables. Second, we know that $\forall U < U^*$, therefore the distribution of the inputs to other branches is different from the Gaussian in Eq. 4.17. Hence we can write, that

$$p[a_s|U^*] = \mathbb{G}\left(a_s|\frac{(N-1)\mu_F^* + F(U^*)}{R+N+1}, \frac{(N-1){\sigma_F^*}^2}{(R+N+1)^2}\right), \tag{4.26}$$

where μ_F^* and ${\sigma_F^*}^2$ are the conditional expectation and variance of the distribution $p[F(U)|U < U^*]$. We calculate μ_F^* and ${\sigma_F^*}^2$ by integrating Equations 4.9-4.10 from $-\infty$ to U^*:

$$\mu_F^* = \lambda(U^*)\int_{-\infty}^{U^*} p[U]F(U)\mathrm{d}U = \lambda(U^*)\int_{-\infty}^{U^*} \mathbb{G}(U|\mu,\sigma^2)F(U)\mathrm{d}U, \tag{4.27}$$

$${\sigma_F^*}^2 = \lambda(U^*)\int_{-\infty}^{U^*} \mathbb{G}(U|\mu,\sigma^2)(F(U)-\mu_F)^2\mathrm{d}U, \tag{4.28}$$

where $\lambda(U^*) = 1/\int_{-\infty}^{U^*} p(U)\mathrm{d}U$ is a normalization factor. Finally we calculate the last term of Eq. 4.24, the distribution of U^* as follows:

$$p[U^*] = \left[(P(U))^N\right]' = \left[\left(\frac{1}{2} + \frac{1}{2}\mathrm{erf}\left\{\frac{U-\mu}{\sqrt{2}\sigma}\right\}\right)^N\right]' \tag{4.29}$$

where $P(U)$ is the cumulative distribution function (CDF) of U and $[X]'$ marks derivation. The intuition behind Equation 4.29 is that: First, $P(U)$ is the probability that a given input is smaller than U. Second, $P(U)^N$ is the probability that all inputs are smaller than U, also the (CDF) of U^*. Third, its derivative $\left[P(U)^N\right]'$ gives us the probability density function (PDF) of U^*. The PDF of U is a Gaussian function, its CDF can be expressed with the Gauss error function (erf{}).

4.5.4 Coupling Between Dendritic Subunits

To calculate the dependence of the dendritic activation on the inputs, we first repeat Eq. 4.6:

$$a_i = \frac{RF(\mathbb{G}(U_i|\mu,\sigma^2)) + a_s}{R+1}. \tag{4.30}$$

Next, we substitute a_s in Equation 4.30 with Eq. 4.7:

$$\begin{aligned} a_i &= \frac{RF(\mathbb{G}(U_i|\mu,\sigma^2)) + \frac{\sum_{j=1}^{N} F(U_j)}{R+N+1}}{R+1} = \\ &= \frac{R}{R+1}F(U_i) + \frac{F(U_i) + \sum_{j\neq i} F(U_j)}{(R+1)(R+N+1)} \\ &= F(U_i)\left(\frac{R}{R+1} + \frac{1}{(R+N+1)(R+1)}\right) + \frac{\sum_{j\neq i} F(U_j)}{(R+1)(R+N+1)}. \end{aligned} \tag{4.31}$$

The two terms of the sum in Eq. 4.31 are independent, because U_i is independent from U_js, therefore we can calculate the distribution of a_i by the convolution of two distributions (corresponding to the two terms in the sum). The second term in Eq. 4.31 is the sum of independent random variables and we approximate it with a Gaussian (similarly as we did it for a_s previously, Eq. 4.8). The distribution of U_i is a Gaussian (Eq. 4.17), that we can transform into the first term of Eq. 4.31 by a Jacobian factor (Bishop, 2006):

$$p_V(V) = p_U(U)\left|\frac{\mathrm{d}U}{\mathrm{d}V}\right|, \tag{4.32}$$

where $V = F(U)$. We get the distribution $p(a_i|U_i)$ by substituting the first term of Eq. 4.31 by a Dirac delta distribution. Similarly, we can calculate $p(a_j|U_i)$ by first computing a conditional sum in the second term ($U_j + \sum_{k\neq\{i,j\}} U_k$) as described by Eq. 4.22 and then performing the convolution.

Part III

Canon

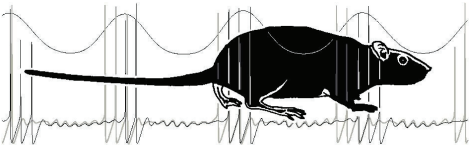

5

Conclusions and main results

In this very last chapter we try to link the three levels of investigations described in the present dissertation. At the beginning of the chapter we give a short overview of our results emphasizing the main contributions to the field.

5.1 Main Results

5.1.1 Hippocampal theta

In Chapter 2 we gave a model for the medial septal circuitry involved in the generation of the hippocampal theta oscillation. According to this model medial septal neurons are able to pace the hippocampal oscillations by rhythmically driving hippocampal interneurons during type II (atropine sensitive) theta. During type I (atropine resistant, locomotion related) theta medial septum is in a good position to intensify the hippocampal theta by resonance mechanism and to increase the coherence of the oscillation across the hippocampal formation. In the following list we describe the proposed role of each element in the septo-hippocampal theta-generating circuit. The first two items are highlighted as they serve as theses of the present dissertation.

- *Septal glutamatergic neurons, endowed with intrinsic cluster-firing property, form a pacemaker network for the septo-hippocampal theta rhythm.*

- *Septal GABAergic fast-spiking neurons show bursting behavior due to emergent network dynamics: a subpopulation of these cells is driven by rhythmic EPSPs originating from the local glutamatergic pacemaker network; the other subpopulation is driven by IPSPs from the first GABAergic subpopulation.*

- The two GABAergic subpopulations fire at opposite phases of the hippocampal theta rhythm. They innervate different classes of hippocampal interneurons and transmit the septal rhythm to the hippocampus.
- The hippocampal network resonate with the septal drive and amplify it; it may also generate intrinsic oscillations.
- The hippocampo-septal feed-back loop may regulate the frequency and the strength of the septal drive or it may recruit septal neurons that amplify oscillations intrinsic to the hippocampus.
- Cholinergic neurons have slow, permissive action on both septal and hippocampal theta generating circuit.

5.1.2 Associative Memory for Places

In Chapter 3 we described an entorhino-hippocampal reciprocal loop where the integrated place representation in the hippocampus is used to correct for the accumulating noise in the entorhinal path integration system. The same mechanism could contribute to the associative retrieval of an episode based on a partial cue available during the recall. In the following list we point out our main results serving as theses of the present dissertation.

- *Feed back connections from the integrated place cell representation in the hippocampus account for the robust, noise-free path integration realized by the grid cells in the entorhinal cortex.*
- *Parametric changes in grid cell activity following morphing of the environment and remapping of place cells in a new environment are the result of a reciprocal interaction between hippocampal place- and entorhinal grid-cell activities.*

5.1.3 Spatial Representation

In Chapter 4 we studied whether individual dendritic branches, beside being integrative compartments, are able to *individually* influence the output of the neuron. We built a simplified computational model and calculated that in certain neurons relatively

small dendritic branches were able to independently trigger somatic firing. Therefore in these cells an action potential mirrors the activity of a small dendritic subunit rather than the input arriving to the whole dendritic tree. These neurons can be regarded as a network of a few independent integrator units connected to a common output unit. We demonstrated that a moderately branched dendritic tree of hippocampal granule cells may be optimized for this parallel computation. Finally, we showed that these parallel dendritic computations could explain some aspects of the location dependent activity of hippocampal granule cells.

In the following list we point out the main results of Chapter 4 serving as theses of the present dissertation.

- *Triggering somatic firing by a relatively small dendritic branch requires the amplification of local events by dendritic spiking and synaptic plasticity.*
- *The moderately branching dendritic tree of granule cells seems optimal for this computation since larger dendritic trees favor local plasticity by isolating dendritic compartments, while reliable detection of individual dendritic spikes in the soma requires a low branch number.*
- *These parallel dendritic computations could contribute to the generation of multiple independent place fields of hippocampal granule cells.*

5.2 Interactions

5.2.1 Theta Oscillation and Information Processing

Based on results presented in Chapter 2 we suggest that neurons in the medial septum are able to generate a coherent theta oscillation within the hippocampal formation. Theta-synchronized synaptic inputs arriving on the somatic and the dendritic membrane of principal cells may support neural computations within the hippocampus in several ways (Lengyel et al., 2005a; Buzsáki, 2006). The periodic hyperpolarization of principal cells throughout the hippocampal formation contribute to the segmentation of the inputs and the internal dynamics into temporally distinct but correlated *frames*. These frames correspond to the time steps used in many large-scale models of information processing (e.g., Treves and Rolls (1994); Arleo and Gerstner (2000)) including those presented in Chapters 3-4. During each theta cycle a new winner-take-all process starts in the dentate gyrus and a different population of neurons is activated than in the previous cycle according to the slightly changed input conditions and internal state of the network. The theta periodic inhibition between frames partially resets the state of the network and contributes therefore to the dynamics of cell assembly formation. This effect is more pronounced in the CA3 region where the internal dynamics of the attractor network is repeatedly interrupted by an external theta periodic inhibition to restart the internal dynamics with new initial conditions (Tsodyks et al., 1996). Dynamics of cell assembly formation, which give rise to the phase precession phenomenon at the single cell level (O'Keefe and Recce, 1993; Skaggs et al., 1993; Dragoi and Buzsáki, 2006; Diba and Buzsaki, 2008) may reflect these intrinsic hippocampal computations also in an abstract "memory" space (Eichenbaum et al., 1999; Buzsáki, 2005).

Hippocampal interneurons have a substantial role in shaping the temporal dynamics of the network (Somogyi and Klausberger, 2005). The firing of interneurons in the hippocampal formation is strongly modulated by the theta rhythm (Csicsvári et al., 1999; Klausberger et al., 2003) leading to the synchronous discharge of principal cells within hippocampal subregions (Skaggs et al., 1996; Frank et al., 2001). The relative synchronization of presynaptic spikes by hippocampal theta allows the temporal integration of the postsynaptic potentials in our model (Chapter 4) despite the relatively small time constant of granule cells' membrane (Schmidt-Hieber et al., 2007). Moreover, the synchronization of synaptic inputs can also influence the form of dendritic

integration by switching from linear to nonlinear integration (Gasparini and Magee, 2006).

Effective transfer and processing of information requires interactions between cortical and hippocampal cell assemblies. This temporally organized "communication" between cortical regions is also reflected by the coordinated oscillatory activity among them (Sirota et al., 2003; Battaglia et al., 2004a; Isomura et al., 2006; Peyrache et al., 2009). Neurons, for example in the prefrontal cortex are phase locked to the hippocampal theta rhythm (Siapas et al., 2005; Hyman et al., 2005) and the correlated firing in the two structures is selectively enhanced during behavior that recruits spatial working memory (Jones and Wilson, 2005). The precise coordination of the timing of neural firing throughout the brain might be critical for information processing: the efficacy of synaptic inputs in the hippocampus (Wyble et al., 2000), the magnitude (Pavlides et al., 1988; Orr et al., 2001) and even the direction (Hyman et al., 2003) of long-term synaptic modification varies according to the phase of the ongoing theta oscillation. These theta related changes in the dynamics of the hippocampal circuit provide a plausible mechanism to separate encoding from retrieval (Hasselmo et al., 2002) and thus to prevent interference between old and new memories (Wallenstein and Hasselmo, 1997). Moreover, on the system level, the phase lag between the ongoing theta oscillations at the interacting regions influence the information being transferred: The theta phase determines whether representations of current or upcoming locations are read by the decoder (Jensen, 2001). Although theta oscillation was not incorporated in the models presented in Chapters 3-4, extending these models with temporal dynamics could be an exciting direction for future research.

5.2.2 Representation and Associative Memory

Although neurons in multiple subregions of the hippocampus, including the dentate gyrus and the CA regions, show location dependent firing, there are subtle differences in the fine details of their spatial receptive fields reflecting their specific role in information processing. For example, place fields are more often bidirectional on linear tracks in CA3 than in CA1 (Dragoi and Buzsáki, 2006), the population codes in the CA3 change more abruptly and coherently after environmental alternations compared to the gradual changes in the CA1 (Lee et al., 2004; Leutgeb et al., 2004; Vazdarjanova and Guzowski, 2004) and when moving from one environment into the other,

the CA3 representation of the second environment is biased toward the activity patterns that represent the first one (Leutgeb et al., 2005a). These findings underscore the early theoretical suggestions that the recurrent connectivity in the CA3 region forming an autoassociative attractor-based neural network is critical for spatial and episodic memories (Marr, 1971; Treves and Rolls, 1994; Nakazawa et al., 2002). Based on quantitative statistical analysis Treves and Rolls (1991) (see also Rolls et al. (1997)) suggested that orthogonalization and sparsification of signals before their presentation to autoassociative networks decrease the interference between the patterns stored and therefore increase the capacity of the network. It was proposed, that the dentate gyrus performs this function (Gilbert et al., 2001; McHugh et al., 2007). In section 4.4.5 we argued that larger number of smaller and uncorrelated place fields may help pattern separation in the dentate gyrus which, in turn, increase the efficacy of the autoassociative network in the CA3. A more accurate spatial representation in the hippocampus also increase the precision of the hippocampo-entorhinal feed-back projections used in Chapter 3 to correct the errors accumulated in the path integration system.

A

Appendix

A.1 The membrane dynamics of medial septal neurons

Membrane potential change of the cluster-firing model taken from Wang (2002) is given by the following current balance equation:

$$C_{\mathrm{m}}\mathrm{d}V/\mathrm{d}t = -I_{\mathrm{Na}} - I_{\mathrm{K}} - I_{\mathrm{KS}} - I_{\mathrm{L}} - I_{\mathrm{syn}} + I_{\mathrm{ext}} \tag{A-1}$$

where $C_{\mathrm{m}} = 1\mu\mathrm{F/cm}^2$, I_{syn}, the synaptic and I_{ext}, the external currents are described in the Methods section. The leakage current is described by the following equation: $I_{\mathrm{L}} = (V - E_{\mathrm{L}})/R_{\mathrm{m}}$, where $R_{\mathrm{m}} = 1\,\Omega/\mathrm{m}^2$ and $E_{\mathrm{L}} = -50\,\mathrm{mV}$.

The three voltage-dependent currents were described by the Hodgkin-Huxley formalism where the gating variable x satisfies a first order kinetics: $\mathrm{d}x/\mathrm{d}t = \\ = \alpha_{\mathrm{x}}(V)(1-x) - \beta_{\mathrm{x}}(V)x \equiv (x_{\mathrm{inf}}(V) - x)/\tau_{\mathrm{x}}(V)$. The sodium current ($I_{\mathrm{Na}}$) was in the standard form:

$$I_{\mathrm{Na}} = g_{\mathrm{Na}} m_{\mathrm{inf}}^3 h(V - E_{\mathrm{Na}}) \tag{A-2a}$$

$$m_{\mathrm{inf}} = \alpha_{\mathrm{m}}/(\alpha_{\mathrm{m}} + \beta_{\mathrm{m}}) \tag{A-2b}$$

$$\alpha_{\mathrm{m}} = (-10^2(V + 0.033))/(\exp(-10^2 \cdot (V + 0.033)) - 1) \tag{A-2c}$$

$$\beta_{\mathrm{m}} = 4 \cdot \exp(-(V + 0.058)/0.018) \tag{A-2d}$$

$$\alpha_{\mathrm{h}} = \phi \cdot 70(\exp(-(V + 0.051)/0.010)) \tag{A-2e}$$

$$\beta_{\mathrm{h}} = \phi \cdot 10^3/(\exp(-10^2 \cdot (V + 0.021)) + 1) \tag{A-2f}$$

The delayed rectifier potassium current (I_{K}) was described as:

$$I_{\mathrm{K}} = g_{\mathrm{K}} n^4 (V - E_{\mathrm{K}}) \tag{A-3a}$$

$$\alpha_{\mathrm{n}} = (-\phi \cdot 10^4 \cdot (V + 0.038))/(\exp(-10^2 \cdot (V + 0.038)) - 1) \tag{A-3b}$$

$$\beta_{\mathrm{n}} = 125 \cdot \phi \cdot \exp(-(V + 0.048)/0.080) \tag{A-3c}$$

The slow potassium current (I_{Ks}):

$$I_{\text{Ks}} = g_{\text{Ks}} pq(V - E_{\text{K}}) \tag{A-4a}$$
$$p_{\text{inf}} = 1/(1 + \exp(-(V + 0.034)/0.0065)) \tag{A-4b}$$
$$q_{\text{inf}} = 1/(1 + (\exp(V + 0.065)/0.0066)) \tag{A-4c}$$
$$\tau_{\text{q}} = \tau_{\text{q0}} \cdot (1 + 1/(1 + (\exp -(V + 0.05)/0.0068))) \tag{A-4d}$$

with parameters $\tau_{\text{p}} = 6\,\text{s}, \tau_{\text{q0}} = 0.1\,\text{s}$.

The maximal conductance and the reversal potential of the ion channels were set as follows: $g_{\text{Na}} = 500\,\text{S/m}^2$, $g_{\text{K}} = 80\,\text{S/m}^2$, $g_{\text{Ks}} = 120\,\text{S/m}^2$; $E_{\text{Na}} = 55\,\text{mV}$, $E_{\text{K}} = -85\,\text{mV}$. The membrane surface was taken to be $1.26 \cdot 10^3 \text{mm}^2$, equivalent to the surface area of a sphere of $20\mu\text{m}$ diameter.

To model the MSDB fast-firing, GABAergic neurons we simplified the cluster-firing model by omitting the term I_{Ks} from equation A-1, and changing the ϕ parameter in equation A-2e-f and A-3b-c from 5 to 10.

A.2 Calculation of the Integrals with Different Integration Functions

In this section we compute the integrals in Equations 4.9–4.10 with the two different dendritic integration functions shown on Fig.4.1. To make the comparisons easier, we scaled both functions to have the same expected value ($\text{E}[F(U)] = 0.5$).

A.2.1 Linear Integration Function

In the linear case, we use the $F_L(U) = 0.26U$ integration function. First we calculate the expected value of the function, if the distribution of U is, from Eqn. 4.17, $p[U] = \mathbb{G}(U|\mu, \sigma^2)$:

$$\mu_L = \int_{-\infty}^{\infty} F_L(U)\mathbb{G}(U|\mu,\sigma^2)\mathrm{d}U =$$

$$= \int_{-\infty}^{\infty} \frac{0.26U}{\sqrt{2\pi\sigma^2}} \exp\left\{-\frac{(U-\mu)^2}{2\sigma^2}\right\}\mathrm{d}U = \qquad z = \tfrac{U-\mu}{\sqrt{2}\sigma}$$

$$= \frac{0.26}{\sqrt{\pi}} \int_{-\infty}^{\infty} (z\sqrt{2}\sigma + \mu)\exp\left\{-z^2\right\}\mathrm{d}z =$$

$$= \frac{0.26\sqrt{2}\sigma}{\sqrt{\pi}} \int_{-\infty}^{\infty} z\exp\left\{-z^2\right\}\mathrm{d}z + \frac{0.26\mu}{\sqrt{\pi}} \int_{-\infty}^{\infty} \exp\left\{-z^2\right\}\mathrm{d}z. \tag{A-5}$$

By changing the upper limit of the integrand from ∞ to U^* (z^*), we get the conditional expectations (Eqn. 4.26). We used the integration rules in Eqn. A-15 and A-16 to compute the primitive function of Eqn. A-5:

$$\mu_L^* = \frac{0.26\Lambda(z^*)}{\sqrt{\pi}} \left(\sqrt{2}\sigma\left[-\frac{1}{2}\exp\{-z^{*2}\} + \frac{1}{2}\exp\{-(-\infty)^2\}\right] + \right.$$
$$\left. + \mu\left[\frac{\sqrt{\pi}}{2}\mathrm{erf}\{z^*\} - \frac{\sqrt{\pi}}{2}\mathrm{erf}\{-\infty\}\right]\right), \tag{A-6}$$

where $\Lambda(z^*) = 1/\int_{-\infty}^{z^*} p(z)\mathrm{d}z$ is a normalization factor. Of course, we can use that $\exp\{-\infty\} = 0$, $\mathrm{erf}\{-\infty\} = -1$ and $\mathrm{erf}\{\infty\} = 1$. By substituting z^* with ∞, as in Eqn. A-5, we have:

$$\mu_L = \frac{0.26}{\sqrt{\pi}}\left(\sqrt{2}\sigma\,[0] + \mu\left[\frac{\sqrt{\pi}}{2} + \frac{\sqrt{\pi}}{2}\right]\right) = 0.26\mu. \tag{A-7}$$

We can calculate the variance in a similar way:

$$\sigma_L^2 = \int_{-\infty}^{\infty} \mathbb{G}(U|\mu,\sigma^2)(F_L(U)-\mu_L)^2 \mathrm{d}U =$$

$$= \int_{-\infty}^{\infty} \frac{(0.26U-\mu_L)^2}{\sqrt{2\pi\sigma^2}} \exp\left\{-\frac{(U-\mu)^2}{2\sigma^2}\right\} \mathrm{d}U = \qquad U = \sqrt{2}\sigma z + \mu$$

$$= \frac{1}{\sqrt{\pi}} \int_{-\infty}^{\infty} (0.26\sqrt{2}\sigma z + 0.26\mu - \mu_L)^2 \exp\left\{-z^2\right\} \mathrm{d}z = \qquad 0.26\mu - \mu_L = \Delta\mu$$

$$= \frac{1}{\sqrt{\pi}} \int_{-\infty}^{\infty} (0.26^2 2\sigma^2 z^2 + 0.52\sqrt{2}\sigma z \Delta\mu + \Delta\mu^2) \exp\left\{-z^2\right\} \mathrm{d}z =$$

$$= \frac{0.26^2 2\sigma^2}{\sqrt{\pi}} \int_{-\infty}^{\infty} z^2 \exp\left\{-z^2\right\} \mathrm{d}z +$$
$$+ \frac{0.52\sqrt{2}\sigma\Delta\mu}{\sqrt{\pi}} \int_{-\infty}^{\infty} z \exp\left\{-z^2\right\} \mathrm{d}z + \frac{\Delta\mu^2}{\sqrt{\pi}} \int_{-\infty}^{\infty} \exp\left\{-z^2\right\} \mathrm{d}z. \tag{A-8}$$

And the primitive function of Equation A-8 again to z^*, by using Eqn. A-15–A-17:

$$\sigma_L^{*\,2} = \Lambda(z^*)\left[\frac{0.26^2\sigma^2}{\sqrt{\pi}}\left(\frac{\sqrt{\pi}}{2}\mathrm{erf}\{z^*\} - z^*\exp\{-z^{*2}\} + \frac{\sqrt{\pi}}{2}\right)\right]$$
$$- \Lambda(z^*)\left[\frac{0.26\sqrt{2}\sigma\Delta\mu^*}{\sqrt{\pi}}\exp\{-z^{*2}\} + \frac{\Delta\mu^{*2}}{2}\left(\mathrm{erf}\{z^*\}+1\right)\right], \tag{A-9}$$

where we used that $\lim_{x\to\infty}\exp\{-x^2\} = 0$, $\lim_{x\to-\infty}\mathrm{erf}\{x\} = -1$, $\lim_{x\to\infty}\mathrm{erf}\{x\} = 1$ and $\lim_{x\to\infty} x\exp\{-x^2\} = 0$. Here $\Delta\mu^* = 0.26\mu - \mu_L^*$. Substituting z^* by ∞, we got that:

$$\sigma_L^2 = 0.26^2\sigma^2 - 0 + \Delta\mu^{*2} = 0.26^2\sigma^2. \tag{A-10}$$

A.2.2 Quadratic Integration Function

In the quadratic case, we chose the $F_Q(U) = kU^2$ integration function, with $k = 0.13$, where $F_Q(0) = 0$ and $\mu_Q \approx 0.5$, as we show below.

$$\mu_Q = \int_{-\infty}^{\infty} F_Q(U)\mathbb{G}(U|\mu,\sigma^2)\mathrm{d}U =$$

$$= \int_{-\infty}^{\infty} \frac{kU^2}{\sqrt{2\pi\sigma^2}} \exp\left\{-\frac{(U-\mu)^2}{2\sigma^2}\right\}\mathrm{d}U = \qquad z = \tfrac{U-\mu}{\sqrt{2}\sigma}$$

$$= \frac{k}{\sqrt{\pi}} \int_{-\infty}^{\infty} \left(\sigma\sqrt{2}z + \mu\right)^2 \exp\{-z^2\}\mathrm{d}z =$$

$$= \frac{2k\sigma^2}{\sqrt{\pi}} \int_{-\infty}^{\infty} z^2 \exp\{-z^2\}\mathrm{d}z + \\ + \frac{2k\sqrt{2}\sigma\mu}{\sqrt{\pi}} \int_{-\infty}^{\infty} z\exp\{-z^2\}\mathrm{d}z + \frac{k\mu^2}{\sqrt{\pi}} \int_{-\infty}^{\infty} \exp\{-z^2\}\mathrm{d}z. \tag{A-11}$$

The integration of Eqn A-11 using Eqns. (A-15–A-17) leads to:

$$\mu_Q^* = k\Lambda(z^*)\left[\frac{\sigma^2}{\sqrt{\pi}}\left(\frac{\sqrt{\pi}}{2}\mathrm{erf}\{z^*\} - z^*\exp\{-z^{*2}\} + \frac{\sqrt{\pi}}{2}\right) + \right. \\ \left. - \frac{\sqrt{2}\sigma\mu}{\sqrt{\pi}}\exp\{-x^{*2}\} + \frac{\mu^2}{2}(\mathrm{erf}\{z^*\} + 1)\right]. \tag{A-12}$$

Substituting z^* with ∞ in Equation A-12, we got that $\mu_Q = k(\mu^2 + \sigma^2)$. We chose the parameter $k = 0.13$, then $\mu_Q = 0.498 \approx 0.5$. And the variance:

$$\sigma_Q^2 = \int_{-\infty}^{\infty} \frac{(kU^2 - \mu_Q)^2}{\sqrt{2\pi\sigma^2}} \exp\left\{-\frac{(U-\mu)^2}{2\sigma^2}\right\}\mathrm{d}U = \qquad z = \tfrac{U-\mu}{\sqrt{2}\sigma}$$

$$= \frac{1}{\sqrt{\pi}} \int_{-\infty}^{\infty} (k(\sigma\sqrt{2}z + \mu)^2 - \mu_Q)^2 \exp\left\{-z^2\right\}\mathrm{d}z$$

$$= \frac{1}{\sqrt{\pi}} \int_{-\infty}^{\infty} (2k\sigma^2z^2 + 2k\sqrt{2}\sigma\mu z + k\mu^2 - \mu_Q)^2 \exp\left\{-z^2\right\}\mathrm{d}z = \qquad \begin{array}{r} c = k\sigma^2 \\ d = 2k\sqrt{2}\sigma\mu \\ k\mu^2 - \mu_Q = e \end{array}$$

$$= \frac{1}{\sqrt{\pi}} \int_{-\infty}^{\infty} (4c^2z^4 + 4cdz^3 + (d^2 + 4ce)z^2 + 2dez + e^2)\exp\left\{-z^2\right\}\mathrm{d}z = \tag{A-13}$$

The integration of Eqn A-13 using Eqns. (A-15–A-19) leads to:

$$\begin{aligned}{\sigma_Q^*}^2 = \Lambda(z^*)\Bigg[\frac{c^2}{\sqrt{\pi}}\left(\left(-2z^{*3}-3z^*\right)\exp\{-z^{*2}\}+\frac{3\sqrt{\pi}}{2}\mathrm{erf}\{z^*\}+\frac{3\sqrt{\pi}}{2}\right)+\\ -\frac{2cd}{\sqrt{\pi}}\exp\{-z^{*2}\}(z^{*2}+1)+\\ +\frac{d^2+4ce}{\sqrt{\pi}}\left(\frac{\sqrt{\pi}}{4}\mathrm{erf}\{z^*\}-\frac{z^*}{2}\exp\{-z^{*2}\}+\frac{\sqrt{\pi}}{4}\right)+\\ -\frac{de}{\sqrt{\pi}}\exp\{-z^{*2}\}+\frac{e^2}{2}(\mathrm{erf}\{z^*\}+1)\Bigg]. \quad \text{(A-14)}\end{aligned}$$

Substituting z^* with ∞ in Equation A-14, we got that $\sigma_Q^2 = 2c^2 + d/2 = 0.0348$.

A.2.3 Integration Rules

To compute the above integrals, we used the following integration rules:

$$\int \exp\left\{-x^2\right\}\mathrm{d}x = \frac{\sqrt{\pi}}{2}\mathrm{erf}\{x\} \quad \text{(A-15)}$$

$$\int x\exp\left\{-x^2\right\}\mathrm{d}x = -\frac{1}{2}\exp\{-x^2\} \quad \text{(A-16)}$$

$$\int x^2\exp\left\{-x^2\right\}\mathrm{d}x = \frac{\sqrt{\pi}}{4}\mathrm{erf}\{x\} - \frac{1}{2}x\exp\{-x^2\} \quad \text{(A-17)}$$

$$\int x^3\exp\left\{-x^2\right\}\mathrm{d}x = -\frac{1}{2}\exp\{-x^2\}(x^2+1) \quad \text{(A-18)}$$

$$\int x^4\exp\left\{-x^2\right\}\mathrm{d}x = \left(-\frac{x^3}{2}-\frac{3x}{4}\right)\exp\{-x^2\}+\frac{3\sqrt{\pi}}{8}\mathrm{erf}\{x\} \quad \text{(A-19)}$$

Bibliography

Acsády, L. and Káli, S. (2007). Models, structure, function: the transformation of cortical signals in the dentate gyrus. *Prog Brain Res.*, 163:577–599.

Amaral, D. and Lavenex, P. (2007). Hippocampal neuroanatomy. In Andersen, P., Morris, R., Amaral, D., Bliss, T., and O'Keefe, J., editors, *The Hippocampus Book*, pages 37–114. Oxford University Press.

Amaral, D. G. and Witter, M. P. (1989). The three dimensional organization of the hippocampal formation: a review of anatomical data. *Neuroscience*, 31:571–591.

Andersen, P., Bliss, T., and Skrede, K. (1971). Lamellar organization of the hippocampal excitatory pathways. *Exp. Brain Res.*, 13:222–238.

Andersen, P., Morris, R., Amaral, D., Bliss, T., and O'Keefe, J. (2007). *The Hippocampus Book*. Oxford University Press.

Arbib, M. A., Érdi, P., and Szentágothai, J. (1997). *Neural Organization: Structure, Function and Dynamics*. MIT Press.

Archie, K. A. and Mel, B. W. (2000). A model for intradendritic computation of binocular disparity. *Nat Neurosci*, 3(1):54–63.

Ariav, G., Polsky, A., and Schiller, J. (2003). Submillisecond precision of the input-output transformation function mediated by fast sodium dendritic spikes in basal dendrites of CA1 pyramidal neurons. *J Neurosci*, 23(21):7750–8.

Arleo, A. and Gerstner, W. (2000). Spatial cognition and neuro-mimetic navigation: a model of hippocampal place cell activity. *Biol Cybern*, 83(3):287–99.

Assisi, C., Stopfer, M., Laurent, G., and Bazhenov, M. (2007). Adaptive regulation of sparseness by feedforward inhibition. *Nat Neurosci*, 10(9):1176–84.

Baker, P. M., Pennefather, P. S., Orser, B. A., and Skinner, F. K. (2002). Disruption of coherent oscillations in inhibitory networks with anesthetics: role of GABA(A) receptor desensitization. *J Neurophysiol.*, 88(5)(5):2821–33.

Barnes, C. A., McNaughton, B. L., Mizumori, S. J., Leonard, B. W., and Lin, L. H. (1990). Comparison of spatial and temporal characteristics of neuronal activity in sequential stages of hippocampal processing. *Prog Brain Res*, 83:287–300.

Barry, C. and Burgess, N. (2007). Learning in a geometric model of place cell firing. *Hippocampus*, 17(9):786–800.

Barry, C., Hayman, R., Burgess, N., and Jeffery, K. J. (2007). Experience-dependent rescaling of entorhinal grids. *Nature Neuroscience*, 10:682–684.

Barry, C., Lever, C., Hayman, R., Hartley, T., Burton, S., O'Keefe, J., Jeffery, K., and Burgess, N. (2006). The boundary vector cell model of place cell firing and spatial memory. *Reviews in the Neurosciences*, 17:71–97.

Bartos, M., Vida, I., Frotscher, M., Geiger, J. R., and Jonas, P. (2001). Rapid signaling at inhibitory synapses in a dentate gyrus interneuron network. *J Neurosci*, 21(8):2687–98.

Battaglia, F. P., Sutherland, G. R., and McNaughton, B. L. (2004a). Hippocampal sharp wave bursts coincide with neocortical "up-state" transitions. *Learn Mem*, 11(6):697–704.

Battaglia, F. P., Sutherland, G. R., and McNaughton, B. L. (2004b). Local sensory cues and place cell directionality: additional evidence of prospective coding in the hippocampus. *J Neurosci*, 24(19):4541–50.

Berger, T. W., Rinaldi, P. C., Weisz, D. J., and Thompson, R. F. (1983). Single-unit analysis of different hippocampal cell types during classical conditioning of rabbit nictitating membrane response. *J Neurophysiol*, 50(5):1197–219.

Bernander, O., Douglas, R. J., Martin, K. A., and Koch, C. (1991). Synaptic background activity influences spatiotemporal integration in single pyramidal cells. *Proc Natl Acad Sci USA*, 88(24):11569–73.

Bi, G. Q. and Poo, M. M. (1998). Synaptic modifications in cultured hippocampal neurons: dependence on spike timing, synaptic strength, and postsynaptic cell type. *J Neurosci*, 18(24):10464–72.

Bishop, C. (2006). *Pattern Recognition and Machine Learning*. Springer.

Blair, H. T., Welday, A. C., and Zhang, K. (2007). Scale-invariant memory representations emerge from moiré interference between grid fields that produce theta oscillations: a computational model. *Journal of Neuroscience*, 27:3211–3229.

Bland, B., Konopacki, J., Kirk, I., Oddie, S., and Disckson, C. (1995). Discharge patterns of hippocampal theta-related cells in the caudal diencephalon of the urethan-anesthetized rat. *J Neurophysiol*, 74:322–333.

Bland, B. H., Oddie, S. D., and Colom, L. V. (1999). Mechanisms of neural synchrony in the septohippocampal pathways underlying hippocampal theta generation. *J Neurosci.*, 19(8):3223–37.

Blasco-Ibanez, J. M. and Freund, T. F. (1995). Synaptic input of horizontal interneurons in stratum oriens of the hippocampal CA1 subfield: structural basis of feedback activation. *Eur J Neurosci*, 7(10):2170–80.

Blaxter, T. J., Carlen, P. L., and Niesen, C. (1989). Pharmacological and anatomical separation of calcium currents in rat dentate granule neurones in vitro. *J Physiol*, 412:93–112.

Bliss, T. V. and Collingridge, G. L. (1993). A synaptic model of memory: Long-term potentiation in the hippocampus. *Nature*, 361:31–39.

Bliss, T. V. and Lømo, T. (1973). Long-lasting potentiation of synaptic transmission in the dentate area of the anaesthetized rabbit following stimulation of the perforant path. *J Physiol*, 232(2):331–56.

Borhegyi, Z., Varga, V., Szilágyi, N., Fabó, D., and Freund, T. F. (2004). Phase segregation of medial septal GABAergic neurons during hippocampal theta activity. *J. of Neuroscience*, 24(39):8470–79.

Bower, J. M. and Beeman, D. (1998). *The Book of GENESIS: Exploring Realistic Neural Models with the GEneral NEural SImulation System*. Springer–Verlag, 2 edition.

Branco, T., Staras, K., Darcy, K. J., and Goda, Y. (2008). Local dendritic activity sets release probability at hippocampal synapses. *Neuron*, 59(3):475–85.

Brashear, H. R., Zaborszky, L., and Heimer, L. (1986). Distribution of GABAergic and cholinergic neurons in the rat diagonal band. *Neuroscience*, 17(2):439–51.

Brazhnik, E. S. and Fox, S. E. (1997). Intracellular recordings from medial septal neurons during hippocampal theta rhythm. *Exp Brain Res.*, 114(3):442–53.

Brazhnik, E. S. and Fox, S. E. (1999). Action potentials and relations to the theta rhythm of medial septal neurons in vivo. *Exp Brain Res.*, 127(3):244–58.

Buckmaster, P. S., Wenzel, H. J., Kunkel, D. D., and Schwartzkroin, P. A. (1996). Axon arbors and synaptic connections of hippocampal mossy cells in the rat in vivo. *J Comp Neurol*, 366(2):271–92.

Burgess, N. (2007). Computational Models of The Spatial and Mnemonic Functions of the Hippocampus. In Andersen, P., Morris, R., Amaral, D., Bliss, T., and O'Keefe, J., editors, *The Hippocampus Book*, pages 715–750. Oxford University Press.

Burgess, N., Barry, C., and O'Keefe, J. (2007). An oscillatory interference model of grid cell firing. *Hippocampus*, 17(9):801–812.

Burgess, N., Jackson, A., Hartley, T., and O'Keefe, J. (2000). Predictions derived from modelling the hippocampal role in navigation. *Biological Cybernetics*, 83(3):301–312.

Burgess, N., Maguire, E., and O'Keefe, J. (2002). The human hippocampus and spatial and episodic memory. *Neuron*, 35:625–41.

Burgess, N. and O'Keefe, J. (1996). Neuronal computations underlying the firing of place cells and their role in navigation. *Hippocampus*, 6:749–762.

Burgess, N., Recce, M., and O'Keefe, J. (1994). A model of hippocampal function. *Neural Networks*, 7:1065–1081.

Burwell, R. D. (2000). The parahippocampal region: corticocortical connectivity. *Ann N Y Acad Sci*, 911:25–42.

Buzsáki, G. (1984). Feed-forward inhibition in the hippocampal formation. *Prog Neurobiol*, 22(2):131–53.

Buzsáki, G. (1986). Hippocampal sharp waves: their origin and significance. *Brain Res*, 382:242–52.

Buzsáki, G. (2002). Theta oscillations in the hippocampus. *Neuron*, 33(3):325–40.

Buzsáki, G. (2006). *Rhythms of the Brain*. Oxford University Press.

Buzsáki, G., Horváth, Z., Urioste, R., Hetke, J., and Wise, K. (1992). High-frequency network oscillation in the hippocampus. *Science*, 256:1025–1027.

Buzsáki, G. (2005). Theta rhythm of navigation: Link between path integration and landmark navigation, episodic and semantic memory. *Hippocampus*, 15(7):827–840.

Cai, X., Liang, C. W., Muralidharan, S., Kao, J. P., Tang, C. M., and Thompson, S. M. (2004). Unique roles of SK and Kv4.2 potassium channels in dendritic integration. *Neuron*, 44(2):351–64.

Caplan, J., Madsen, J., Schulze-Bonhage, A., Aschenbrenner-Scheibe, R., Newman, E., and Kahana, M. (2003). Human theta oscillations related to sensorimotor integration and spatial learning. *J Neurosci*, 23:4726–4736.

Chapman, C. A. and Lacaille, J. C. (1999). Intrinsic theta-frequency membrane potential oscillations in hippocampal CA1 interneurons of stratum lacunosum-moleculare. *J. Neurophysiol.*, 81:1296–307.

Chen, W. R., Midtgaard, J., and Shepherd, G. M. (1997). Forward and backward propagation of dendritic impulses and their synaptic control in mitral cells. *Science*, 278(5337):463–7.

Claiborne, B. J., Amaral, D. G., and Cowan, W. M. (1990). Quantitative, three-dimensional analysis of granule cell dendrites in the rat dentate gyrus. *J Comp Neurol*, 302(2):206–19.

Colbert, C. M., Magee, J. C., Hoffman, D. A., and Johnston, D. (1997). Slow recovery from inactivation of Na+ channels underlies the activity-dependent attenuation of dendritic action potentials in hippocampal CA1 pyramidal neurons. *J Neurosci*, 17(17):6512–21.

Cole, A. E. and Nicoll, R. A. (1984). Characterization of a slow cholinergic post-synaptic potential recorded in vitro from rat hippocampal pyramidal cells. *J Physiol.*, 352:173–88.

Collett, T. and Zeil, J. (1998). Places and landmarks: an arthropod perspective. In Healy, S., editor, *Spatial representation in animals*, pages 18–53. Oxford University Press.

Colom, L. V., Castaneda, M. T., Reyna, T., Hernandez, S., and Garrido-Sanabria, E. (2005). Characterization of medial septal glutamatergic neurons and their projection to the hippocampus. *Synapse*, 58(3):151–64.

Csicsvári, J., Hirase, H., Czurkó, A., Mamiya, A., and Buzsáki, G. (1999). Oscillatory coupling of hippocampal pyramidal cells and interneurons in the behaving Rat. *J Neurosci*, 19(1):274–87.

Csicsvári, J., Hirase, H., Mamiya, A., and Buzsáki, G. (2000). Ensemble patterns of hippocampal CA3-CA1 neurons during sharp wave-associated population events. *Neuron*, 28(2):585–94.

Csicsvári, J., Jamieson, B., Wise, K., and Buzsáki, G. (2003). Mechanisms of gamma oscillations in the hippocampus of the behaving rat. neuron 37:311322. *Neuron*, 37:311–322.

Dan, Y. and Poo, M. M. (2006). Spike timing-dependent plasticity: from synapse to perception. *Physiol Rev*, 86(3):1033–48.

Day, M., Langston, R., and Morris, R. G. (2003). Glutamate-receptor-mediated encoding and retrieval of paired-associate learning. *Nature*, 424(6945):205–9.

Dayan, P. and Abbot, L. F. (2001). *Theoretical neuroscience: Computational and mathematical modeling of neural systems*. The MIT press.

de Almeida, L., Idiart, M., and Lisman, J. E. (2009). The input-output transformation of the hippocampal granule cells: from grid cells to place fields. *J Neurosci*, 29(23):7504–12.

Destexhe, A. (2000). Modelling corticothalamic feedback and the gating of the thalamus by the cerebral cortex. *J Physiol (Paris)*, 94:391–410.

Destexhe, A. and Paré, D. (1999). Impact of network activity on the integrative properties of neocortical pyramidal neurons in vivo. *J Neurophysiol*, 81(4):1531–47.

Diba, K. and Buzsaki, G. (2008). Hippocampal network dynamics constrain the time lag between pyramidal cells across modified environments. *J Neurosci*, 28(50):13448–56.

Dolorfo, C. L. and Amaral, D. G. (1998). Entorhinal cortex of the rat: topographic organization of the cells of origin of the perforant path projection to the dentate gyrus. *J Comp Neurol*, 398(1):25–48.

Douglas, R. M., McNaughton, B. L., and Goddard, G. V. (1983). Commissural inhibition and facilitation of granule cell discharge in fascia dentata. *J Comp Neurol*, 219(3):285–94.

Dragoi, G. and Buzsáki, G. (2006). Temporal encoding of place sequences by hippocampal cell assemblies. *Neuron*, 50(1):145–57.

Dragoi, G., Carpi, D., Recce, M., Csicsvári, J., and Buzsáki, G. (1999). Interactions between hippocampus and medial septum during sharp waves and theta oscillation in the behaving rat. *J. Neurosci.*, 19:6191–99.

Eghbali, M., Curmi, J. P., Birnir, B., and Gage, P. W. (1997). Hippocampal GABA(A) channel conductance increased by diazepam. *Nature*, 388(6637):71–5.

Eichenbaum, H. (2004). Hippocampus: cognitive processes and neural representations that underlie declarative memory. *Neuron*, 44(1):109–20.

Eichenbaum, H., Dudchenko, P., Wood, E., Shapiro, M., and Tanila, H. (1999). The hippocampus, memory, and place cells: Is it spatial memory or a memory space? *Neuron*, 23:209–226.

Érdi, P., Kiss, T., Tóth, J., Ujfalussy, B., and Zalányi, L. (2006). From systems biology to dynamical neuropharmacology: proposal for a new methodology. *Syst Biol (Stevenage)*, 153(4):299–308.

Etienne, A. S., Berlie, J., Georgakopoulos, J., and Maurer, R. (1998). Role of dead reckoning in navigation. In Healy, S., editor, *Spatial representation in animals*, pages 54–68. Oxford University Press.

Etienne, A. S. and Jeffery, K. J. (2004). Path integration in mammals. *Hippocampus*, 14:180–192.

Etienne, A. S., Maurer, R., and Séguinot, V. (1996). Path integration in mammals and its interaction with visual landmarks. *Journal of Experimental Biology*, 199:201–209.

Fellous, J. M. and Sejnowski, T. J. (2000). Cholinergic induction of oscillations in the hippocampal slice in the slow (0.5-2 Hz), theta (5-12 Hz), and gamma (35-70 Hz) bands. *Hippocampus*, 10(2):187–97.

Ferbinteanu, J. and Shapiro, M. L. (2003). Prospective and retrospective memory coding in the hippocampus. *Neuron*, 40(6):1227–39.

Fisher, R. E., Gray, R., and Johnston, D. (1990). Properties and distribution of single voltage-gated calcium channels in adult hippocampal neurons. *J Neurophysiol*, 64(1):91–104.

Forster, E., Zhao, S., and Frotscher, M. (2006). Laminating the hippocampus. *Nat Rev Neurosci*, 7(4):259–67.

Foster, D. J. and Wilson, M. A. (2007). Hippocampal theta sequences. *Hippocampus*, 17(11):1093–9.

Frank, L. M., Brown, E. N., and Wilson, M. (2001). A comparison of the firing properties of putative excitatory and inhibitory neurons from CA1 and the entorhinal cortex. *J Neurophysiol*, 86(4):2029–2040.

Frankland, P. W. and Bontempi, B. (2005). The organization of recent and remote memories. *Nat Rev Neurosci*, 6(2):119–30.

Freund, T. F. (1989). GABAergic septohippocampal neurons contain parvalbumin. *Brain Res.*, 478(2):375–81.

Freund, T. F. and Antal, M. (1988). GABA-containing neurons in the septum control inhibitory interneurons in the hippocampus. *Nature*, 336(6195):170–173.

Freund, T. F. and Buzsáki, G. (1996). Interneurons of the hippocampus. *Hippocampus*, 6(4):347–470.

Fricke, R. A. and Prince, D. A. (1984). Electrophysiology of dentate gyrus granule cells. *J Neurophysiol*, 51(2):195–209.

Fried, I., MacDonald, K. A., and Wilson, C. L. (1997). Single neuron activity in human hippocampus and amygdala during recognition of faces and objects. *Neuron*, 18(5):753–65.

Frotscher, M. and Leranth, C. (1985). Cholinergic innervation of the rat hippocampus as revealed by choline acetyltransferase immunocytochemistry: a combined light and electron microscopic study. *J Comp Neurol.*, 239(2):237–46.

Fuhs, M. C. and Touretzky, D. S. (2006). A spin glass model of path integration in rat medial entorhinal cortex. *Journal of Neuroscience*, 26:4266–4276.

Fyhn, M., Hafting, T., Treves, A., Moser, M.-B., and Moser, E. I. (2007). Hippocampal remapping and grid realignment in entorhinal cortex. *Nature*, 446:190–194.

Fyhn, M., Molden, S., Witter, M. P., Moser, E. I., and Moser, M.-B. (2004). Spatial representation in the entorhinal cortex. *Science*, 305:1258–1264.

Gao, B. and Fritschy, J. M. (1994). Selective allocation of GABAA receptors containing the alpha 1 subunit to neurochemically distinct subpopulations of rat hippocampal interneurons. *Eur J Neurosci*, 6(5):837–53.

Gao, B., Hornung, J. P., and Fritschy, J. M. (1995). Identification of distinct GABA-A-receptor subtypes in cholinergic and parvalbumin-positive neurons of the rat and marmoset medial septum-diagonal band complex. *Neuroscience.*, 65(1):101–17.

Garner, H. L., Whittington, M. A., and Henderson, Z. (2005). Induction by kainate of theta frequency rhythmic activity in the rat medial septum-diagonal band complex in vitro. *J Physiol.*, 564(Pt 1):83–102.

Gasparini, S. and Magee, J. C. (2006). State-dependent dendritic computation in hippocampal CA1 pyramidal neurons. *J Neurosci*, 26(7):2088–100.

Gaussier, P., Banquet, J. P., Sargolini, F., Giovannangeli, C., Save, E., and Poucet, B. (2007). A model of grid cells involving extra hippocampal path integration, and the hippocampal loop. *Journal of Integrative Neuroscience*, 6:447–476.

Gerstner, W. and Kistler, W. (2002). *Spiking Neuron Models*. Cambridge University Press.

Gilbert, P. E., Kesner, R. P., and Lee, I. (2001). Dissociating hippocampal subregions: double dissociation between dentate gyrus and CA1. *Hippocampus*, 11(6):626–36.

Gillies, M. J., Traub, R. D., LeBeau, F. E. N., Davies, C. H., Gloveli, T., Buhl, E. H., and Whittington, M. A. (2002). A model of atropine-resistant theta oscillations in rat hippocampal area CA1. *Journal of Physiology*, 543:779–793.

Giocomo, L., Zilli, E., Fransen, E., and Hasselmo, M. (2007). Temporal frequency of subthreshold oscillations scales with entorhinal grid cell field spacing. *Science*, 315(5819):1719–1722.

Golding, N., Staff, N., and Spruston, N. (2002). Dendritic spikes as a mechanism for cooperative long-term potentiation. *Nature*, 418(6895):326–331.

Gordon, U., Polsky, A., and Schiller, J. (2006). Plasticity compartments in basal dendrites of neocortical pyramidal neurons. *J Neurosci*, 26(49):12717–26.

Gothard, K. M., Skaggs, W. E., and McNaughton, B. L. (1996). Dynamics of mismatch correction in the hippocampal ensemble code for space: Interaction between path integration and environmental cues. *Journal of Neuroscience*, 16:8027–8040.

Goutagny, R., Manseau, F., Jackson, J., Danik, M., and Williams, S. (2008). In vitro activation of the medial septum-diagonal band complex generates atropine-sensitive and atropine-resistant hippocampal theta rhythm: an investigation using a complete septohippocampal preparation. *Hippocampus*, 18(6):531–5.

Govindarajan, A., Kelleher, R. J., and Tonegawa, S. (2006). A clustered plasticity model of long-term memory engrams. *Nat Rev Neurosci*, 7(7):575–83.

Green, J. D. and Arduini, A. A. (1954). Hippocampal electrical activity in arousal. *J Neurophysiol*, 17(6):533–57.

Griffith, W. (1988). Membrane properties of cell types within guinea pig basal forebrain nuclei in vitro. *J Neurophysiol*, 59(5):1590–612.

Griffith, W. and Matthews, R. (1986). Electrophysiology of AChE-positive neurons in basal forebrain slices. *Neurosci Lett*, 71(2):169–74.

Griffith, W., Sim, J., and Matthews, R. (1991). Electrophysiologic characteristics of basal forebrain neurons in vitro. *Adv Exp Med Biol*, 295:143–55.

Guanella, A. and Verschure, P. F. M. J. (2006). A model of grid cells based on a path integration mechanism. In Kollias, S., Stafylopatis, A., Duch, W., and Oja, E., editors, *Artificial Neural Networks – ICANN 2006*, volume 4131 of *Lecture Notes in Computer Science*, pages 740–749. Springer-Verlag Berlin Heildelberg.

Hafting, T., Fyhn, M., Bonnevie, T., Moser, M.-B., and Moser, E. I. (2008). Hippocampus-independent phase precession in entorhinal grid cells. *Nature*, 453(7199):1248–1252.

Hafting, T., Fyhn, M., Molden, S., Moser, M.-B., and Moser, E. I. (2005). Microstructure of a spatial map in the entorhinal cortex. *Nature*, 436:801–806.

Haider, B., Duque, A., Hasenstaub, A. R., and McCormick, D. A. (2006). Neocortical network activity in vivo is generated through a dynamic balance of excitation and inhibition. *J Neurosci*, 26(17):4535–45.

Hájos, N., Nusser, Z., Rancz, E. A., Freund, T. F., and Mody, I. (2000). Cell type- and synapse-specific variability in synaptic GABA-A receptor occupancy. *Eur J Neurosci.*, 12(3):810–18.

Hajszan, T., Alreja, M., and Leranth, C. (2004). Intrinsic vesicular glutamate transporter 2-immunoreactive input to septohippocampal parvalbumin-containing neurons: novel glutamatergic local circuit cells. *Hippocampus*, 14(4):499–509.

Halasy, K. and Somogyi, P. (1993). Subdivisions in the multiple GABAergic innervation of granule cells in the dentate gyrus of the rat hippocampus. *Eur J Neurosci*, 5(5):411–29.

Hangya, B. (2009). *Identified, putative pacemaker neurons of the medial septum lead the hippocampal network during theta activity*. PhD thesis, Semmelweis University, János Szentágothai School of PhD studies.

Hangya, B., Borhegyi, Z., Szilagyi, N., Freund, T. F., and Varga, V. (2009). GABAergic neurons of the medial septum lead the hippocampal network during theta activity. *J Neurosci*, 29(25):8094–102.

Hargreaves, E. L., Rao, G., Lee, I., and Knierim, J. J. (2005). Major dissociation between medial and lateral entorhinal input to dorsal hippocampus. *Science*, 308(5729):1792–4.

Harris, K., Csicsvári, J., Hirase, H., Dragoi, G., and Buzsáki, G. (2003). Organization of cell assemblies in the hippocampus. *Nature*, 424:552–556.

Harvey, C. D. and Svoboda, K. (2007). Locally dynamic synaptic learning rules in pyramidal neuron dendrites. *Nature*, 450(7173):1195–200.

Harvey, C. D., Yasuda, R., Zhong, H., and Svoboda, K. (2008). The spread of Ras activity triggered by activation of a single dendritic spine. *Science*, 321(5885):136–40.

Hasselmo, M. E., Giocomo, L., and Zilli, E. (2007). Grid cell firing may arise from interference of theta frequency membrane potential oscillations in single neurons. *Hippocampus*, 17(12):1252–1271.

Hasselmo, M. E., Hay, J., Ilyn, M., and Gorchetchnikov, A. (2002). Neuromodulation, theta rhythm and rat spatial navigation. *Neural Netw.*, 15(4-6):689–707.

Hausser, M. and Mel, B. (2003). Dendrites: Bug or feature? *Current Opinion in Neurobiology*, 13:372–383.

Hausser, M., Spruston, N., and Stuart, G. J. (2000). Diversity and dynamics of dendritic signaling. *Science*, 290(5492):739–44.

Hayman, R. M. and Jeffery, K. J. (2008). How heterogeneous place cell responding arises from homogeneous grids–a contextual gating hypothesis. *Hippocampus*, 18(12):1301–13.

Hebb, D. O. (1949). *The organization of behavior*. Wiley, New York.

Henderson, Z., Fiddler, G., S Saha, A. B., and Halasy, K. (2004). A parvalbumin-containing, axosomatic synaptic network in the rat medial septum: relevance to rhythmogenesis. *Eur. J Neurosci.*, 19(10):2753–98.

Henderson, Z., Morris, N., Grimwood, P., Fiddler, G., Yang, H., and Appenteng, K. (2001). Morphology of local axon collaterals of electrophysiologically characterised neurons in the rat medial septal/ diagonal band complex. *J Comp Neurol*, 430(3):410–32.

Herz, A. V., Gollisch, T., Machens, C. K., and Jaeger, D. (2006). Modeling single-neuron dynamics and computations: a balance of detail and abstraction. *Science*, 314(5796):80–5.

Huhn, Z., Somogyvári, Z., Kiss, T., and Érdi, P. (2009). Distance coding strategies based on the entorhinal grid cell system. *Neural Netw*, 22(5-6):536–43.

Hutcheon, B. and Yarom, Y. (2000). Resonance, oscillation and the intrinsic frequency preferences of neurons. *Trends Neurosci*, 23(5):216–22.

Hyman, J. M., Wyble, B. P., Goyal, V., Rossi, C. A., and Hasselmo, M. E. (2003). Stimulation in hippocampal region CA1 in behaving rats yields long-term potentiation when delivered to the peak of theta and long-term depression when delivered to the trough. *J Neurosci*, 23(37):11725–31.

Hyman, J. M., Zilli, E. A., Paley, A. M., and Hasselmo, M. E. (2005). Medial prefrontal cortex cells show dynamic modulation with the hippocampal theta rhythm dependent on behavior. *Hippocampus*, 15(6):739–49.

Isomura, Y., Sirota, A., Ozen, S., Montgomery, S., Mizuseki, K., Henze, D. A., and Buzsáki, G. (2006). Integration and segregation of activity in entorhinal-hippocampal subregions by neocortical slow oscillations. *Neuron*, 52(5):871–82.

Jeffery, K. J. (1998). Learning of landmark stability and instability by hippocampal place cells. *Neuropharmacology*, 37:677–687.

Jeffery, K. J. (2007). Integration of the sensory inputs to place cells: What, where, why, and how? *Hippocampus*, 17:775–785.

Jeffery, K. J., Donnett, J. G., Burgess, N., and O'Keefe, J. M. (1997). Directional control of hippocampal place fields. *Exp Brain Res*, 117(1):131–42.

Jeffery, K. J. and O'Keefe, J. (1999). Learned interaction of visual and idiothetic cues in the control of place field orientation. *Experimental Brain Research*, 127:151–161.

Jensen, O. (2001). Information transfer between rhythmically coupled networks: Reading the hippocampal phase code. *Neural Comput.*, 13(12):2743–2761.

Jensen, O. (2005). Reading the hippocampal code by theta phase-locking. *Trends Cogn Sci*, 9(12):551–3.

Jensen, O. and Lisman, J. E. (1996). Theta/gamma networks with slow NMDA channels learn sequences and encode episodic memory: role of NMDA channels in recall. *Learn Mem*, 3(2-3):264–78.

Jinno, S., Klausberger, T., Marton, L. F., Dalezios, Y., Roberts, J. D., Fuentealba, P., Bushong, E. A., Henze, D., Buzsáki, G., and Somogyi, P. (2007). Neuronal diversity in GABAergic long-range projections from the hippocampus. *J Neurosci*, 27(33):8790–804.

Johnston, D. and Narayanan, R. (2008). Active dendrites: colorful wings of the mysterious butterflies. *Trends Neurosci*, 31(6):309–16.

Jones, M. W. and Wilson, M. A. (2005). Theta rhythms coordinate hippocampal-prefrontal interactions in a spatial memory task. *PLoS Biol*, 3(12):e402.

Jung, H. Y., Mickus, T., and Spruston, N. (1997). Prolonged sodium channel inactivation contributes to dendritic action potential attenuation in hippocampal pyramidal neurons. *J Neurosci*, 17(17):6639–46.

Jung, M. and McNaughton, B. (1993). Spatial selectivity of unit activity in the hippocampal granular layer. *Hippocampus*, 3(2):165–82.

Jung, M. W., Wiener, S. I., and McNaughton, B. L. (1994). Comparison of spatial firing characteristics of units in dorsal and ventral hippocampus of the rat. *The Journal of Neuroscience*, 74(12):7347–7356.

Kahana, M., Sekuler, R., Caplan, J., Kirschen, M., and Madsen, J. (1999). Human theta oscillations exhibit task dependence during virtual maze navigation. *Nature*, 399:781–784.

Káli, S. and Dayan, P. (2000). The involvement of recurrent connections in area CA3 in establishing the properties of place fields: a model. *Journal of Neuroscience*, 20:7463–7477.

Kamondi, A., Acsády, L., Wang, X., and Buzsáki, G. (1998). Theta oscillation in somata and dendrites of hippocampal pyramidal cells in vivo: activity-dependent phase-precession of action potentials. *Hippocampus*, 8:244–261.

Kaplan, M. S. and Hinds, J. W. (1977). Neurogenesis in the adult rat: electron microscopic analysis of light radioautographs. *Science*, 197(4308):1092–4.

Kee, N., Teixeira, C. M., Wang, A. H., and Frankland, P. W. (2007). Preferential incorporation of adult-generated granule cells into spatial memory networks in the dentate gyrus. *Nat Neurosci*, 10(3):355–62.

King, C., Recce, M., and O'Keefe, J. (1998). The rhythmicity of cells of the medial septum/diagonal band of broca in the awake freely moving rat: relationships with behaviour and hippocampal theta. *European Journal of Neuroscience*, 10:464–477.

Kiss, J., Patel, A. J., Baimbridge, K. G., and Freund, T. F. (1990). Topographical localization of neurons containing parvalbumin and choline acetyltransferase in the medial septum-diagonal band region of the rat. *Neuroscience*, 36(1):61–72.

Kjelstrup, K. B., Solstad, T., Brun, V. H., Hafting, T., Leutgeb, S., Witter, M. P., Moser, E. I., and Moser, M. B. (2008). Finite scale of spatial representation in the hippocampus. *Science*, 321(5885):140–3.

Klausberger, T., Magill, P. J., Márton, L. F., Roberts, J. D. B., Cobden, P. M., Buzsáki, G., and Somogyi, P. (2003). Brain-state- and cell-type-specific firing of hippocampal interneurons in vivo. *Nature*, 421:844–8.

Klausberger, T. and Somogyi, P. (2008). Neuronal diversity and temporal dynamics: The unity of hippocampal circuit operations. *Science*, 321:53–57.

Kloosterman, F., Van Haeften, T., Witter, M. P., and Lopes Da Silva, F. H. (2003). Electrophysiological characterization of interlaminar entorhinal connections: an essential link for re-entrance in the hippocampal-entorhinal system. *European Journal of Neuroscience*, 18:3037–3052.

Knapp, J., Morris, N., Henderson, Z., and Matthews, R. (2000). Electrophysiological characteristics of non-bursting, glutamate decarboxylase messenger RNA-positive neurons of the medial septum/diagonal band nuclei of guinea-pig and rat. *Neuroscience*, 98(4):661–8.

Knierim, J. J., Kudrimoti, H. S., and McNaughton, B. L. (1995). Place cells, head direction cells, and the learning of landmark stability. *Journal of Neuroscience*, 15:1648–1659.

Koch, C. (1999). *Biophysics of Computation: Information Processing in Single Neurons.* Oxford University Press.

Koch, C., Poggio, T., and Torre, V. (1983). Nonlinear interactions in a dendritic tree: localization, timing, and role in information processing. *Proc Natl Acad Sci USA*, 80(9):2799–802.

Kocsis, B., Bragin, A., and Buzsáki, G. (1999). Interdependence of multiple theta generators in the hippocampus: a partial coherence analysis. *J. Neurosci*, 19:6200–212.

Kocsis, B. and Vertes, R. (1997). Phase relations of rhythmic neuronal firing in the supramammillary nucleus and mammillary body to the hippocampal theta ac- tivity in urethane anesthetized rats. *Hippocampus*, 7:207–214.

Konopacki, J., MacIver, M. B., Bland, B. H., and Roth, S. H. (1987). Carbachol-induced EEG 'theta' activity in hippocampal brain slices. *Brain Res*, 405(1):196–8.

Kramis, R., Vanderwolf, C., and Bland, B. (1975). Two types of hippocampal rhythmical slow activity in both the rabbit and the rat: relations to behavior and effects of atropine, diethyl ether, urethane, and pentobarbital. *Exp Neurol*, 49:58–85.

Kreiman, G., Koch, C., and Fried, I. (2000). Category-specific visual responses of single neurons in the human medial temporal lobe. *Nat Neurosci*, 3(9):946–53.

Kropff, E. and Treves, A. (2008). The emergence of grid cells: Intelligent design or just adaptation? *Hippocampus*, 18(12):1256–69.

Larkum, M. E. and Nevian, T. (2008). Synaptic clustering by dendritic signalling mechanisms. *Curr Opin Neurobiol*, 18(3):321–31.

Larkum, M. E., Nevian, T., Sandler, M., Polsky, A., and Schiller, J. (2009). Synaptic integration in tuft dendrites of layer 5 pyramidal neurons: a new unifying principle. *Science*, 325(5941):756–60.

Lawson, V. H. and Bland, B. H. (1993). The role of the septohippocampal pathway in the regulation of hippocampal field activity and behavior: analysis by the intraseptal microinfusion of carbachol, atropine, and procaine. *Exp Neurol*, 120(1):132–44.

Lee, I., Yoganarasimha, D., Rao, G., and Knierim, J. J. (2004). Comparison of population coherence of place cells in hippocampal subfields CA1 and CA3. *Nature*, 430(6998):456–9.

Lee, M. G., Chrobak, J. J., Sik, A., Wiley, R. G., and Buzsaki, G. (1994). Hippocampal theta activity following selective lesion of the septal cholinergic system. *Neuroscience*, 62(4):1033–47.

Leibold, C., Gundlfinger, A., Schmidt, R., Thurley, K., Schmitz, D., and Kempter, R. (2008). Temporal compression mediated by short-term synaptic plasticity. *Proc Natl Acad Sci U S A*, 105(11):4417–22.

Lengyel, M. (2003). *The theta switch: Rate and phase coding in the entorhino-hippocampal system*. PhD thesis, Eötvös Loránd University, Faculty of Natural Sciences, Biology PhD School.

Lengyel, M., Huhn, Z., and Érdi, P. (2005a). Computational theories on the function of theta oscillations. *Biol Cybern.*, 92(6):393–408.

Lengyel, M., Kwag, J., Paulsen, O., and Dayan, P. (2005b). Matching storage and recall: hippocampal spike timing-dependent plasticity and phase response curves. *Nature Neuroscience*, 8(12):1677–1683.

Leung, L. and Borst, J. (1987). Electrical activity of the cingulate cortex. i. generating mechanisms and relations to behavior. *Brain Res*, 407:68–80.

Leung, L. and Shen, B. (2004). Glutamatergic synaptic transmission participates in generating the hippocampal EEG. *Hippocampus*, 14(4):510–25.

Leung, L. S. and Yu, H. W. (1998). Theta-frequency resonance in hippocampal CA1 neurons in vitro demonstrated by sinusoidal current injection. *J Neurophysiol*, 79(3):1592–6.

Leutgeb, J., Leutgeb, S., Treves, A., Meyer, R., Barnes, C., McNaughton, B., Moser, M.-B., and Moser, E. (2005a). Progressive transformation of hippocampal neuronal representations in "morphed" environments. *Neuron*, 48:345–58.

Leutgeb, J. K., Leutgeb, S., Moser, M.-B., and Moser, E. I. (2007). Pattern separation in the dentate gyrus and CA3 of the hippocampus. *Science*, 315:961–966.

Leutgeb, S., Leutgeb, J., Barnes, C., Moser, E., McNaughton, B., and Moser, M. (2005b). Independent codes for spatial and episodic memory in hippocampal neuronal ensembles. *Science*, 309:619–623.

Leutgeb, S., Leutgeb, J., Treves, A., Moser, M.-B., and Moser, E. (2004). Distinct ensemble codes in hippocampal areas CA3 and CA1. *Science*, 305:1295–1298.

Lever, C., Burton, S., Jeewajee, A., O'Keefe, J., and Burgess, N. (2009). Boundary vector cells in the subiculum of the hippocampal formation. *J Neurosci*, 29(31):9771–7.

Lever, C., Wills, T., Cacucci, F., Burgess, N., and O'Keefe, J. (2002). Long-term plasticity in hippocampal place-cell representation of environmental geometry. *Nature*, 416:90–94.

Lipton, P. A. and Eichenbaum, H. (2008). Complementary roles of hippocampus and medial entorhinal cortex in episodic memory. *Neural Plast*, 2008:258467.

Lisman, J. E. and Otmakhova, N. A. (2001). Storage, recall, and novelty detection of sequences by the hippocampus: elaborating on the socratic model to account for normal and aberrant effects of dopamine. *Hippocampus*, 11:551–568.

Lőrincz, A. and Buzsáki, G. (2000). Two-phase computational model training long-term memories in the entorhinal-hippocampal region. *Annals of the New York Academy of Sciences*, 911:83–111.

Losonczy, A. and Magee, J. C. (2006). Integrative properties of radial oblique dendrites in hippocampal CA1 pyramidal neurons. *Neuron*, 50(2):291–307.

Losonczy, A., Makara, J. K., and Magee, J. C. (2008). Compartmentalized dendritic plasticity and input feature storage in neurons. *Nature*, 452(7186):436–41.

Lynch, G. S., Dunwiddie, T., and Gribkoff, V. (1977). Heterosynaptic depression: a postsynaptic correlate of long-term potentiation. *Nature*, 266(5604):737–9.

Maaswinkel, H. and Whishaw, I. Q. (1999). Homing with locale, taxon, and dead reckoning strategies by foraging rats: sensory hierarchy in spatial navigation. *Behavioural Brain Research*, 99:143–152.

Maccaferri, G. and Lacaille, J. (2003). Interneuron diversity series: Hippocampal interneuron classifications making things as simple as possible, not simpler. *Trends. Neurosci.*, 26:564–71.

Magee, J. C. and Johnston, D. (1997). A synaptically controlled, associative signal for Hebbian plasticity in hippocampal neurons. *Science*, 275(5297):209–13.

Maguire, E., Burgess, N., Donnett, J., Frith, C., Frackowiak, R., and O'Keefe, J. (1998). Knowing where and getting there: a human navigation network. *Science*, 280:921–24.

Manseau, F., Danik, M., and Williams, S. (2005). A functional glutamatergic neurone network in the medial septum and diagonal band area. *J Physiol.*, 566(3):865–84.

Manseau, F., Goutagny, R., Danik, M., and Williams, S. (2008). The hippocamposeptal pathway generates rhythmic firing of GABAergic neurons in the medial septum and diagonal bands: an investigation using a complete septohippocampal preparation in vitro. *J Neurosci*, 28(15):4096–107.

Markus, E. J., Barnes, C. A., McNaughton, B. L., Gladden, V. L., and Skaggs, W. E. (1994). Spatial information content and reliability of hippocampal CA1 neurons: effects of visual input. *Hippocampus*, 4(4):410–21.

Marr, A. (1971). Simple memory: a theory for archicortex. *Philosophical transactions of the Royal Society of London. Series B, Biological sciences*, 262:23–81.

Martin, S. J., Grimwood, P. D., and Morris, R. G. (2000). Synaptic plasticity and memory: an evaluation of the hypothesis. *Annu Rev Neurosci*, 23:649–711.

Maurer, A. P., Vanrhoads, S. R., Sutherland, G. R., Lipa, P., and McNaughton, B. L. (2005). Self-motion and the origin of differential spatial scaling along the septo-temporal axis of the hippocampus. *Hippocampus*, 15(7):841–52.

McHugh, T. J., Jones, M. W., Quinn, J. J., Balthasar, N., Coppari, R., Elmquist, J. K., Lowell, B. B., Fanselow, M. S., Wilson, M. A., and Tonegawa, S. (2007). Dentate gyrus NMDA receptors mediate rapid pattern separation in the hippocampal network. *Science*, 317(5834):94–9.

McNaughton, B. L., Barnes, C., Gerrard, J., Gothard, K., Jung, M., Knierim, J., Kudrimoti, H., Qin, Y., Skaggs, W., Suster, M., and Weaver, K. (1996). Deciphering the hippocampal polyglot: the hippocampus as a path integration system. *Journal of Experimental Biology*, 199:173–185.

McNaughton, B. L., Barnes, C. A., and O'Keefe, J. (1983). The contributions of position, direction, and velocity to single unit activity in the hippocampus of freely-moving rats. *Exp Brain Res*, 52(1):41–9.

McNaughton, B. L., Battaglia, F. P., Jensen, O., Moser, E. I., and Moser, M.-B. (2006). Path integration and the neural basis of the "cognitive map". *Nature Reviews Neurosci.*, 7(8):663–678.

McNaughton, B. L., Douglas, R. M., and Goddard, G. V. (1978). Synaptic enhancement in fascia dentata: cooperativity among coactive afferents. *Brain Res*, 157(2):277–93.

Mel, B. W. (1993). Synaptic integration in an excitable dendritic tree. *J Neurophysiol*, 70(3):1086–101.

Mel, B. W., Ruderman, D. L., and Archie, K. A. (1998). Translation-invariant orientation tuning in visual "complex" cells could derive from intradendritic computations. *J Neurosci*, 18(11):4325–34.

Michel, O. (2004). Webots: Professional mobile robot simulation. *Journal of Advanced Robotics Systems*, 1(1):39–42.

Milojkovic, B. A., Radojicic, M. S., and Antic, S. D. (2005). A strict correlation between dendritic and somatic plateau depolarizations in the rat prefrontal cortex pyramidal neurons. *J Neurosci*, 25(15):3940–51.

Mohler, H., Fritschy, J. M., and Rudolph, U. (2002). A new benzodiazepine pharmacology. *J Pharmacol Exp Ther.*, 300(1):2–8.

Monmaur, P., Collet, A., Puma, C., Frankel-Kohn, L., and Sharif, A. (1997). Relations between acetylcholine release and electrophysiological characteristics of theta rhythm: a microdialysis study in the urethane-anesthetized rat hippocampus. *Brain Res Bull*, 42(2):141–6.

Mori, M., Abegg, M. H., Gahwiler, B. H., and Gerber, U. (2004). A frequency-dependent switch from inhibition to excitation in a hippocampal unitary circuit. *Nature*, 431(7007):453–6.

Morris, N. P., Harris, S. J., and Henderson, Z. (1999). Parvalbumin-immunoreactive, fast-spiking neurons in the medial septum/diagonal band complex of the rat: intracellular recordings in vitro. *Neuroscience*, 92(2):589–600.

Morris, R. G. and Frey, U. (1997). Hippocampal synaptic plasticity: role in spatial learning or the automatic recording of attended experience? *Philos Trans R Soc Lond B Biol Sci*, 352(1360):1489–503.

Muller, R., Bostock, E., Taube, J., and Kubie, J. (1994). On the directional firing properties of hippocampal place cells. *J Neurosci*, 14:7235–7251.

Muller, R. U. and Kubie, J. L. (1987). The effects of changes in the environment on the spatial firing of hippocampal complex-spike cells. *Journal of Neuroscience*, 7:1951–1968.

Murayama, M., Perez-Garci, E., Luscher, H. R., and Larkum, M. E. (2007). Fiberoptic system for recording dendritic calcium signals in layer 5 neocortical pyramidal cells in freely moving rats. *J Neurophysiol*, 98(3):1791–805.

Murayama, M., Perez-Garci, E., Nevian, T., Bock, T., Senn, W., and Larkum, M. E. (2009). Dendritic encoding of sensory stimuli controlled by deep cortical interneurons. *Nature*, 457(7233):1137–41.

Nadel, L. and Moscovitch, M. (1997). Memory consolidation, retrograde amnesia and the hippocampal complex. *Curr Opin Neurobiol*, 7(2):217–27.

Nakazawa, K., Quirk, M. C., Chitwood, R. A., Watanabe, M., Yeckel, M. F., Sun, L. D., Kato, A., Carr, C. A., Johnston, D., Wilson, M. A., and Tonegawa, S. (2002).

Requirement for hippocampal CA3 NMDA receptors in associative memory recall. *Science*, 297(5579):211–8.

Nardini, M., Jones, P., Bedford, R., and Braddick, O. (2008). Development of cue integration in human navigation. *Current Biology*, 18:689–693.

Nevian, T., Larkum, M. E., Polsky, A., and Schiller, J. (2007). Properties of basal dendrites of layer 5 pyramidal neurons: a direct patch-clamp recording study. *Nat Neurosci*, 10(2):206–14.

Nusser, Z., Sieghart, W., Benke, D., Fritschy, J. M., and Somogyi, P. (1996). Differential synaptic localization of two major gamma-aminobutyric acid type A receptor alpha subunits on hippocampal pyramidal cells. *PNAS*, 93(21):11939–44.

O'Keefe, J. (1976). Place units in the hippocampus of the freely moving rat. *Exp Neurol*, 51(1):78–109.

O'Keefe, J. (1999). Do hippocampal pyramidal cells signal non-spatial as well as spatial information? *Hippocampus*, 9(4):352–64.

O'Keefe, J. and Burgess, N. (1996). Geometric determinants of the place fields of hippocampal neurons. *Nature*, 381:425–28.

O'Keefe, J. and Burgess, N. (2005). Dual phase and rate coding in hippocampal place cells: theoretical significance and relationship to entorhinal grid cells. *Hippocampus*, 15:853–866.

O'Keefe, J. and Dostrovsky, J. (1971). The hippocampus as a spatial map. Preliminary evidence from unit activity in the freely-moving rat. *Brain Research*, 34:171–175.

O'Keefe, J. and Nadel, L. (1978). *The Hippocampus as a Cognitive Map*. Oxford University Press.

O'Keefe, J. and Recce, M. L. (1993). Phase relationship between hippocampal place units and the EEG theta rhythm. *Hippocampus*, 3:317–30.

Orbán, G., Kiss, T., and Érdi, P. (2006). Intrinsic and synaptic mechanisms determining the timing of neuron population activity during hippocampal theta oscillation. *Journal of Neurophysiology*, 96:2889–2904.

Orr, G., Rao, G., Houston, F. P., McNaughton, B. L., and Barnes, C. A. (2001). Hippocampal synaptic plasticity is modulated by theta rhythm in the fascia dentata of adult and aged freely behaving rats. *Hippocampus*, 11(6):647–54.

Parra, P., Gulyás, A., and Miles, R. (1998). How many subtypes of inhibitory cells in the hippocampus? *Neuron*, 20:983–93.

Paré, D. and Collins, D. (2000). Neuronal correlates of fear in the lateral amygdala: multiple extracellular recordings in conscious cats. *J Neurosci*, 20:2701–2710.

Pastalkova, E., Serrano, P., Pinkhasova, D., Wallace, E., Fenton, A. A., and Sacktor, T. C. (2006). Storage of spatial information by the maintenance mechanism of LTP. *Science*, 313(5790):1141–4.

Pavlides, C., Greenstein, Y. J., Grudman, M., and Winson, J. (1988). Long-term potentiation in the dentate gyrus is induced preferentially on the positive phase of theta-rhythm. *Brain Res*, 439(1-2):383–7.

Petsche, H., Stumpf, C., and Gogolak, G. (1962). The significance of the rabbit's septum as a relay station between the mid-brain and the hippocampus. I The control of hippocampal arousal activity by the septum cells. *Electroencephalogr Clin Neurophysiol*, 14:202–211.

Peyrache, A., Khamassi, M., Benchenane, K., Wiener, S. I., and Battaglia, F. P. (2009). Replay of rule-learning related neural patterns in the prefrontal cortex during sleep. *Nat Neurosci*, 12(7):919–26.

Poirazi, P., Brannon, T., and Mel, B. W. (2003a). Arithmetic of subthreshold synaptic summation in a model CA1 pyramidal cell. *Neuron*, 37(6):977–87.

Poirazi, P., Brannon, T., and Mel, B. W. (2003b). Pyramidal neuron as two-layer neural network. *Neuron*, 37(6):989–99.

Poirazi, P. and Mel, B. W. (2001). Impact of active dendrites and structural plasticity on the memory capacity of neural tissue. *Neuron*, 29(3):779–96.

Polsky, A., Mel, B. W., and Schiller, J. (2004). Computational subunits in thin dendrites of pyramidal cells. *Nat Neurosci*, 7(6):621–7.

Puma, C. and Bizot, J. C. (1999). Hippocampal theta rhythm in anesthetized rats: role of AMPA glutamate receptors. *Neuroreport*, 10(11):2297–300.

Quirk, G., Muller, R., and Kubie, J. (1990). The firing of hippocampal place cells in the dark depends on the rat's recent experience. *J Neurosci*, 10:2008–2017.

Quiroga, R. Q., Reddy, L., Kreiman, G., Koch, C., and Fried, I. (2005). Invariant visual representation by single neurons in the human brain. *Nature*, 435(7045):1102–7.

R Development Core Team (2005). *R: A language and environment for statistical computing*. R Foundation for Statistical Computing, Vienna, Austria. ISBN 3-900051-07-0.

Rall, W. (1989). Cable Theory for Dendritic Neurons. In Koch, C. and Segev, I., editors, *Methods in Neuronal Modeling*, pages 9–62. MIT press.

Redish, A. (1999). *Beyond the cognitive map: from place cells to episodic memory*. A Bradford Book. Cambridge, MA: The MIT Press.

Rodriguez-Pallares, J., Caruncho, H. J., Lopez-Real, A., Wojcik, S., Guerra, M. J., and Labandeira-Garcia, J. L. (2001). Rat brain cholinergic, dopaminergic, noradrenergic and serotonergic neurons express GABAA receptors derived from the alpha3 subunit. *Receptors Channels*, 7(6):471–8.

Rolls, E. T. (1995). A model of the operation of the hippocampus and entorhinal cortex in memory. *International Journal of Neural Systems*, 6:51–71.

Rolls, E. T. and Kesner, R. P. (2006). A computational theory of hippocampal function, and empirical tests of the theory. *Progress in Neurobiology*, 79:1–48.

Rolls, E. T., Miyashita, Y., Cahusac, P. M., Kesner, R. P., Niki, H., Feigenbaum, J. D., and Bach, L. (1989). Hippocampal neurons in the monkey with activity related to the place in which a stimulus is shown. *J Neurosci*, 9(6):1835–45.

Rolls, E. T., Robertson, R. G., and Georges-Francois, P. (1997). Spatial view cells in the primate hippocampus. *Eur J Neurosci*, 9(8):1789–94.

Rolls, E. T., Stringer, S. M., and Elliot, T. (2006). Entorhinal cortex grid cells can map to hippocampal place cells by competitive learning. *Network*, 17:447–465.

Samu, D. (2008). Biológiai alapú navigáció a gridsejt-rendszer és a hippokampusz modellezése alapján. Master's thesis, Budapest University of Technology and Economics.

Sargolini, F., Fyhn, M., Hafting, T., McNaughton, B. L., Witter, M. P., Moser, M.-B., and Moser, E. I. (2006). Conjunctive representation of position, direction, and velocity in entorhinal cortex. *Science*, 312(5774):758–762.

Save, E., Nerad, L., and Poucet, B. (2000). Contribution of multiple sensory information to place field stability in hippocampal place cells. *Hippocampus*, 10(1):64–76.

Schacter, D. L. and Wagner, A. D. (1999). Medial temporal lobe activations in fMRI and PET studies of episodic encoding and retrieval. *Hippocampus*, 9(1):7–24.

Schiller, J., Major, G., Koester, H. J., and Schiller, Y. (2000). NMDA spikes in basal dendrites of cortical pyramidal neurons. *Nature*, 404(6775):285–9.

Schiller, J., Schiller, Y., Stuart, G., and Sakmann, B. (1997). Calcium action potentials restricted to distal apical dendrites of rat neocortical pyramidal neurons. *J Physiol*, 505 (Pt 3):605–16.

Schmidt-Hieber, C., Jonas, P., and Bischofberger, J. (2004). Enhanced synaptic plasticity in newly generated granule cells of the adult hippocampus. *Nature*, 429(6988):184–7.

Schmidt-Hieber, C., Jonas, P., and Bischofberger, J. (2007). Subthreshold dendritic signal processing and coincidence detection in dentate gyrus granule cells. *The Journal of Neuroscience*, 27(31):8430–8441.

Scoville, W. B. and Milner, B. (1957). Loss of recent memory after bilateral hippocampal lesions. *Journal of Neurology, Neurosurgery and Psychiatry*, 20:11–21.

Segev, I. and Rall, W. (1988). Computational study of an excitable dendritic spine. *J Neurophysiol*, 60(2):499–523.

Séguinot, V., Maurer, R., and Etienne, A. S. (1993). Dead reckoning in a small mammal: the evaluation of distance. *Journal of Comparative Physiology A.*, 173:103–113.

Serafin, M., Williams, S., Khateb, A., Fort, P., and Muhlethaler, M. (1996). Rhythmic firing of medial septum non-cholinergic neurons. *Neuroscience.*, 75(3):671–5.

Sharp, P. E. (1991). Computer simulation of hippocampal place cells. *Psychobiology*, 19(2):103–115.

Sharp, P. E., Blair, H. T., Etkin, D., and Tzanetos, D. B. (1995). Influences of vestibular and visual motion information on the spatial firing patterns of hippocampal place cells. *J Neurosci*, 15(1 Pt 1):173–89.

Shepherd, G. M. and Brayton, R. K. (1987). Logic operations are properties of computer-simulated interactions between excitable dendritic spines. *Neuroscience*, 21(1):151–65.

Shu, Y., Hasenstaub, A., and McCormick, D. A. (2003). Turning on and off recurrent balanced cortical activity. *Nature*, 423(6937):288–93.

Si, B. and Treves, A. (2009). The role of competitive learning in the generation of DG fields from EC inputs. *Cogn Neurodyn*, 3(2):177–87.

Siapas, A. G., Lubenov, E. V., and Wilson, M. A. (2005). Prefrontal phase locking to hippocampal theta oscillations. *Neuron*, 46(1):141–51.

Sik, A., Penttonen, M., and Buzsáki, G. (1997). Interneurons in the hippocampal dentate gyrus: an in vivo intracellular study. *Eur J Neurosci*, 9(3):573–88.

Simon, A. P., Poindessous-Jazat, F., Dutar, P., Epelbaum, J., and Bassant, M. H. (2006). Firing properties of anatomically identified neurons in the medial septum of anesthetized and unanesthetized restrained rats. *J Neurosci*, 26(35):9038–46.

Sirota, A., Csicsvári, J., Buhl, D., and Buzsáki, G. (2003). Communication between neocortex and hippocampus during sleep in rodents. *Proc Natl Acad Sci USA*, 100(4):2065–9.

Skaggs, W. E., McNaughton, B. L., Gothard, K. M., and Markus, E. J. (1993). An information theoretic approach to deciphering the hippocampal code. *Advances in neural information processing systems.*, pages 1030–1037.

Skaggs, W. E., McNaughton, B. L., Wilson, M. A., and Barnes, C. A. (1996). Theta phase precession in hippocampal neuronal populations and the compression of temporal sequences. *Hippocampus*, 6(2):149–72.

Solstad, T., Boccara, C. N., Kropff, E., Moser, M.-B., and Moser, E. I. (2008). Representation of geometric borders in the entorhinal cortex. *Science*, 19(5909):1865–1868.

Solstad, T., Moser, E. I., and Einevoll, G. T. (2006). From grid cells to place cells: a mathematical model. *Hippocampus*, 16:1026–1031.

Somogyi, P. and Klausberger, T. (2005). Defined types of cortical interneurons structure space and spike timing in the hippocampus. *J Physiol*, 562(1):9–26.

Somogyvari, Z., Zalanyi, L., Ulbert, I., and Erdi, P. (2005). Model-based source localization of extracellular action potentials. *J Neurosci Methods*, 147(2):126–37.

Song, H., Kempermann, G., Overstreet Wadiche, L., Zhao, C., Schinder, A. F., and Bischofberger, J. (2005). New neurons in the adult mammalian brain: synaptogenesis and functional integration. *J Neurosci*, 25(45):10366–8.

Song, S., Miller, K. D., and Abbott, L. F. (2000). Competitive Hebbian learning through spike-timing-dependent synaptic plasticity. *Nat Neurosci*, 3(9):919–26.

Sotty, F., Danik, M., Manseau, F., Quirion, R., and Williams, S. (2003). Distinct electrophysiological properties of glutamatergic, cholinergic and GABAergic rat septohippocampal neurons: novel implications for hippocampal rhythmicity. *J Physiol*, 551:927–943.

Spruston, N. (2008). Pyramidal neurons: dendritic structure and synaptic integration. *Nat Rev Neurosci*, 9(3):206–21.

Stent, G. S. (1973). A physiological mechanism for Hebb's postulate of learning. *Proc Natl Acad Sci USA*, 70(4):997–1001.

Stewart, M. and Fox, S. E. (1989). Two populations of rhythmically bursting neurons in rat medial septum are revealed by atropine. *J Neurophysiol.*, 61(5):982–93.

Stewart, M. and Fox, S. E. (1990). Do septal neurons pace the hippocampal theta rhythm? *Trends Neurosci.*, 13(5):163–8.

Stumpf, C., Petsche, H., and Gogolak, G. (1962). The significance of the rabbit's septum as a relay station between the midbrain and the hippocampus. II. The differential influence of drugs upon both the septal cell firing pattern and the hippocampus theta activity. *Electroencephalogr Clin Neurophysiol*, 14:212–9.

Takacs, V. T., Freund, T. F., and Gulyas, A. I. (2008). Types and synaptic connections of hippocampal inhibitory neurons reciprocally connected with the medial septum. *Eur J Neurosci*, 28(1):148–64.

Takahashi, S. and Sakurai, Y. (2007). Coding of spatial information by soma and dendrite of pyramidal cells in the hippocampal CA1 of behaving rats. *Eur J Neurosci*, 26(7):2033–45.

Tanila, H., Shapiro, M. L., and Eichenbaum, H. (1997). Discordance of spatial representation in ensembles of hippocampal place cells. *Hippocampus*, 7(6):613–23.

Taube, J. S., Muller, R. U., and Ranck, Jr, J. B. (1990). Head-direction cells recorded from the postsubiculum in freely moving rats. I. Description and quantitative analysis. *J Neurosci*, 10(2):420–35.

Thompson, L. T. and Best, P. J. (1990). Long-term stability of the place-field activity of single units recorded from the dorsal hippocampus of freely behaving rats. *Brain Res*, 509(2):299–308.

Touretzky, D. S. and Redish, A. D. (1996). Theory of rodent navigation based on interacting representations of space. *Hippocampus*, 6(3):247–270.

Treves, A. and Rolls, E. T. (1991). What determines the capacity of autoassociative memories in the brain? *Network*, 2:371–397.

Treves, A. and Rolls, E. T. (1992). Computational constraints suggest the need for two distinct input systems to the hippocampal CA3 network. *Hippocampus*, 2(2):189–99.

Treves, A. and Rolls, E. T. (1994). Computational analysis of the role of the hippocampus in memory. *Hippocampus*, 4:374–391.

Treves, A., Tashiro, A., Witter, M. E., and Moser, E. I. (2008). What is the mammalian dentate gyrus good for? *Neuroscience*, 154(4):1155–72.

Tsay, D., Dudman, J. T., and Siegelbaum, S. A. (2007). HCN1 channels constrain synaptically evoked Ca2+ spikes in distal dendrites of CA1 pyramidal neurons. *Neuron*, 56(6):1076–89.

Tse, D., Langston, R. F., Kakeyama, M., Bethus, I., Spooner, P. A., Wood, E. R., Witter, M. P., and Morris, R. G. (2007). Schemas and memory consolidation. *Science*, 316(5821):76–82.

Tsodyks, M. (2005). Attractor neural networks and spatial maps in hippocampus. *Neuron*, 48:168–169.

Tsodyks, M. V., Skaggs, W. E., Sejnowski, T. J., and McNaughton, B. L. (1996). Population dynamics and theta rhythm phase precession of hippocampal place cell firing: a spiking neuron model. *Hippocampus*, 6(3):271–80.

Turrigiano, G. G. (1999). Homeostatic plasticity in neuronal networks: the more things change, the more they stay the same. *Trends Neurosci*, 22(5):221–7.

Tóth, K., Borhegyi, Z., and Freund, T. F. (1993). Postsynaptic targets of GABAergic hippocampal neurons in the medial septum-diagonal band of broca complex. *J Neurosci*, 13(9):3712–24.

Tóth, K., Freund, T., and R, M. (1997). Disinhibition of rat hippocampal pyramidal cells by GABAergic afferents from the septum. *J Physiol (Lond)*, 500:463–74.

Ujfalussy, B. (2005). Pacemaker sejtek hálózati topológiája felelős a theta szinkronizációért a mediális szeptumban: kísérleti eredmények számítógépes modellezése. Master's thesis, Eötvös Loránd University.

Ujfalussy, B., Eros, P., Somogyvári, Z., and Kiss, T. (2008). Episodes in space: A modelling study of hippocampal place representation. In Asada, M., Hallam, J. C. T., Meyer, J., and Tani, J., editors, *From Animals to Animats 10*, volume 5040 of *Lecture Notes in Artificial Intelligence*, pages 123–136. Springer.

Ujfalussy, B. and Kiss, T. (2006). How do glutamatergic and GABAergic cells contribute to synchronization in the medial septum? *J Comput Neurosci*, 21(3):343–57.

Ujfalussy, B., Kiss, T., and Érdi, P. (2009). Parallel computational subunits in dentate granule cells generate multiple place fields. *PLoS Comput Biol*, 5(9):e1000500.

Ujfalussy, B., Kiss, T., Orbán, G., Hoffmann, W. E., Érdi, P., and Hajós, M. (2007). Pharmacological and computational analysis of alpha-subunit preferential GABA(A) positive allosteric modulators on the rat septo-hippocampal activity. *Neuropharmacology*, 52(3):733–43.

van Haeften, T., Baks-te-Bulte, L., Goede, P. H., Wouterlood, F. G., and Witter, M. P. (2003). Morphological and numerical analysis of synaptic interactions between neurons in deep and superficial layers of the entorhinal cortex of the rat. *Hippocampus*, 13:943–952.

Vanderwolf, C. H. (1969). Hippocampal electrical activity and voluntary movement in the rat. *Electroencephalogr Clin Neurophysiol*, 26(4):407–418.

Vanderwolf, C. H. (1988). Cerebral activity and behavior: control by central cholinergic and serotonergic systems. *Int Rev Neurobiol*, 30:225–340.

Vargha-Khadem, F., Gadian, D. G., Watkins, K. E., Connelly, A., Van Paesschen, W., and Mishkin, M. (1997). Differential effects of early hippocampal pathology on episodic and semantic memory. *Science*, 277(5324):376–80.

Vazdarjanova, A. and Guzowski, J. F. (2004). Differences in hippocampal neuronal population responses to modifications of an environmental context: evidence for distinct, yet complementary, functions of CA3 and CA1 ensembles. *J Neurosci*, 24(29):6489–96.

Vértes, R. P. and Kocsis, B. (1997). Brainstem-diencephalo-septohippocampal systems controlling the theta rhythm of the hippocampus. *Neuroscience*, 81:893–926.

Vetter, P., Roth, A., and Hausser, M. (2001). Propagation of action potentials in dendrites depends on dendritic morphology. *J Neurophysiol*, 85(2):926–37.

Vinogradova, O., Brazhnik, E., Karanov, A., and Zhadina, S. (1980). Neuronal activity of the septum following various types of deafferentation. *Brain Res*, 187(2):353–68.

Vinogradova, O. S. (1995). Expression, control, and probable functional significance of the neuronal theta-rhythm. *Prog Neurobiol.*, 45(6):523–583.

Wainger, B., DeGennaro, M., Santoro, B., Siegelbaum, S., and Tibbs, G. (2001). Molecular mechanism of cAMP modulation of HCN pacemaker channels. *Nature*, 411(6839):805–10.

Wallenstein, G. V. and Hasselmo, M. E. (1997). GABAergic modulation of hippocampal population activity: sequence learning, place field development, and the phase precession effect. *J Neurophysiol*, 78(1):393–408.

Wang, X. J. (2002). Pacemaker neurons for the theta rhythm and their synchronization in the septohippocampal reciprocal loop. *J Neurophysiol.*, 87(2):889–900.

Wang, X. J. and Buzsáki, G. (1996). Gamma oscillation by synaptic inhibitionin a hippocampal interneuronl network model. *J Neurosci.*, 16:6402–6413.

Wei, D. S., Mei, Y. A., Bagal, A., Kao, J. P., Thompson, S. M., and Tang, C. M. (2001). Compartmentalized and binary behavior of terminal dendrites in hippocampal pyramidal neurons. *Science*, 293(5538):2272–5.

Welinder, P. E., Burak, Y., and Fiete, I. R. (2008). Grid cells: the position code, neural network models of activity, and the problem of learning. *Hippocampus*, 18(12):1283–300.

Wiener, S. I., Korshunov, V. A., Garcia, R., and Berthoz, A. (1995). Inertial, substratal and landmark cue control of hippocampal CA1 place cell activity. *European Journal of Neuroscience*, 7:2206–2219.

Wiener, S. I., Paul, C. A., and Eichenbaum, H. (1989). Spatial and behavioral correlates of hippocampal neuronal activity. *J Neurosci*, 9(8):2737–63.

Wiener, S. I. and Taube, J. S., editors (2005). *Head Direction Cells and the Neural Mechanisms of Spatial Orientation*. MIT Press.

Williams, S. R. (2004). Spatial compartmentalization and functional impact of conductance in pyramidal neurons. *Nat Neurosci*, 7(9):961–7.

Wills, T., Lever, C., Cacucci, F., Burgess, N., and O'Keefe, J. (2005). Attractor dynamics in the hippocampal representation of the local environment. *Science*, 308:873–876.

Wilson, M. A. and McNaughton, B. L. (1993). Dynamics of the hippocampal ensemble code for space. *Science*, 261:1055–1058.

Witter, M. P., Groenewegen, H. J., Lopes da Silva, F. H., and Lohman, A. H. (1989). Functional organization of the extrinsic and intrinsic circuitry of the parahippocampal region. *Prog Neurobiol*, 33(3):161–253.

Witter, M. P., Naber, P. A., van Haeften, T., Machielsen, W. C. M., Rombouts, S. A. R. B., Barkhof, F., Scheltens, P., and Lopes da Silva, F. H. (2000). Cortico-hippocampal communication by way of parallel parahippocampal-subicular pathways. *Hippocampus*, 10:398–410.

Wood, E. R., Dudchenko, P. A., and Eichenbaum, H. (1999). The global record of memory in hippocampal neuronal activity. *Nature*, 397(6720):613–6.

Wood, E. R., Dudchenko, P. A., Robitsek, R. J., and Eichenbaum, H. (2000). Hippocampal neurons encode information about different types of memory episodes occurring in the same location. *Neuron*, 27(3):623–33.

Wyble, B. P., Linster, C., and Hasselmo, M. E. (2000). Size of CA1-evoked synaptic potentials is related to theta rhythm phase in rat hippocampus. *J Neurophysiol*, 83(4):2138–44.

Yoder, R. M. and Pang, K. C. (2005). Involvement of GABAergic and cholinergic medial septal neurons in hippocampal theta rhythm. *Hippocampus*, 15(3):381–92.

Zipser, D. (1985). A computational model of hippocampal place fields. *Behavioral Neuroscience*, 99(5):1006–1018.

Zola-Morgan, S., Squire, L. R., and Amaral, D. G. (1986). Human amnesia and the medial temporal region: enduring memory impairment following a bilateral lesion limited to field CA1 of the hippocampus. *J Neurosci*, 6(10):2950–67.

Zucker, R. S. and Regehr, W. G. (2002). Short-term synaptic plasticity. *Annu Rev Physiol*, 64:355–405.

Zugaro, M. B., Berthoz, A., and Wiener, S. I. (2001). Background, but not foreground, spatial cues are taken as references for head direction responses by rat anterodorsal thalamus neurons. *J Neurosci*, 21(14):RC154.

Összefoglalás

Jelen dolgozat a hippocampális formáció működését közelíti meg három különböző, mégis egymással összefüggő irányból, modellezi azt három különböző szinten. Az első fejezetben részletes egysejtmodelleket használva vizsgáljuk a hippocampális theta ritmus kialakulását. Ez az oszcilláció jellemző a rágcsálók hippocampusára különféle felderítő viselkedésformák alatt. A modellben a mediális szeptum glutamáterg sejtjei intrinsic klaszter-tüzelő sejtek. A sejtek theta-periodikus klaszterei szinkronizálódnak, így a hálózat ritmusgenerátorként funkcionál. A szeptális gyorstüzelő GABAerg sejtek theta-periodikus burstjeit a hálózati dinamika hozza létre: a sejtek egy része periodikus serkentő szinaptikus bemeneteket fogad a fenti glutamáterg populációtól, míg a másik részüket az első csoporttól eredő GABAerg gátlás vezérli. A szeptális GABAerg sejtek hippocampális interneuronokat beidegezve közvetítitk a ritmust a hippocampusba.

A hippocampusnak igen fontos szerepe van a térinformáció feldolgozásában, az emléknyomok kontextusfüggő eltárolásában. A hippocampusból a neocortexbe vezető pályák pedig az emléknyomok előhívásában játszanak közre. A dolgozat második részében megmutatjuk, hogy a magasan szervezett hippocampális helyreprezentációból eredő visszacsatolás hozzájárul az útintegráció hibatűréséhez. Az útintegrációt vegző entorhinális kérgi gridsejtek tüzelési mintázata megváltozik ha a környezet alakja módosul. A hippocampus és az entorhinális kéreg kétirányú kapcsolatát leíró modellünk ezeket a változásokat jól visszaadja, megmagyarázza.

A hippocampusz kapujában található gyrus dentatusnak különösen fontos szerepe van a helyreprezentáció kialakításában. Hogyan alakul ki a gyrus dentatus-beli szemcsesejtek térbeli tüzelési mintázata? Erre keressük a válasz a dolgozat harmadik részében. Megmutatjuk, hogy a ezeknek az idegsejteknek a mérsékelten elágazó dendritfája alkalmas párhuzamos információfeldolgozásra. Ezzel szemben a túl kompakt dendritfa nem tesz lehetővé lokális folyamatokat (pl. szinaptikus plaszticitást) míg egy túl nagy dendritfán a lokális folyamatoknak nincsen kellően nagy hatásuk a sejt kimenetére. Végül megmutatjuk, hogy a modell magyarázatot ad a szemcsesejtek többszörös helymezőinek kialakulására.

Summary

In the present dissertation we describe three lines of research focusing on different aspects of hippocampal computations. First we give a new conductance-based model for the generation of the theta oscillation which is the dominant EEG pattern during exploratory behavior in the rodent hippocampus. According to the model medial septal glutamatergic neurons, endowed with intrinsic cluster-firing property, form a pacemaker network for the theta rhythm. Septal GABAergic fast-spiking neurons show bursting behavior due to emergent network dynamics: a subpopulation of these cells is driven by rhythmic EPSPs originating from the local glutamatergic pacemaker network; the other subpopulation is driven by IPSPs from the first GABAergic subpopulation. We suggest that these GABAergic neurons innervate hippocampal interneurons and transmit the septal rhythm to the hippocampus.

The hippocampus in implicated in the rapid encoding of information in relation to their spatio-temporal context, and back projection to the neocortex contribute to the retrieval of the stored information based on noisy or partial cues. In the second part, we show that feed-back connections from the integrated place cell representation in the hippocampus account for the robust, noise-free path integration realized by the grid cells in the entorhinal cortex. Our model also suggest that parametric changes in grid cell activity following morphing of the environment and remapping of place cells in a new environment are the result of a reciprocal interaction between hippocampal place- and entorhinal grid-cell activities.

The dentate gyrus has a pivotal role in the emergence of a robust place representation within the hippocampus, thus, in the third part, we explore the computations performed by dentate granule cells. We demonstrate that the moderately branching dendritic tree of these neurons is suitable for parallel information processing since larger dendritic trees favor local plasticity by isolating dendritic compartments, while reliable detection of individual dendritic events in the soma requires a low branch number. These parallel dendritic computations could contribute to the generation of multiple independent place fields of hippocampal granule cells.